Spatio-Temporal Patterns in Systems far from Equilibrium

Hira Affan Siddiqui

2011

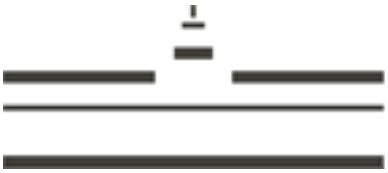

Westfälische
Wilhelms-Universität
Münster

Theoretische Physik

Spatio-Temporal Patterns in Systems far from Equilibrium

Inauguraldissertation
zur Erlangung des Doktorgrades
der Naturwissenschaften im Fachbereich Physik
der Mathematisch-Naturwissenschaftlichen Fakultät
der Westfälischen Wilhelms-Universität Münster

vorgelegt von
Hira Affan Siddiqui
aus Lahore

– 2011 –

Dekan:	Prof. Dr. Tilmann Kuhn
Erster Gutachter:	Prof. Dr. Rudolf Friedrich
Zweiter Gutachter:	Prof. Dr. Andreas Heuer
Tag der mündlichen Prüfung:	_____
Tag der Promotion:	_____

Dedicated to My Mother

Kurzfassung

In dieser Arbeit wurde die Strukturbildung in räumlich ausgedehnten Systemen anhand von zwei kanonischen Beispielen untersucht. Zum einen das Rayleigh-Bénard-System, das bei der Untersuchung hydrodynamischer Instabilitäten eine große Rolle spielt, und zum anderen ein Reaktions-Diffusions System, das bei der Beschreibung von Strukturbildung in chemischen Systemen benutzt wird.

Zuerst wurde das Rayleigh-Bénard System in der Nähe der konvektiven Instabilität untersucht. Im Rahmen der Beschreibung mittels der verallgemeinerten Swift-Hohenberg-Gleichung, bei der das mittlere Feld die Hauptrolle spielt, konnte die Entwicklung eines Zustandes, der Spiral-defekt-chaos genannt wird, numerisch beobachtet werden. Das Modell bestand aus einer Ordnungsparametergleichung für das Temperaturfeld, die an eine Gleichung zur Beschreibung des mittleren Strömungsfeldes gekoppelt ist. Die in der Dynamik des mittleren Strömungsfeldes auftretenden Nichtlinearitäten führen auf eine zweidimensionale Navier-Stokes Gleichung, die an eine Swift-Hohenberg Gleichung gekoppelt ist. Um die Rolle des mittleren Strömungsfeldes zu quantifizieren, wurde das Feld numerisch abgekoppelt, während die dynamisch Temperaturfelds weiterhim wirksam ist. Hier konnte gezeigt werden, dass den spezielle Rollenstrukturen bend rolls genannt werden. Das zeigt, dass das mittlere Feld für das Spiral-defekt-chaos verantwortlicher ist.

Der zweite Teil der Arbeit befasst sich mit der raum-zeitlichen Strukturbildung in Advektions-Reaktions-Diffusions Systemen, in denen die chemischen Spezies mit der hydrodynamischen Strömung interagieren. Durch das Zusammenspiel beider erhält man in Modellen, bei dem der Reaktions-Diffusions Teil ein Aktivator-Inhibitor System darstellt, wieder den Spiral-Defekt-Chaos genannten Zustand. Für dieses System wurde eine verallgemeinerte Swift-Hohenberg Gleichung formuliert. Anschließend wurde die Entwicklung von fraktalen Fronten, die sich aufgrund der starken Nichtlinearität an der Grenzschicht zwischen zwei chemischen Spezies bilden, numerisch untersucht. Motiviert durch die numerischen Ergebnisse, wurde eine Gleichung für die Propagation der Front in Abhängigkeit

von ihrer räumlichen Struktur zusammen mit einer mittlere Feld Gleichung für die Front analytisch abgeleitet.

Abstract

We studied the pattern formation in spatially extended systems by considering two canonical systems; one is the Rayleigh-Bénard system representing a hydrodynamic fluid and the other is a Reaction-Diffusion system representing a chemical system.

We began our investigation for the Rayleigh-Bénard system undergoing convective instability in hydrodynamic fluids. The evolution of spiral defect chaos is seen numerically within the framework of the generalized Swift-Hohenberg equations where the mean field plays the major role. The model equations consist of an order parameter equation for the temperature field coupled to an equation for the mean flow field. The nonlinearities which are retained in the dynamics of the mean flow lead to a two-dimensional Navier-Stokes equation coupled to a Swift-Hohenberg equation. In order to quantify the role of mean field, we quenched the mean field numerically and the temperature field was advanced in time where we showed that the spirals then lead to the bent rolls. This proved that the mean field is responsible for the spiral defect chaos.

The second part of the thesis comprises of the studies of spatio-temporal patterns in Advection-Reaction-Diffusion systems in which the chemical species interact with the hydrodynamic fluid. Due to the interplay between the two, we obtained the spiral defect chaos in the activator-inhibitor type model. We formulated the generalized Swift-Hohenberg type model for this system. Then the evolution of fractal boundaries due to the effect of the strong non-linearity at the interface of the two chemical species is studied numerically. Motivated by our numerical findings, we derived the equation for the evolution of front propagation due to the spatial variation of the front analytically together with the mean field equation for the front.

Contents

1 Introduction

1.1 Pattern Formation

Our Universe is made up of matter with amazing patterns. If one looks into the telescope then he could view thousands of colorful patterns spread all over the sky. Our Earth consists of oceans, mountains, atmosphere and is changing itself continuously by tectonic motion, atmospheric processes, oceanic currents. Since the birth of the universe, it is in a non-equilibrium state.

Pattern formation is a phenomenon observed in many fields of physics, chemistry, material science, as well as in biology. The study of the spontaneous evolution and appearance of such patterns has been in the focus of research in such fields since several decades. The patterns that we are concerned about are macroscopic spatio-temporal patterns. Similar patterns may appear in quite different systems on the macroscopic scale having different microscopic properties. The formation of such spatio-temporal patterns and the related breaking of spatial symmetries seen in our nature can be considered as the result of instabilities caused by nonlinear processes under non-equilibrium conditions.

The emerging patterns can be initiated by a flux of energy or matter, e.g. caused by the existence of externally imposed temperature variations as in convection, or by the through-flow of chemicals in an open flow reactor. In this perspective in 1952, the remarkable idea of Alan Turing [74] gave the most direct evidence that the interplay between diffusion and reaction may lead to the growth of a pattern. This idea was a surprise as diffusion was understood as a source of smoothing process, and, hence should tend to stabilize a systems. Later in the 1990's, experiments supported Turing's idea. Since then a wide range of research has been directed to investigate chemical pattern formation.

It has been nearly during the last thirty years that pattern formation has emerged as a new field of research. The aim is to understand the dynamics and the formation of spontaneous patterns which appear in non- equilibrium systems.

Understanding the phenomenon, especially in dissipative systems, is the main challenge in the field of nonlinear sciences and it is expected that new concepts resulting from this field will influence the development of other fields of research. Pattern formation is common to many other spatially extended nonlinear non-equilibrium systems in physics, chemistry, and biology [42], [55], [24]. Patterns observed in diverse systems are often strikingly similar, and their understanding in terms of general, unifying concepts has long been a main direction of research [42].

From the theoretical side, the main problems in the field of non-equilibrium pattern formation are

- to classify instabilities occurring in dissipative systems,
- to predict the selection of patterns,
- to assess the stability of spatio-temporal patterns.

Non-equilibrium systems are represented by nonlinear partial differential equations which are notoriously difficult to solve. However, close to instabilities bifurcation theory and the physical concept of order parameters and order parameter dynamics has been developed [42]. It has been stressed that the same mathematical structures are at the basis of pattern forming processes in quite different physical, chemical, and biological systems, irrespective of the nature of their microscopic constituents.

1.2 Outline of Thesis

The thesis is concerned with aspects of processes leading to spatially disordered patterns. One of the central issue are the states usually denoted as spiral defect chaos. Furthermore, we shall deal with instabilities of fronts in chemical advection-reaction-diffusion systems. The thesis is organised as follows:

- Chapter 2 concerns with the first model of our investigation, where an introduction to the Rayleigh-Bénard system is given. Then the concepts of order parameters and order parameter dynamics is introduced.
- Chapter 3 concerns with an example of complex spatiotemporal patterns namely, spiral defect chaos observed in Rayleigh-Bénard systems. We

investigate an order parameter equation, the generalized Swift-Hohenberg equation, coupled to the dynamics of a vortical fluid motion described by the mean field equation. We theoretically and numerically investigate the influence of quenching of the mean flow onto the dynamics

- In Chapter 4, our second system is introduced in terms of a reaction diffusion system in the form of an activator and inhibitor model. We include the effects due to advection of the chemical fields by fluid flows and formulate models for active fluids and an inter-facial reaction.
- In Chapter 5, the emerging patterns are discussed for our advection-diffusion-reaction system. It is shown that spiral defect chaos can also be observed in such systems. Furthermore, for different sets of control parameters, we find an instability of fronts leading to fractal like patterns.
- Chapter 6 deals with the fractal boundaries or fronts. Here we derive an evolution equation for the front and discuss the stability of planar fronts
- In Chapter 7, an introduction to the applied numerical techniques is provided.
- Chapter 8 closes the Thesis with a summary.

2 Pattern Formation in Rayleigh-Bénard Convection

In this chapter we give an introduction to Rayleigh-Bénard convection as a non-equilibrium system exhibiting a variety of spatio-temporal patterns. Furthermore, we introduce a simple model equation for this system. An extension of this simple model will be the starting point for our investigation of spatio-temporal chaos.

2.1 Rayleigh-Bénard Convection

Thermal convection is one of the most common processes observed in fluid systems. From the microscopic scale of nano devices till the macroscopic scale of the Earth and Stars, we observe similar phenomena. It has been shown that even the displacement of the tectonic plates in the earth's core, atmospheric motions etc. are the result of convective motions. It is well noted that the application of convection is not bounded only to natural phenomenon, but is highly important also for industrial applications.

Rayleigh-Bénard convection is one of the simplest and widely studied examples for pattern formation. A variety of spatio-temporal patterns is observed ranging from the simplest roll pattern, over chaotic patterns, complex spiral defect chaos up to highly turbulent convection. Its study started from the experiment of Bénard in 1900 [17], followed by later theoretically studies of Lord Rayleigh [66] in 1916. Although it has to be noted that Bénard observed the phenomenon where the instability arises due to surface tension effects commonly known as Bénard Marangoni effect, whereas Rayleigh studied the effects of instability where the variation of temperature and hence density of the fluid played a major role in driving the instability. According to A. Newell et al. [3], Rayleigh-Bénard convection is *the granddaddy of canonical examples used to study pattern formation and behavior in spatially extended systems.*

Let us briefly describe the arrangement of the convection experiment. It consists of a thin layer of fluid between two horizontal plates, heated from below, as shown in fig. (2.1). Let the temperature at the top be T_1 while that at the bottom be T_2. The fluid remains at rest as long as the dissipation forces balance the buoyancy force due to the gravitational gravity. In other words, heat is transported due to heat conduction only. When the temperature difference $\Delta T = T_2 - T_1$ increases to a critical value, the diffusive forces no longer counter-balance the buoyancy force and the fluid starts to convect. Lighter fluid close to the bottom starts to move towards the upper plate and heavier fluid from the top starts moving down.

2.1.1 Oberbeck-Boussinesq Approximation

The Rayleigh-Bénard system is generally considered on the basis of the Boussinesqian approximation, according to which only density is affected by the variation in temperature

$$\rho - \rho_0 = -\rho_0 \alpha (T - T_0) \tag{2.1}$$

ρ_0 is the density of the fluid at some mean temperature T_0. We consider that the thermal expansion coefficient α is small so that the characteristics of the fluid (kinematic diffusivity ν, thermal diffusivity χ and α itself) vary little within the horizontal layer of the fluid. Then the density of the fluid can be considered as constant everywhere except for the density variation in the buoyancy term. Furthermore, the fluid is assumed to be incompressible. This is usually denoted as Boussinesq description of convection.

The basic equations of motion are then the Navier-Stokes equation including the temperature dependent buoyancy term and the equation of heat conduction for the temperature field.

$$\begin{aligned}
\left(\frac{\partial}{\partial t} + \boldsymbol{U}(\boldsymbol{r},t)\cdot\boldsymbol{\nabla}\right)\boldsymbol{U}(\boldsymbol{r},t) &= -\nabla(\frac{p}{\rho_0}) + \nu\Delta U(\boldsymbol{r},t) + \boldsymbol{g}\frac{\rho}{\rho_0} \\
\left(\frac{\partial}{\partial t} + \boldsymbol{U}(\boldsymbol{r},t)\cdot\boldsymbol{\nabla}\right)T &= \kappa\Delta T \\
\boldsymbol{\nabla}\cdot\boldsymbol{U}(\boldsymbol{r},t) &= 0
\end{aligned} \tag{2.2}$$

Here, $\boldsymbol{U}$,T and P are velocity, temperature and pressure of the fluid and the other quantities like ρ, ν, g, α and κ are density, kinematic viscosity, gravity,

thermal expansion coefficient and thermal diffusivity respectively. The thickness of the layer is denoted by d.

These equations allow for a stationary state, where heat is transported purely by heat conduction, implying $\boldsymbol{u}(\boldsymbol{x},t)=0$, and

$$\frac{\partial^2}{\partial z^2}T_0(z) \tag{2.3}$$

The boundary conditions then lead to

$$T_z(0) = T_2 + z(T_1 - T_2)/d \tag{2.4}$$

In order to consider the convective state, one introduces deviations from the basic state according to

$$\begin{aligned} p &= p_0 + p \\ T &= T_0 + \theta \end{aligned} \tag{2.5}$$

The resulting equations for the deviations can be put into dimensionless form by scaling distance with d, the height of the fluid layer, time with the vertical diffusion time $t_\nu = \frac{d^2}{\kappa}$ and velocity with $\frac{d}{t_\nu}$:

$$\begin{aligned} \frac{1}{Pr}\left(\frac{\partial}{\partial t} + \boldsymbol{U}(\boldsymbol{r},t)\cdot\boldsymbol{\nabla}\right)\boldsymbol{U}(\boldsymbol{r},t) &= -\nabla P + \Delta\boldsymbol{U}(\boldsymbol{r},t) + \theta(\boldsymbol{r},t)e_z \\ \left(\frac{\partial}{\partial t} + \boldsymbol{U}(\boldsymbol{r},t)\cdot\boldsymbol{\nabla}\right)\theta(\boldsymbol{r},t) &= \Delta\theta(\boldsymbol{r},t) + Re_z\cdot\boldsymbol{U}(\boldsymbol{r},t) \\ \boldsymbol{\nabla}\cdot\boldsymbol{U}(\boldsymbol{r},t) &= 0 \end{aligned} \tag{2.6}$$

Temperature is measured in terms of the temperature difference $\Delta T = T_2 - T_1$. Here, two new quantities known as Rayleigh and Prandtl number arise

$$\begin{aligned} R &= \frac{\alpha g \Delta T d^3}{\kappa\nu} \\ Pr &= \frac{\nu}{\kappa} \end{aligned} \tag{2.7}$$

These two quantities play a major role in the dynamics of the system. The Rayleigh number R defines the competition between the buoyancy and the

dissipative forced. Convection only occurs when the buoyancy overcomes the dissipative forces. Thus, we expect that there is a critical Rayleigh number. When the Rayleigh number is increased to a critical value R_c, convection starts and roll pattern of a certain wavelength appear. For the rigid boundaries, which is the realistic case for experimental conditions, the value of the critical Rayleigh number is $R_c \approx 1706$ and the wave vector of rolls at onset is $k_c \approx 3.116$. The Prandtl number Pr is the ratio between kinematic viscosity to thermal diffusivity or can be expressed alternatively as ratio of vertical thermal diffusive timescale to the vertical velocity diffusive time scale.

2.1.2 Large Prandtl numbers

A simplification arises for the case of infinite Prandtl number since then the inertial terms in the Navier-Stokes equation can be neglected:

$$0 = -\nabla P + \Delta U(\boldsymbol{r}, t) + R\mathbf{e}_z\theta(\boldsymbol{r}, t) \tag{2.8}$$

Making the ansatz

$$U(\boldsymbol{r}, t) = \nabla \times \nabla \times e_z S(\boldsymbol{r}, t) \tag{2.9}$$

we can eliminate the velocity field in terms of the temperature field

$$S = R\Delta^{(-2)}\Delta^2\theta(\boldsymbol{r}, t) \tag{2.10}$$

Here $\Delta^2 = \frac{\partial^2}{\partial x^2} + \frac{\partial^2}{\partial y^2}$ denotes the Laplacian in the horizontal plane. $\Delta^{(-1)}$ denotes the inverse Laplacian. For the following we shall use the coordinates $\boldsymbol{r} = [\boldsymbol{x}, z] = [x, y, z]$.

Eliminating S using the eq. (2.8), we can reduce the basic equations eq. (2.6) to an evolution equation for the field $\theta(\boldsymbol{x}, z, t)$:

$$\left(\frac{\partial}{\partial t} + R(\nabla \times \nabla \times e_z\Delta\theta(\boldsymbol{x}, t)\right) \cdot \nabla\theta(\boldsymbol{x}, t) = \Delta\theta(\boldsymbol{x}, t) - R\Delta^2\Delta^{-2}\theta(\boldsymbol{x}, t) \tag{2.11}$$

For the following, we shall rewrite this evolution equation in the form, introducing the linear part and the nonlinear part [18]:

$$\partial_t\theta(\boldsymbol{x}, z, t) = L\theta(\boldsymbol{x}, z, t) + \Gamma : \theta(\boldsymbol{x}, z, t) : \theta(\boldsymbol{x}, z, t) \tag{2.12}$$

The linear operator L is defined according to

$$L\Delta\theta(\boldsymbol{x},t) - R\Delta^2\Delta^{-2}\theta(\boldsymbol{x},t) \tag{2.13}$$

and the definition of the nonlinear term is obtained from a comparison of eqs. (2.12) with (2.11).

The basic state is given by the solution $\theta = 0$.

2.2 Two-Dimensional Model

The theoretical treatment of the complicated periodic structures, already for the case of high Prandtl numbers, eq. (2.11) for three dimensional flows is rather involved.

Therefore, a model equation has been formulated, based on the observation that the behavior in vertical direction is relatively simple close to onset of convection. The reason is that for many parameter ranges the vertical dependence has a standard form [39].

The most simplest and widely used model equation for studying pattern formation in Rayleigh-Bénard systems in so-called large aspect ratio systems is the well known Swift-Hohenberg (SH) equation. It was originally introduced for studying the noise induced fluctuation very close to threshold ($\epsilon \ll 1$) [72]. This equation is useful for studying the Rayleigh-Bénard convection at ($\epsilon \approx O(1)$) [61]. Since convection creates quasi two-dimensional patterns in a wide range of parameters, the two-dimensional model seems a natural choice for studying the convection as they are known to capture the essential features of the dynamics involved in such systems. It takes the form

$$\partial_t\psi(\boldsymbol{x},t) = \epsilon\psi(\boldsymbol{x},t) - (k_c^2 + \nabla^2)^2\psi(\boldsymbol{x},t) - \psi^3(\boldsymbol{x},t) \tag{2.14}$$

where ψ models the temperature field in the mid plane of the layer. It is a real function, ∇ is the gradient in two-dimensions. The quantity k_c is related to the wavelength $\lambda = 2\pi/k_c$ of the emerging patterns.

In the next section, we shall briefly discuss how the application of this equation to the description of pattern formation can be justified.

2.3 Pattern Formation and The Order Parameter Concept

In this section, we outline the basic treatment of instabilities in non-equilibrium systems close to instabilities. It has turned out that close to instability systems of quite different nature like fluids, liquid crystals, binary fluids, lasers, to name just a few, can be described by the same type of equations. This approach is denoted as the order parameter concept [42]. It is an extension of the Ginzburg-Landau theory [49] to non-equilibrium systems.

The order parameter equations for non-equilibrium systems can be derived from the basic equations governing the behavior of the system under consideration close to instability. However, they may, like the Ginzburg-Landau theory, also be stated using symmetry arguments.

2.4 Derivation of the Order Parameter Equation

In this section we briefly review the derivation of rotationally invariant order parameter equations, following closely the treatment of Bestehorn and Friedrich [18]. We formulate the basic equation in the form (2.12)

$$\partial_t \theta(\boldsymbol{x}, z, t) = L\theta(\boldsymbol{x}, z, t) + \Gamma : \theta(\boldsymbol{x}, z, t) : \theta(\boldsymbol{x}, z, t) \tag{2.15}$$

The generalization to more complex situations is given in [18].

2.4.1 Linear Stability Analysis

The first step consists of the linear stability analysis neglecting the nonlinear term. A linear equation always can be solved by an exponential ansatz

$$\theta(\boldsymbol{x}, z, t) = \exp(\lambda_n(\boldsymbol{k}t))\theta_{n\boldsymbol{k}}(\boldsymbol{x}, z) \tag{2.16}$$

with the modes

$$\theta_{n\boldsymbol{k}}(\boldsymbol{x}, z) = \theta_n(\boldsymbol{k}, z)\exp(\mathrm{i}\boldsymbol{k}\cdot\boldsymbol{x}) \tag{2.17}$$

Here, we have taken into account that in the horizontal directions, we have periodic boundary conditions. n denotes a discrete index distinguishing the modes with respect to their behavior in z-direction, $\boldsymbol{k}$ is the wave vector for the

plane wave ansatz in horizontal directions. The modes are defined as eigenmodes of the linear operator with eigenvalue $\lambda_n(\boldsymbol{k})$:

$$\lambda_n \theta_n(\boldsymbol{k}, z) \exp(\mathrm{i}\boldsymbol{k} \cdot \boldsymbol{x}) = L(\boldsymbol{\nabla}, \epsilon)\theta_n(\boldsymbol{k}, z) \exp(\mathrm{i}\boldsymbol{k} \cdot \boldsymbol{x}) \tag{2.18}$$

For simplicity, we shall assume that the linear operator is self-adjoint. Then we have real eigenvalues and the set of modes form a complete basis of a Hilbert space with the scalar product Now here we define the scalar product for separable Hilbert space,

$$\langle u|v\rangle = \int_0^1 lz \int d^2\boldsymbol{x} u(\boldsymbol{x}, z)^* v(\boldsymbol{x}, z) \tag{2.19}$$

We have assumed the modes to be normalized

$$\langle \theta_{n\boldsymbol{k}} | \theta_{m\boldsymbol{k}'} \rangle = \delta_{nm}\delta_{\boldsymbol{k}\boldsymbol{k}'} \tag{2.20}$$

Let us explicitly consider the calculations for Rayleigh-Bénard convection at large Prandtl number. The linear operator is just given by

$$L = \Delta - R\Delta^{-2}\Delta_2 \tag{2.21}$$

The ansatz for the modes is

$$\theta_n(\boldsymbol{k}, z) \exp(\mathrm{i}\boldsymbol{k} \cdot \boldsymbol{x}) = N sin(n\pi z) \exp(\mathrm{i}\boldsymbol{k} \cdot \boldsymbol{x}) \qquad n = 1, ... \tag{2.22}$$

This ansatz obeys the boundary conditions $\theta_n(\boldsymbol{k}, z) \exp(\mathrm{i}\boldsymbol{k} \cdot \boldsymbol{x}) = 0$ for $z = 0$, $z = 1$, i.e. the deviation from the linear temperature profile vanishes at the top and bottom boundary of the fluid. The eigenvalues are then obtained using the identities

$$\begin{aligned} \Delta\theta_n(\boldsymbol{k}, z) \exp(\mathrm{i}\boldsymbol{k} \cdot \boldsymbol{x}) &= -(\pi^2 n^2 + \boldsymbol{k}^2)\theta_n(\boldsymbol{k}, z) \exp(\mathrm{i}\boldsymbol{k} \cdot \boldsymbol{x}) \\ \Delta^2\theta_n(\boldsymbol{k}, z) \exp(\mathrm{i}\boldsymbol{k} \cdot \boldsymbol{x}) &= -\boldsymbol{k}^2\theta_n(\boldsymbol{k}, z) \exp(\mathrm{i}\boldsymbol{k} \cdot \boldsymbol{x}) \end{aligned} \tag{2.23}$$

They are explicitly given by

$$\lambda_n(k) = -(\pi^2 n^2 + k^2) + R\frac{k^2}{(\pi^2 n^2 + k^2)^2} \tag{2.24}$$

The largest eigenvalues belong to the band of modes with $n = 1$. An instability arises when $\lambda_1(k)$ becomes positive for a certain Rayleigh number R. This happens for a critical wave number denotes as k_c. the conditions are

$$\begin{aligned} \lambda_1(k) &= 0 \\ \frac{\partial}{\partial k}\lambda_1(k) &= 0 \end{aligned} \tag{2.25}$$

The result is $R_c = \frac{27\pi^4}{4}$, $k_c = \frac{\pi}{\sqrt{2}}$. The modes with $n = 2, ...$ are strongly damped.

2.4.2 Amplitude Equations

In the next step we expand the state vector into the complete set of modes

$$\theta(\boldsymbol{x}, t) = \sum_n \sum_{\boldsymbol{k}} A_n(\boldsymbol{k}, t)\theta_n(\boldsymbol{k}, z)\exp(\mathrm{i}\boldsymbol{k}\cdot x) = \sum_n \sum_{\mathbf{k}} A_n(\boldsymbol{k}, t)\theta_{n\boldsymbol{k}}(\boldsymbol{x}, z) \tag{2.26}$$

Inserting this ansatz in the eq. (2.12), and, subsequently forming the scalar product with the mode $\theta_{m\boldsymbol{k}}(\boldsymbol{x}, z)$ we end up with the following set of infinite ordinary differential equations.

$$\begin{aligned} \dot{A}_n(\boldsymbol{k}, t) = \lambda_n A_n(\boldsymbol{k}, t) + \sum_{n',n''} \sum_{\boldsymbol{k}',\boldsymbol{k}''} \delta_{\boldsymbol{k},k'+k''} \\ \times\Gamma_{n;n',n''}(\boldsymbol{k};\boldsymbol{k}',\boldsymbol{k}'')A_{n'}(\boldsymbol{k}', t)A_{n''}(\boldsymbol{k}'', t) \end{aligned} \tag{2.27}$$

where $A_n(\boldsymbol{k}, t)$ denotes the amplitudes of the full modes. The linear part of this equation is diagonal as we can see from eq. (2.18). The matrix element Γ in above eq. (2.27) is defined according to

$$\Gamma_{n;n',n''}(\boldsymbol{k};\boldsymbol{k}',\boldsymbol{k}'') = \langle\theta^*_{n,k}(\boldsymbol{x}, z)|\Gamma : \theta_{n',k'}(\boldsymbol{x}, z) : \theta_{n'',k''}(\boldsymbol{x}, z) : \theta_{n''',k'''}(\boldsymbol{x}, z) \tag{2.28}$$

It can be explicitly calculated.

2.4.3 Elimination of Stable Modes

A situation, which is common e.g. for the Rayleigh-Bénard instability and for many other systems, is the fact that close to instability modes from a single band, say the modes with index n=1, get positive real parts, whereas the modes of the

remaining bands ($n = 2, ..$) are strongly damped. Therefore we divide the modes into two parts

$$\lambda_n(\boldsymbol{k}): \qquad \lambda_u(\boldsymbol{k}) \qquad , \qquad \lambda_s(\boldsymbol{k}) \tag{2.29}$$

where the index $u = 1$, and s takes the values $s = 2, 3...$ A_s denotes the stable and A_u the unstable amplitudes.

The evolution equation for the modes of the unstable band takes the form

$$\begin{aligned} \dot{A}_s(\boldsymbol{k},t) &= \lambda_s(\boldsymbol{k})A_s(\boldsymbol{k},t) \\ &+ \sum_{\boldsymbol{k}',\boldsymbol{k}''} \Gamma_{s;uu}(\boldsymbol{k};\boldsymbol{k}',\boldsymbol{k}'')A_u(\boldsymbol{k}',t)A_u(\boldsymbol{k}'',t) + O(A_uA_s) \end{aligned} \tag{2.30}$$

The sums always involve the summation such that $\boldsymbol{k} = \boldsymbol{k}' + \boldsymbol{k}''$.

Since the amplitudes $A_s(\boldsymbol{k},t)$ of the stable modes are strongly damped we are allowed to eliminate them adiabatically [43]. To lowest order in $A_u(\boldsymbol{k},t)$ we obtain

$$A_s(\boldsymbol{k},t) = \frac{1}{-\lambda_s(\boldsymbol{k})} \sum_{\boldsymbol{k}',\boldsymbol{k}''} \Gamma_{s;u,u}(\boldsymbol{k};\boldsymbol{k}',\boldsymbol{k}'')A_u(\boldsymbol{k}',t)A_u(\boldsymbol{k}'',t) \tag{2.31}$$

The evolution equation for the modes of the unstable band takes the form

$$\begin{aligned} \dot{A}_u(\boldsymbol{k},t) &= \lambda_u(\boldsymbol{k})A_u(\boldsymbol{k},t) \\ &+ \sum_{s} \sum_{\boldsymbol{k}',\boldsymbol{k}''} \Gamma_{u;us}(\boldsymbol{k};\boldsymbol{k}',\boldsymbol{k}'')A_u(\boldsymbol{k}',t)A_s(\boldsymbol{k}'',t) \\ &+ \sum_{s} \sum_{\mathbf{s}',\boldsymbol{k}''} \Gamma_{u;su}(\boldsymbol{k};\boldsymbol{k}',\boldsymbol{k}'')A_u(\boldsymbol{k}',t)A_s(\boldsymbol{k}'',t) + O(A_s^2) \end{aligned} \tag{2.32}$$

Now using the adiabatic approximation [43] and inserting the stable modes into unstable mode , we get the final order parameter equation as

$$\begin{aligned} \dot{A}_u(\boldsymbol{k},t) &= \lambda_u A_u(\boldsymbol{k},t) \\ &+ \sum_{(\boldsymbol{k}',\boldsymbol{k}'',\boldsymbol{k}''')} \delta_{\boldsymbol{k},k'+k''+k'''} \times \Gamma^3(\boldsymbol{k};\boldsymbol{k}',\boldsymbol{k}'',\boldsymbol{k}''')A_u(\boldsymbol{k}',t)A_u(\boldsymbol{k}'',t)A_u(\boldsymbol{k}''',t) \end{aligned}$$

Thereby, we have defined the third order mode coupling term

$$\Gamma^3(\boldsymbol{k};\boldsymbol{k}',\boldsymbol{k}'',\boldsymbol{k}''') = \Gamma_{u;us}(\boldsymbol{k};\boldsymbol{k}',\boldsymbol{k}_s) + \Gamma_{u;su}(\boldsymbol{k};\boldsymbol{k}_s,\boldsymbol{k}')\frac{1}{\lambda_s(\boldsymbol{k}_s)}\Gamma_{s;uu}(\boldsymbol{k}_s;\boldsymbol{k}'',\boldsymbol{k}''') \tag{2.33}$$

Again, the sum is restricted to $\boldsymbol{k}_s = \boldsymbol{k}'' + \boldsymbol{k}'''$, $\boldsymbol{k} = \boldsymbol{k}' + \boldsymbol{k}_s$ Due to the adiabatic elimination of the stable modes we arrived at an evolution equation for the amplitudes of modes of the unstable band. The mode coupling terms (2.33) can be explicitly calculated.

2.4.4 Order Parameter Equation in Real Space

The last step in deriving the order parameter equation consists in converting back to real space. To this end we define the order parameter field

$$\psi(\boldsymbol{x},t) = \frac{1}{L_0}\sum_{\boldsymbol{k}} \exp(\mathrm{i}\boldsymbol{k}\cdot\boldsymbol{x})A_u(\boldsymbol{k},t) \tag{2.34}$$

(L_0 denotes the length of the domain in the two dimensional plane) and we obtain an equation of the form

$$\frac{\partial}{\partial t}\psi(\boldsymbol{x},t) = L(-\mathrm{i}\nabla)\psi(\boldsymbol{x},t) + N[\psi(\boldsymbol{x},t)] \tag{2.35}$$

The nonlinear term $N[\psi(\boldsymbol{x},t)]$ in general is a nonlocal functional of the order parameter field.

Swift-Hohenberg Equation

As we have discussed above, Rayleigh-Bénard convection close to onset can be modeled by the Swift-Hohenberg equation. It can be obtained from the order parameter equation by a suitable approximation of the nonlinearity. In general, the third order nonlinear term is nonlocal.

However, frequently it can be approximated by a local term. The simplest approximation consists in assuming $\Gamma(\boldsymbol{k};\boldsymbol{k}',\boldsymbol{k}'',\boldsymbol{k}''')$ to be constant:

$$\Gamma(\boldsymbol{k};\boldsymbol{k}',\boldsymbol{k}'',\boldsymbol{k}''') \approx -\gamma \tag{2.36}$$

Then the order parameter equation takes the form

$$\frac{\partial}{\partial t}\psi(\boldsymbol{x},t) = L(-\mathrm{i}\nabla)\psi(\boldsymbol{x},t) - \gamma\psi(\boldsymbol{x},t)^3 \tag{2.37}$$

We can also make a further approximation. Since we assume that modes with wavenumber close to a critical one, denoted by k_c will be excited close to instability we can approximate the eigenvalues $\lambda(k)$ by

$$\lambda(k) = \epsilon - (k_c^2 - k^2)^2 \tag{2.38}$$

The final result is the Swift-Hohenberg equation

$$\frac{\partial}{\partial t}\psi(\boldsymbol{x},t) = [\epsilon - (k_c^2 + \Delta)^2]\psi(\boldsymbol{x},t) - \psi(\boldsymbol{x},t)^3 \tag{2.39}$$

It is obvious that Swift-Hohenberg equations can be derived not only for Rayleigh-Bénard systems.

2.4.5 Stability Analysis

Now let us consider Swift-Hohenberg equation, setting for our convenience $k_c = 1$. Let $\psi = 0$ be the base solution of the equation. We now consider small perturbations $\delta\psi$ such that we can neglect the nonlinearity.

$$\partial_t\delta\psi = \epsilon\delta\psi - (1 + 2\Delta^2 + \Delta^4)\delta\psi \tag{2.40}$$

We solve this equation by the ansatz

$$\delta\psi(\boldsymbol{x},t) = \hat{\psi}\exp(\mathrm{i}\boldsymbol{k}\cdot\boldsymbol{x})\exp(\lambda(k)t) \tag{2.41}$$

where k denotes the wave vector. The growth rate of the modes is then given by

$$\lambda = \epsilon - (k^2 - k_c^2)^2$$

Hence we can solve the system for each k. In order to determine k we need to specify the boundary condition. Let us consider that the system is periodic in

space so for the lateral length of L we can write the boundary condition as

$$\delta\psi_k(x+L,t) = \delta\psi_k(x,t) \tag{2.42}$$

For our model equation, maximum growth rate is $\lambda = \epsilon$ occurs at $k = k_c = 1$. If $\epsilon < 0$, the base solution is stable and all eigenvalues are negative while for $\epsilon > 0$, the base state is unstable. The solution of the model equation can be expressed as a linear superposition of the modes. All those modes with $\lambda_k < 0$ will decay and the pattern will contain the modes for which $\lambda_k > 0$, growing exponentially. The nonlinear term in the Swift-Hohenberg equation will lead to a saturation of the linear growth, and, as it turns out, to a selection of roll patterns.

It is very important to note here that the Swift-Hohenberg model is a so-called potential system. It can be rewritten in the form

$$\frac{\partial}{\partial t}\psi(\boldsymbol{x},t) = -\frac{\delta}{\delta\psi(\boldsymbol{x},t)}V[\psi] \tag{2.43}$$

Here, $\frac{\delta}{\delta\psi(\boldsymbol{x},t)}$ denotes the variational derivative. The potential reads

$$V = \int[-\frac{1}{2}\epsilon\psi^2 + \frac{1}{4}\psi^4 + \frac{1}{2}[(\nabla^2+1)\psi]^2] \tag{2.44}$$

This functional V is called a Lyapunov functional. This means that the system evolves in time until it reaches a stationary state, which corresponds to a minimum of the potential V.

2.5 Summary

In this chapter we give an introduction to Rayleigh-Bénard Convection as a paradigm for pattern formation. We listed the basic fluid dynamical equations and formulated the Swift-Hohenberg equation as a model equation for the description of patterns in large aspect ratio systems.

Next we have introduced the order parameter concept which applies to instabilities in non-equilibrium systems. Furthermore, we have shown how the order parameter field can be defined, and we have discussed how one can derive suitable evolution equations from the basic equations under consideration. We

have indicated, that the Swift-Hohenberg equation is an approximation to the order parameter equation.

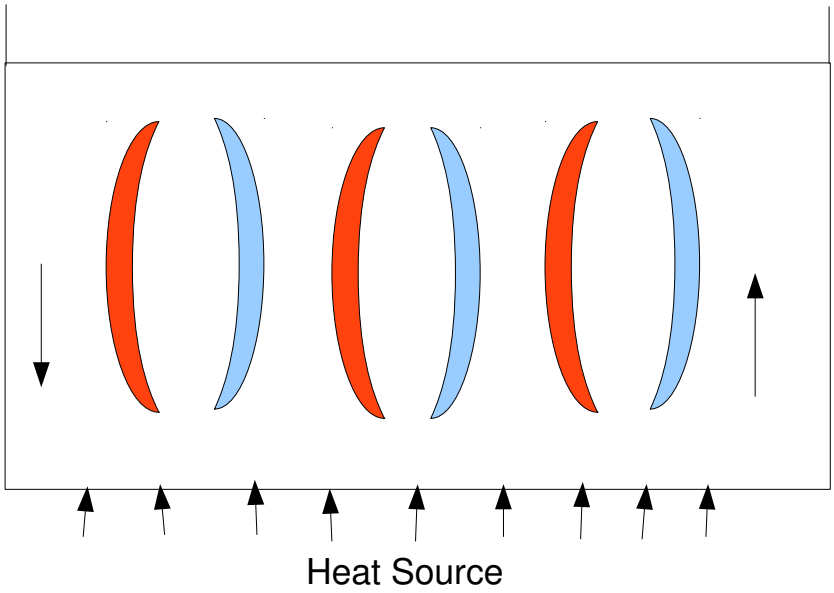

Figure 2.1 Schematic representation of Rayleigh-Bénard convection, where red colored warm fluid moves up and blue colored cold fluid sinks down.

3 Spiral Defect Chaos

A system which exhibits irregular behavior in time is denoted to be chaotic. Chaos is mainly concerned with disordered behavior which is sensitive to initial conditions. Examples of chaotic systems are rather diverse, and range from weather, turbulence, chemical reactions to heart fibrillation.

Spatio-temporal chaos means that in addition to chaotic evolution in time spatial structures are involved due to the interactions among different spatial locations. There is no clear definition of this notion, but it is applied to pattern forming systems which exhibits disordered patterns, where also defects are involved. Although experimentally spatio-temporal chaos has been observed its analysis is yet very difficult [25].

Hence to study some of the characteristics of spatio-temporal chaos we shall explore a model system with the help of numerical simulation. Our first example is related to Rayleigh-Bénard convection since this system has played an important and historical role in understanding complex behavior by the connection between experiments and theory [8, 69]. Rayleigh-Bénard experiment is not only a paradigm of a non-equilibrium system but exhibits also more exotic behaviors like chaos. It has played a major role in the understanding of routes to chaos for states, where only a few active modes determine the spatio-temporal dynamics.

A prominent example of spatio-temporal chaos in Rayleigh-Bénard system is so-called spiral defect chaos, which is observed in large aspect ratio systems and low Prandtl number flows. The accidental discovery of spiral defect chaos in low Prandtl number Rayleigh-Bénard convection experiments [68] motivated a number of experimental as well as theoretical studies.

3.1 Importance of Mean Flow

The result of experimental as well as theoretical work has shown that an important ingredient of spiral defect chaos is the so-called mean flow, which sets in in large

aspect ratio systems, in addition to the cellular flow generated by convection. For small Prandtl number there is a coupling of this mean flow to the cellular motion.

Since then it has been argued that mean flow is responsible for the production of spirals which is a non-relaxational effect in the dynamics of convection rolls. Since the mean flow must be divergence free due to incompressibility, it takes the form of a stirring motion, and may be completely described in terms of a vertical vorticity [23].

The spiral defect chaos state is observed in convection when the strength of the mean flow becomes larger and, as is apparent from experiments, enforcing a bending of convective rolls eventually leading to spiral dynamics. It is interesting to notice that in the experiments [13, 14] the spiral defect patterns turned into target patterns when the Prandtl number Pr was increased from $Pr = 1$ to $Pr = 10$. The parameters for which spiral defect chaos was observed are the Rayleigh number $R \geq 3000$, Prandtl number $Pr \approx 1.0$ and aspect ratio $\Gamma \geq 20$ [31, 52]. The mean flow is driven by the distortion of the patterns or the curvature of roll patterns. This suggests to extend the Swift-Hohenberg equation for the order parameter field $\psi(\boldsymbol{x}, t)$ by an inclusion of a transport due to a mean flow.

3.2 Swift-Hohenberg Equation and Mean Flow

Now we describe the modification of the order parameter equation in order to include the pattern forming processes related with spiral defect chaos. This has been done first by Manneville [55]. Subsequently, it has been established that the dynamics of the behavior of this modified model is qualitatively similar to that of experiments [41]. Experimentally, Bodenschatz et al. [30] observed in a cylindrical large aspect ratio system, the transitions between hexagonal structures and n-armed spirals formed by convective rolls. Croquette et al. [77] experimentally studied the side wall forcing and observed the nucleation of defects in the form of spirals. When the temperature gradient is increased, hexagons are formed due to non Boussinesqian effects [20]. When the temperature gradient is far beyond the critical temperature, hexagons become unstable and the mean flow bends the rolls and creates n-spirals or targets.

The modification of the order parameter equation by the inclusion of the mean

flow leads to the following set of equations

$$\partial_t \psi(\boldsymbol{x},t) + \boldsymbol{U}(\boldsymbol{x},t)\cdot\nabla\psi(\boldsymbol{x},t) = \left(\epsilon - (1+\Delta)^2 - \psi(\boldsymbol{x},t)^2\right)\psi(\boldsymbol{x},t) \tag{3.1}$$

Here, ∇ is a two dimensional gradient. $\boldsymbol{U}$ represents the mean flow which is the two dimensional velocity field and can be expressed in terms of the stream function ϕ

$$\mathbf{U} = \nabla \times \boldsymbol{e}_z\phi(\boldsymbol{x},t) = \begin{pmatrix} \partial_y\phi(\boldsymbol{x},t) \\ -\partial_x\phi(\boldsymbol{x},t) \end{pmatrix} \tag{3.2}$$

Since the mean flow is driven by the curvature or distortion of rolls we can come up with the following equation for the stream function $\chi(\boldsymbol{x},t)$:

$$[\partial_t + \mathbf{U}\cdot\nabla - Pr(-c^2+\Delta)]\Delta\phi = g\,(\nabla\psi\times\nabla\Delta\psi) \tag{3.3}$$

U is the mean velocity defined by a stream function given by above eq. (3.2). Pr is Prandtl number defined as earlier. g is a constant which describes the strength of the mean field and is believed to be inversely proportional to the Prandtl number of the fluid [26]. Hence for larger Prandtl numbers, the mean flow can be neglected. The left hand side of eq. (3.3) is the two-dimensional Navier-Stokes equation, formulated for the stream function. The constant c^2 takes into account a possible damping to to a slight vertical dependence of the mean flow profile.

The model equations (3.1), (3.2) have been investigated by many authors. Bestehorn et al. [53] included the non Boussinesqian effects and found targets and spirals. It is to be noted that in the present work, we have extended the model by taking into account the advection term, which renders the mean field equation nonlinear with respect to the stream function itself.

In fig. (3.1) and fig. (3.2) we show the evolution of spiral defect chaos at different time steps where $g = 100$, $Pr = 1.0$, $c^2 = 12$, $\epsilon = 0.7$. The time step for integration has been taken to be $dt = 0.001$ and the grid point resolution is 256×256. The physical length of the system is chosen as 100.

3.2.1 Quasi Patterns

Whereas spiral defect chaos emerges from random initial conditions, we have been able to calculate spatially regular patterns, starting from certain well-defined

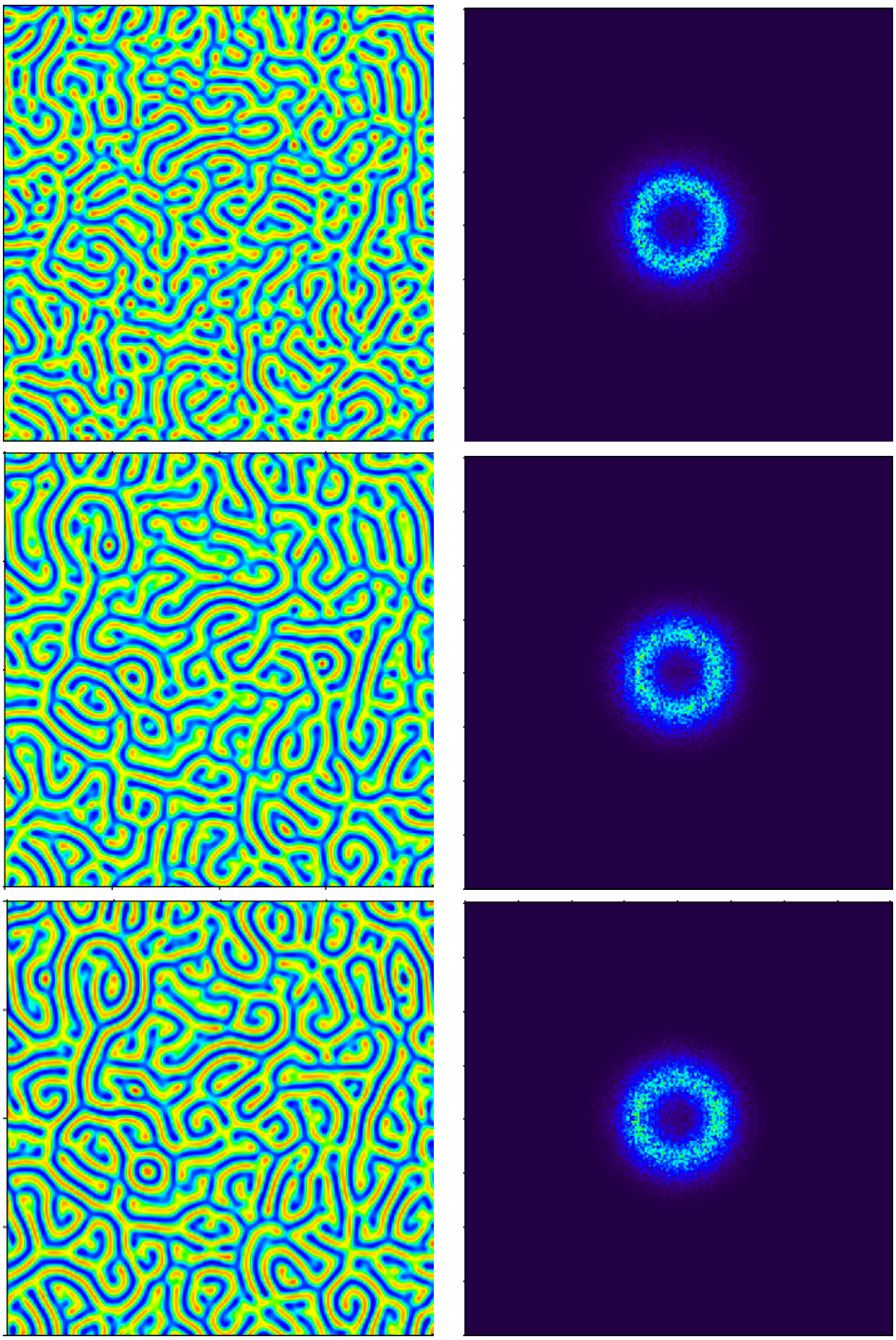

Figure 3.1 Evolution of spiral defect chaos starting from random initial conditions: Order parameter field is shown in left column while Fourier transformed field on the right $g = 100$, $Pr = 1.0$, $c^2 = 12$, $\epsilon = 0.7$,$dt = 0.001$,$resolution = 256 \times 256$, system length=100.

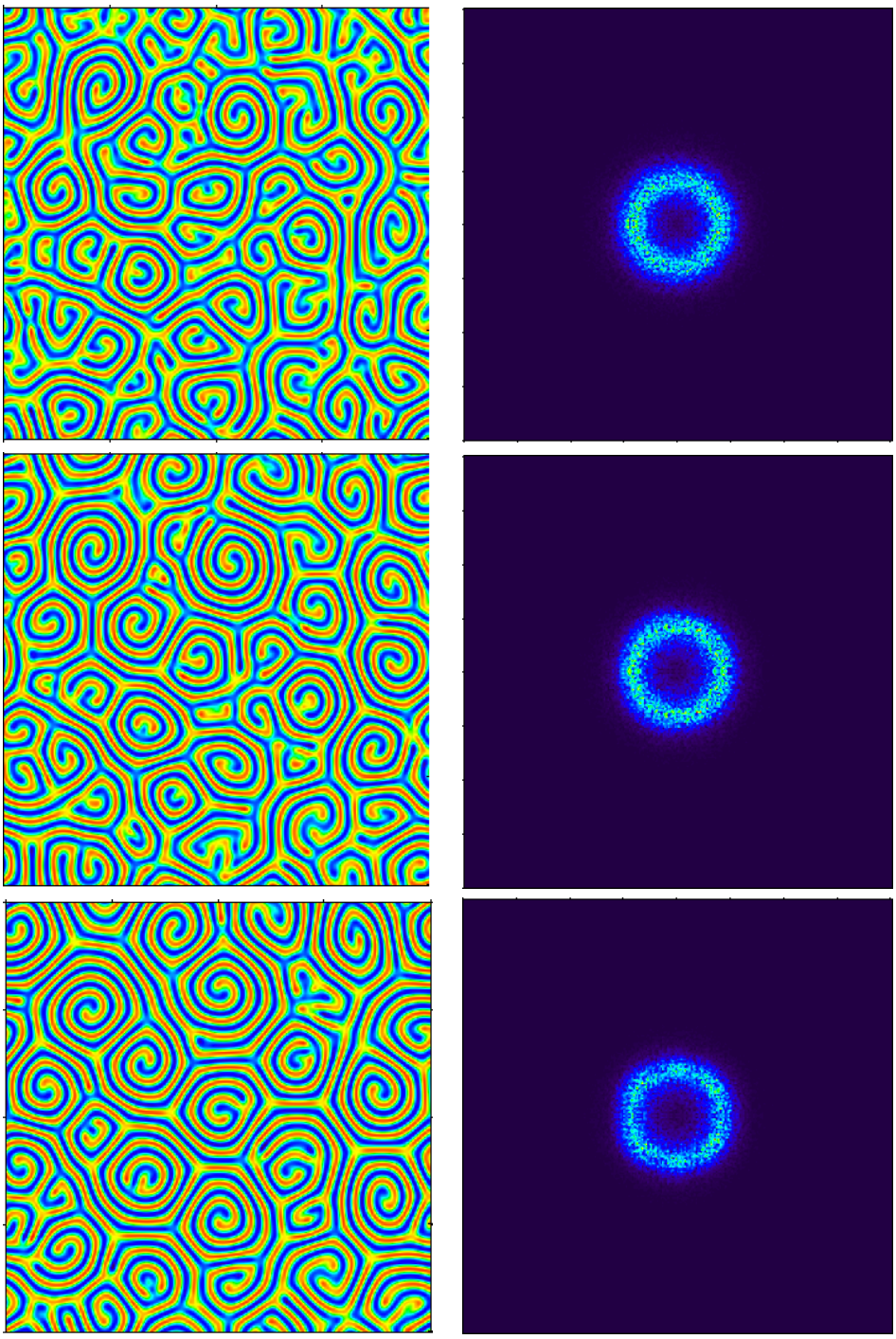

Figure 3.2 Continuation of fig. (3.1): Order parameter field is shown where in left column while Fourier transformed field on the right $g = 100$, $Pr = 1.0$, $c^2 = 12$, $\epsilon = 0.7$,$dt = 0.001$, $resolution = 256 \times 256$, system length=100.

initial conditions. The regular patterns are named quasi-patterns because they are similar to quasi crystals of solid state physics.

Quasi crystal like patterns in non-equilibrium patterns were first found in Faraday's experiments [16], where oscillations are generated on the surface of the fluid by a periodic motion of the fluid layer in the gravitational field. These quasi-patterns are also found in other systems like nonlinear optics [64], liquid crystals [65] and the wave experiments of Faraday [19, 6, 12].

In a recent theoretical article, Iooss and Rucklidge [44] investigated the quasi patterns in the framework of the Swift Hohenberg model and proposed that these quasi patterns are approximate steady solutions of this equation. We obtained these kinds of patterns by using our modified model, eq. (3.1) and eq. (3.3) including the mean field dynamics. It is interesting to see that such non-potential systems also exhibits stationary quasi patterns. We numerically obtained these patterns by appropriately placing fragments of spirals and target patterns as initial conditions as can be seen in figs. (3.3), (3.4), (3.5), (3.6)

3.3 Quenching the Mean Flow

As mentioned above mean flow plays an important role in developing the spatio-temporal chaos in systems like Rayleigh-Bénard convection [4, 69, 7] at low Prandtl numbers. However, the specific reason for the onset of these spatio-temporal chaotic states is not yet clear. Insight into the pattern forming process could be expected by a separation of the dynamics of the order parameter field $\psi(\boldsymbol{x}, t)$ and the mean field $\boldsymbol{U}(\boldsymbol{x}, t)$. This leads us to the idea of quenching: We freeze the mean field after some considerable time when the spiral defect chaos has invaded all over the system, and then study the behavior of the order parameter by comparing its behavior before and after quenching. We also mention that Chiam et al. [45] have analyzed numerically this behavior of quenching of mean flow using the full Navier Stokes model, whereas we investigate the generalized Swift-Hohenberg equation with squeezed mean flow. This will allow us to perform some analytical conclusions.

To develop the understanding of the procedure, we proceed as follows. From

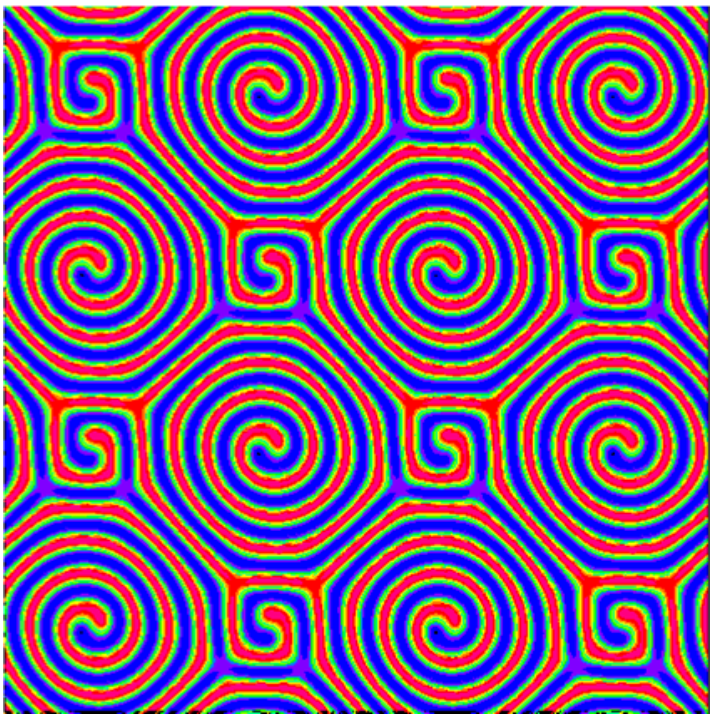

Figure 3.3 Order parameter field at final time step where spiral fragments initially have been placed at different positions and iterated for longer time, while the parameters are the same as in fig. (3.1)

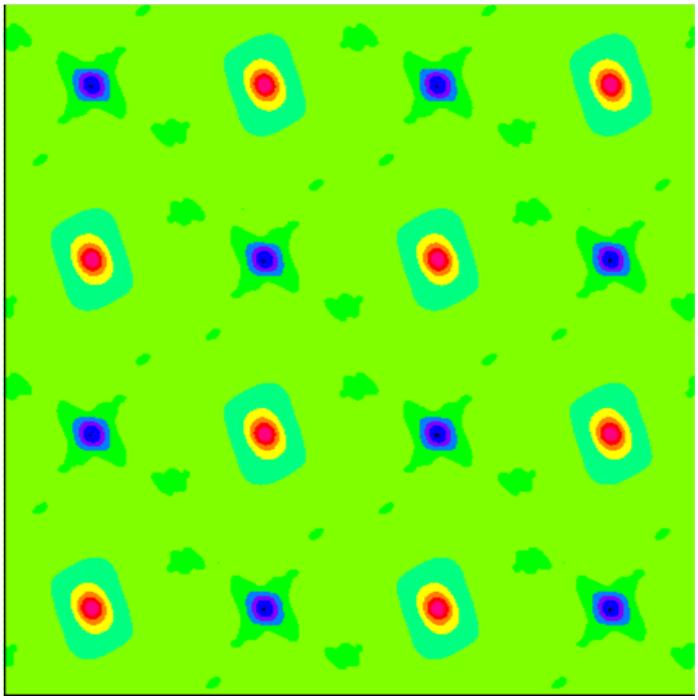

Figure 3.4 Mean Field at final time step corresponding to fig. (3.3).

the definition given above eq. (3.2)

$$\mathbf{U} = -\left[\boldsymbol{e}_z \times \nabla\phi\right]$$

the stream function $\phi(\boldsymbol{x})$ and, correspondingly, the velocity field becomes stationary after quenching.

It is expected that the order parameter field then also has the tendency to become stationary. This becomes possible if the advection term

$$\boldsymbol{U} \cdot \nabla\psi = -\left[\boldsymbol{e}_z \times \nabla\phi\right] \cdot \nabla\psi \tag{3.4}$$

vanishes, since then order parameter field relaxes to a stripe like pattern, due to the variational feature of the order parameter dynamics.

This observation prompts us to make the ansatz, that the order parameter field is a function of the stream function ϕ, i.e. the spatial dependence is prescribed by the stream function, $\phi = \phi(\boldsymbol{x})$. We calculate the gradient of the order parameter

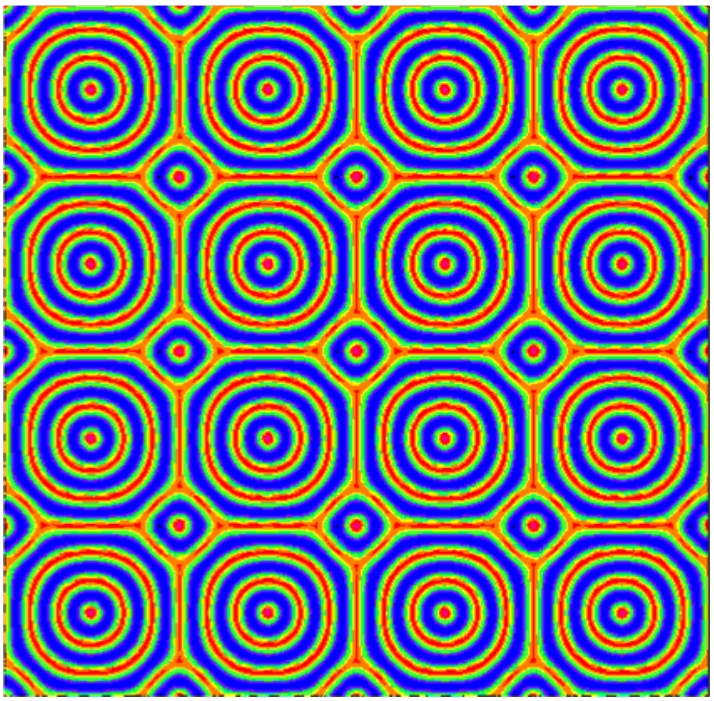

Figure 3.5 Order parameter field at final time step where fragments of targets are placed have been initially placed at different positions and iterated for longer time, while the parameters are the same as in fig. (3.1)

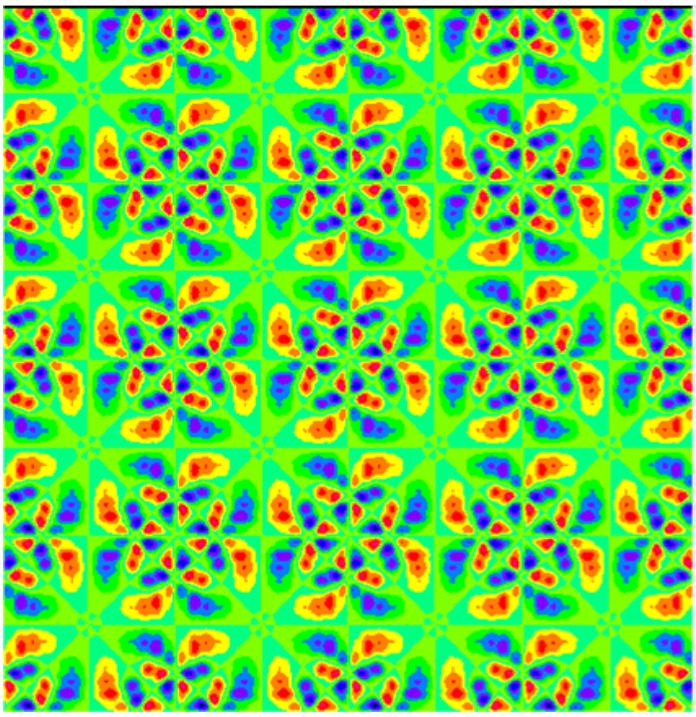

Figure 3.6 Mean field at final time step corresponding to fig. (3.5)

field

$$\nabla\psi\left(\phi(\boldsymbol{x}),t\right)=\nabla\phi(\boldsymbol{x})\frac{\partial}{\partial\phi}\psi(\phi,t) \tag{3.5}$$

As a consequence, the advection term vanishes explicitly and can be put equal to zero.

$$\boldsymbol{U}\cdot\nabla\psi=-[\boldsymbol{e}_z\times\nabla\phi(\boldsymbol{x})]\cdot\nabla\phi(\boldsymbol{x})\frac{\partial}{\partial\phi}\psi(\phi)=0$$

Now we have to calculate $\Delta\psi\left(\phi(\boldsymbol{x},t)\right)$ and $\Delta^2\psi\left(\phi(\boldsymbol{x},t)\right.$, in order to insert the ansatz into the order parameter equation:

$$\nabla\psi=\nabla\phi\cdot\frac{\partial\psi(\phi)}{\partial\phi}$$

$$\Delta\psi=\Delta\phi\frac{\partial\psi}{\partial\phi}+(\nabla\phi)^2\frac{\partial^2\psi}{\partial^2\phi}$$

Similarly we can write

$$\Delta^2\psi\approx(\nabla\phi)^4\frac{\partial^4\psi}{\partial^2\phi}+...$$

Here we use the approximation that as ϕ is slowly varying i.e.,

$$\Delta\phi\ll\nabla\phi$$

we may neglect the higher order derivatives of ϕ. As a consequence, the order parameter equation can be replaced by

$$\partial_t\psi=(\varepsilon-1)\psi+2(\nabla\phi))^2\frac{\partial^2\psi}{\partial^2\phi}-(\nabla\phi)^4\frac{\partial^4\psi}{\partial^2\phi}-\psi^3 \tag{3.6}$$

An approximate solution of the above equation can be written as

$$\psi=\sqrt{\frac{\varepsilon-(1-(\nabla\phi^2))^2}{3}}\sin(\sqrt{(\nabla\phi)^2}\phi+\varphi)$$

A stationary solution exists only if the condition $\varepsilon>(1-(\nabla\phi^2))^2$ or

$$\nabla\phi^2<1 \tag{3.7}$$

is fulfilled. We expect that in regions of space, where this condition is not met, the pattern can not relax inducing a spatio-temporal variation of the order parameter

field $\psi(\boldsymbol{x}, t)$.

Following figures, (3.7), (3.8) exhibit the results of quenching of the mean field after the development of spiral chaos in the order parameter field.

In the fig.(3.7) and fig.(3.8), first column on the left hand side shows the order parameter field, its corresponding Fourier spectrum is shown in the second column. The mean field is quenched after the spirals invade the whole domain so that we can see in the mentioned figures that the mean field remains constant and the order parameter field is continuously advanced in time until the spirals have been relaxed to curved roles or structures with angular bends. The first observation is that the wavelength of the stripes of the patterns changes, the thickness of the stripes apparently decreases. Second, the stripes have the tendency to align with the contour lines of the stream function in regions well separated from the former spiral tip locations. Third, the system does not tend to a stationary state, temporal variations are induced close to the former spiral tips and, also close to grain boundaries. We interpret this observation by the argument that the condition for alignment of order parameter field and stream function, derived above (3.7) is not met. Furthermore, it seems that the quenched dynamics leads to a state quite different from spiral defect chaos due to the change of the wavelength, and, therefore, is only of restricted help in exploring the dynamical mechanisms leading to spiral defect chaos.

3.4 Summary

In this chapter we studied a well-known model for the dynamics of pattern formation in Rayleigh-Bénard convection. Although this model has been studied rather intensively during the last years, still the problem to understand the emergence of spatio-temporal chaos and its quantification remains an open problem. We numerically studied spiral defect chaos and showed here the evolutions of spirals in large aspect ratio system. Next we considered newly studied patterns, namely quasi patterns, which evolve from suitably chosen initial conditions and for the case of periodic boundaries. Furthermore, we discussed that, when the mean field is quenched, the system relaxes to normal roll like patterns. In regions with a weak mean field rolls emerge which are aligned parallel to the lines of constant stream function. Close to strong points where the velocity field exhibits a

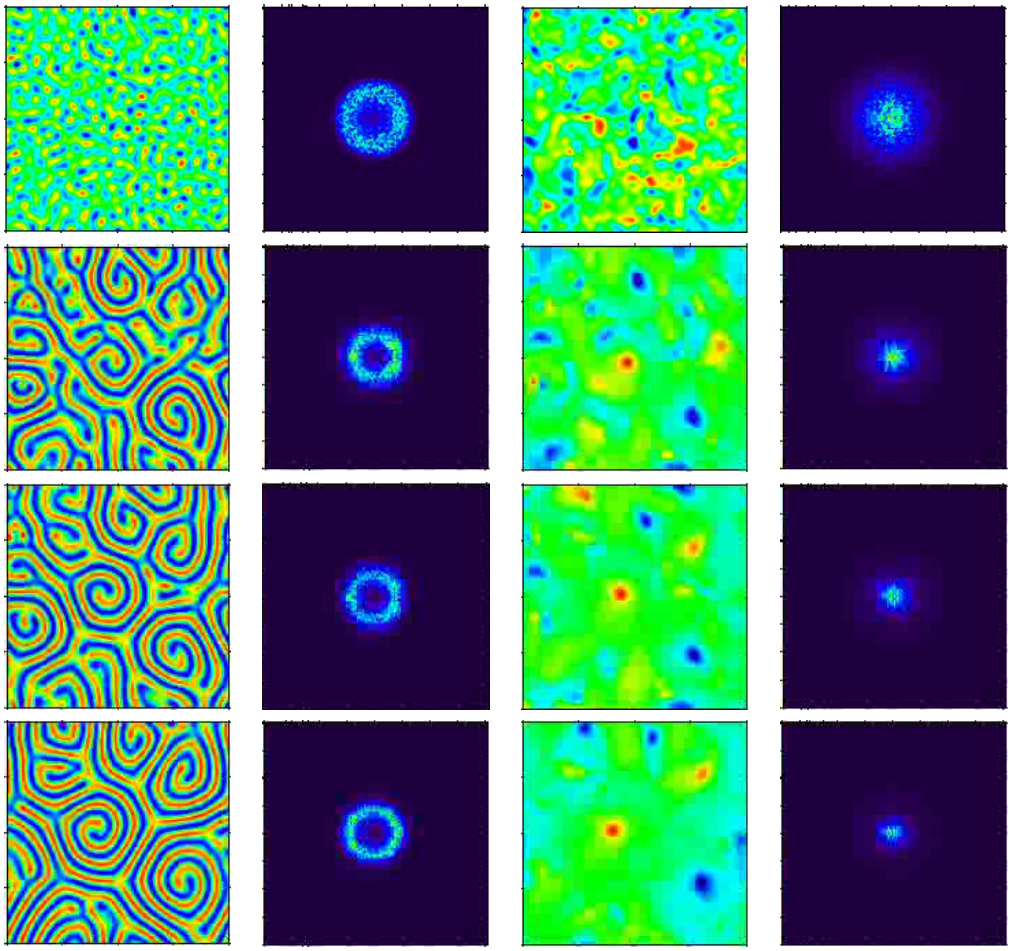

Figure 3.7 Quenching the mean flow: Order parameter field in first column, its Fourier spectrum in second column, mean field in third column and its Fourier Spectrum in last column,The parameters are $g = 100$, $Pr = 1.0$, $c = 12$, $\epsilon = 0.9$, $dt = 0.001$, $resolution = 128 \times 128$, L=100.

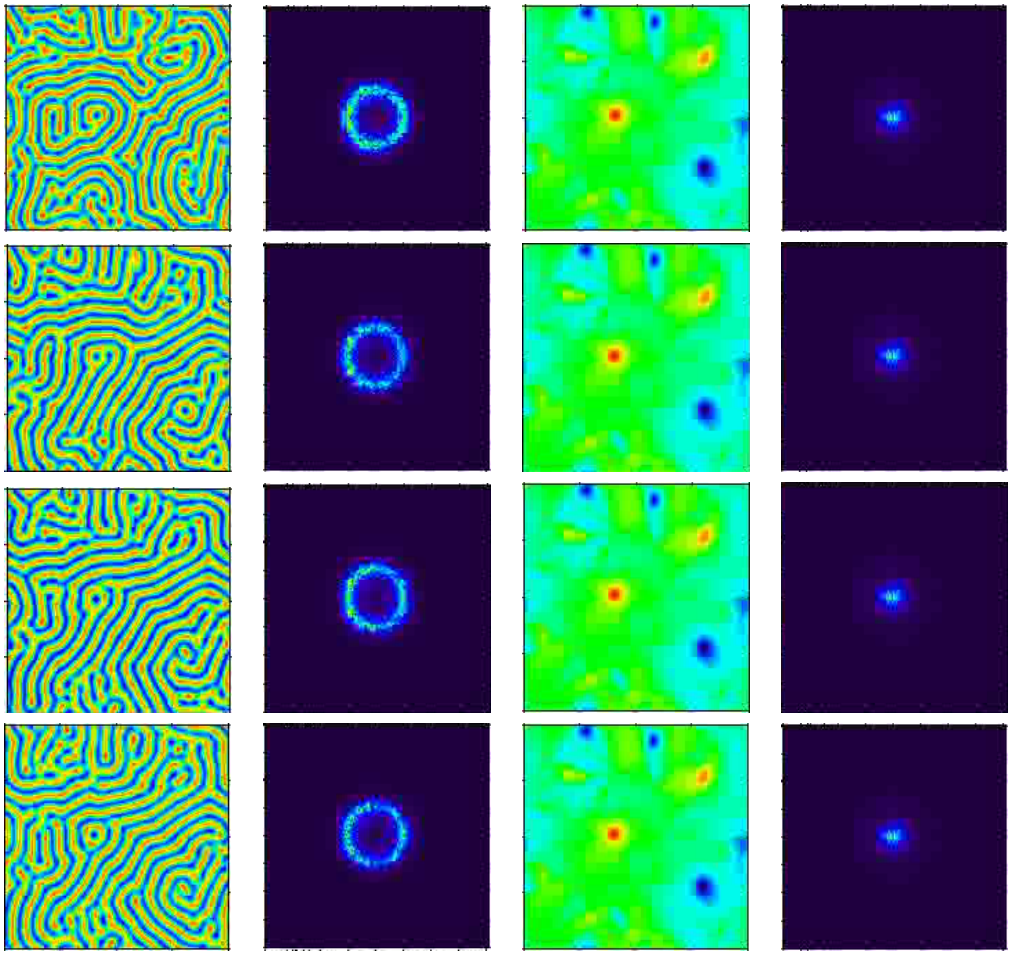

Figure 3.8 Quenching the mean flow: Continuation of fig. (3.7). Order parameter field in first column, its Fourier spectrum in second column, Mean field in third column and its Fourier Spectrum in last column,The parameters are $g = 100$, $Pr = 1.0$, $c = 12$, $\epsilon = 0.9$, $dt = 0.001$, $resolution = 128 \times 128$, L=100.

strong circulation local temporal variations of the patterns are induced. However, quenching seems to be only of minor value for the understanding of the onset of spiral defect chaos.

4 Pattern Formation in Chemical Systems

4.1 Introduction

This chapter addresses the fact that chemical systems also exhibit pattern formation under non-equilibrium conditions. Although pattern formation is a vast topic which has been explored since the midst of the last century, there are still open questions. Especially our understanding of how chemical reactions could create macroscopic structures with temporal and spatial complexity via self-organization is incomplete. The important features which drive the system far away from equilibrium leading to such spatio-temporal structures are nonlinearity, or feedback. In fact Ilya Prigogine [62] was one of the first pioneer chemists who proposed to analyze the self-organization process on the basis of non-equilibrium thermodynamics. Later on it became evident that the analysis of the processes of pattern selection has to be based on bifurcation analysis. As it is by now well-established that stationary or oscillatory patterns appear in chemical systems due to instability [48], [46]. Many different patterns like spirals, standing waves or solitary structures and fronts are found in experimental systems. Furthermore, similar patterns can be described by nonlinear reaction-diffusion models [60], [56]. However it should be emphasized here that these patterns are found as maintained a long as reactants are available [11].

One of the first example is dating back from 1977 where chaos was observed in CSTR (continuously stirred tank reactor [46]). Here, diffusion of the chemical species is suppressed by generating homogeneous solutions by continuous mixing and stirring. Spatio-temporal patterns usually emerge in the presence of diffusion, i.e. without mixing and stirring, like in the famous Belousov- Zhabotinsky (BZ) reactions [81]. The experimental difficulty in studying the spatio-temporal patterns in chemical systems is that the system should be driven far away from equilibrium by a continuous through flow of chemical substances. Therefore, at the beginning of research on reaction-diffusion systems only transients could be

obtained. Many patterns like spirals in the aforementioned BZ reactions, targets and wave like structures are observed in various other systems like cardiac tissue, chicken retina, liquid crystals [32]. The existence of stationary, stripe patterns, hexagonal patterns can be concluded from the work of A. Turing [74]. However, experimentally, such patterns have been realized in experiments only in the end of the last century by the groups of H. Swinney at Austin, Texas [57] and the group in Bordeaux [76].

Theoretically, the existence of stationary, wavelike, and chaotic patterns is shown on the basis of reaction-diffusion systems. Time dependent patterns may emerge on the basis of a Hopf- bifurcation. Furthermore, excitation waves like the BZ-waves are typical for so-called excitable media. Furthermore, we mention that reaction diffusion systems can be used for the description of the spatio-temporal behavior of dislocations of crystals [80]. A brief introduction of reaction-diffusion system is given in the next section.

4.2 Reaction-Diffusion Systems

In this section we want to introduce the mathematical model systems used for the analysis of reaction-diffusion systems. The model system is used not only to describe chemical reactions, but is also applied to fascinating biological patterns, patterns in ecological systems, physico-chemical systems and geochemistry. The spatio-temporal patterns appearing in these systems are expressed in terms of the dynamics of local concentrations of the chemical species, where diffusion plays an important role in describing the chemical kinetics of the system. These system of equations have reaction terms which usually simplifies the chemical kinetics.

Reaction-diffusion systems model chemical processes on the basis of a continuum theory. The basic equation of a continuum theory are balance equations for densities. Let us denote this density by $C(\boldsymbol{x}, t)$, denoting, e.g. the density of a certain chemical element in an aqueous solution. Then the balance equation takes the form

$$\frac{\partial}{\partial t} C(\boldsymbol{x}, t) + \nabla \cdot \boldsymbol{J}_C(\boldsymbol{x}, t) = R(\boldsymbol{x}, t) \tag{4.1}$$

The balance equation contains the current $\boldsymbol{J}_C(\boldsymbol{x}, t)$ and the source term $R(\boldsymbol{x}, t)$.

The meaning of this equation becomes evident by integrating over a volume V:

$$\frac{\partial}{\partial t}\int_V d\boldsymbol{x} C(\boldsymbol{x},t) + \int_V d\boldsymbol{x}\nabla\cdot\boldsymbol{J}_C(\boldsymbol{x},t) = \int_V d\boldsymbol{x} R(\boldsymbol{x},t) \tag{4.2}$$

Using the integral theorem of Gauss we end up with

$$\frac{\partial}{\partial t}\int_V d\boldsymbol{x} C(\boldsymbol{x},t) + \int_{\delta V} d\boldsymbol{A}\cdot\boldsymbol{J}_C(\boldsymbol{x},t) = \int_V d\boldsymbol{x} R(\boldsymbol{x},t) \tag{4.3}$$

where $d\boldsymbol{A}$ denotes the surface element of the volume V. From this relation it becomes obvious that the fraction of the chemical described by the concentration field $C(\boldsymbol{x},t)$ contained in the volume V changes due to fluxes across the surface, described by the flux $\mathbf{J}_C$, and a production or destruction rate with density $R(\boldsymbol{x},t)$.

If there are several chemicals (Number n) involved, a balance equation can be formulated for each concentration $C_\alpha(\boldsymbol{x},t)$, $\alpha = 1,..,n$:

$$\begin{aligned}
\frac{\partial}{\partial t}C_1 + \nabla\cdot\mathbf{J}_1[C_1,..C_n] &= R_1[C_1,..,C_n] \\
&\cdots\cdots \\
\frac{\partial}{\partial t}C_n + \nabla\cdot\boldsymbol{J}_n[C_1,..C_n] &= R_n[C_1,..,C_n]
\end{aligned} \tag{4.4}$$

Thereby, we have already taken into account that the fluxes $\mathbf{J}_\alpha$ and the reaction rates R_α may depend on all the concentrations C_α involved in the reaction.

Spatial effects enter due to the processes of diffusion. Reactions in aqueous solutions are characterized by the fact that the involved chemical molecules undergo Brownian motion so that the concentrations diffuse. This is taken into account by Fick's law:

$$\boldsymbol{J}_\alpha = \boldsymbol{U}(\boldsymbol{x},t)C_\alpha(\boldsymbol{x},t) - D_\alpha\nabla C_\alpha(\boldsymbol{x},t) \tag{4.5}$$

D_α denotes a diffusion constant for the chemical with concentration $C_\alpha(\boldsymbol{x},t)$ in the solution, $\boldsymbol{U}(\boldsymbol{x},t)$ is a possible velocity field.

Let us now be specific and consider two chemical species whose chemical concentrations are denoted by $u(\boldsymbol{x},t)$ and $v(\boldsymbol{x},t)$ at position $\boldsymbol{x}$ in time t. The

reaction-diffusion system then explicitly reads

$$\begin{aligned}\frac{\partial}{\partial t}u(\boldsymbol{x},t) &= f(u(\boldsymbol{x},t),v(\boldsymbol{x},t)) + D_u\Delta u(\mathbf{x},t)\\ \frac{\partial}{\partial t}v(\boldsymbol{x},t) &= g(u(\boldsymbol{x},t),v(\boldsymbol{x},t)) + D_v\Delta v(\boldsymbol{x},t)\end{aligned} \tag{4.6}$$

The spatial vector $\boldsymbol{x}$ can be one, two or three dimensional. The first terms on the right hand side of both equations $f(u,v)$ and $g(u,v)$ denote the chemical reaction rates, and, in general, are nonlinear. The second terms describe the diffusion processes where D_u and D_v are the diffusion coefficients. It is evident that the type of patterns formed in these systems strongly depends upon the non linearity and the spatial inhomogeneity due to diffusion. Also as in principle no free energy exists in such kind of systems, the emerging patterns can not be understood on the basis of variational principles.

When we consider a diffusive system in the absence of reaction then diffusion smears out the concentrations, and, hence, no pattern formation is observed. However, the interplay between reaction and diffusion leads to the emergence of spatio-temporal patterns, as has been emphasized by A. Turing [74].

In this thesis we are mainly concerned with a FitzHugh-Nagumo model [37] for an activator $u(\boldsymbol{x},t)$ and an inhibitor $v(\boldsymbol{x},t)$. It reads

$$\begin{aligned}\dot{u}(\boldsymbol{x},t) &= D_u\Delta u(\boldsymbol{x},t) + \epsilon u(\boldsymbol{x},t) - u(\boldsymbol{x},t)^3 - \kappa v(\boldsymbol{x},t)\\ \tau\dot{v}(\boldsymbol{x},t) &= D_v\Delta v(\boldsymbol{x},t) - v(\boldsymbol{x},t) + u(\boldsymbol{x},t)\end{aligned} \tag{4.7}$$

4.2.1 Homogeneous state

Here we will give general methods to investigate the bifurcation of reaction diffusion system. In order to calculate instability points, we begin with stationary solution, which, in addition, is spatially homogeneous. Let us consider that u_0 and v_0 be the solutions of the above eq. (4.6):

$$\begin{aligned}\frac{\partial}{\partial t}u(\boldsymbol{x},t) &= f(u(\boldsymbol{x},t),v(\boldsymbol{x},t)) = 0\\ \frac{\partial}{\partial t}v(\boldsymbol{x},t) &= g(u(\boldsymbol{x},t),v(\boldsymbol{x},t)) = 0\end{aligned} \tag{4.8}$$

Let us then consider a small perturbations around the stable state given by $u = u_0 + u_1$ and $v = v_0 + v_1$. Let us expand the system near the steady state using Taylor expansion which is valid if $|\frac{u_0}{u_1}| \ll 1$

$$f(u) = f(u_0) + \frac{\partial f}{\partial u}_{u_0,v_0} \cdot u_1 + \frac{\partial f}{\partial v}_{u_0,v_0} \cdot v_1 \tag{4.9}$$

and similarly for the inhibitor$v$, we can write the Jacobian of the linearized system at perturbed point as

$$J = \begin{pmatrix} f_u & f_v \\ g_u & g_v \end{pmatrix}$$

Defining the vector $\boldsymbol{w} = [u_1, v_1]$ we can rewrite the set of linear equations in matrix form

$$\frac{\partial}{\partial t}\boldsymbol{w} = J\boldsymbol{w} \tag{4.10}$$

Let us now calculate the solution in order to find the condition for stability. Using the exponential ansatz $\boldsymbol{w} = \boldsymbol{w}_0 e^{\lambda t}$ we obtain the linear eigenvalue problem

$$\lambda \boldsymbol{w} = J\boldsymbol{w}$$

The eigenvalues are determined as roots of the characteristic equation

$$\lambda^2 - \lambda TrJ + DetJ = 0$$

where TrJ and $DetJ$ are given by respectively as

$$\begin{aligned} TrJ &= f_u + g_v \\ DetJ &= f_u g_v - f_v g_u \end{aligned} \tag{4.11}$$

The solutions read

$$\lambda_{1,2} = \frac{TrJ}{2} \pm \sqrt{(\frac{TrJ}{2})^2 - DetJ} \tag{4.12}$$

We have to distinguish the case where the eigenvalues are complex from the case of real eigenvalues.

Complex eigenvalues are obtained for

$$DetJ > \left(\frac{TrJ}{2}\right)^2 \tag{4.13}$$

The solution is unstable provided

$$TrJ > 0 \tag{4.14}$$

Real eigenvalues are obtained in the opposite case:

$$DetJ < \left(\frac{TrJ}{2}\right)^2 \tag{4.15}$$

A single positive real eigenvalue is obtained in the case

$$DetJ < 0 \tag{4.16}$$

Two negative real eigenvalues arise for

$$TrJ < 0 \qquad , \qquad 0 < DetJ < \left(\frac{TrJ}{2}\right)^2 \tag{4.17}$$

The existence of at least one eigenvalue with positive real parts indicates instability.

This classifies the stability of the homogeneous solution of the two-component reaction-diffusion system.

FitzHugh-Nagumo Model

Let us turn to the consideration of the FitzHugh-Nagumo system. We first consider the fixed point $u = v = 0$. We explicitly obtain the Jacobian as

$$J = \begin{pmatrix} \epsilon & -\kappa \\ \frac{1}{\tau} & -\frac{1}{\tau} \end{pmatrix} \tag{4.18}$$

Explicitly,

$$\begin{aligned} TrJ &= \epsilon - \frac{1}{\tau} \\ DetJ &= -\left(\frac{\epsilon}{\tau} + \frac{\kappa}{\tau}\right) \end{aligned} \tag{4.19}$$

The above criterion on the stability of the homogeneous state $u = v = 0$ allows one to investigate instability boundaries in the ϵ-τ-plane.

4.3 Turing Instability

Since the seminal work of Turing [74] it is well-known that if the diffusion process of the inhibitor is faster as compared to that of the activator, pattern formation is observed. The intention of Turing was to provide an explanation of morphogenesis, i.e. the process of the development of shapes or forms in living organisms. The idea of a Turing pattern can be basically demonstrated by a two-component reaction-diffusion model consisting of two species, denoted as activator and inhibitor, respectively. An activator causes to increase the concentration of itself and the inhibitor, while the inhibitor does the reverse. In connection with diffusion this leads to Turing patterns.

The basic phenomenology can be described as the competition between the diffusion and chemical kinetics. Although this type of pattern was studied in the context of patterns developed in biology at first but its appearance can be interpreted in many other fields like physics [15], chemistry [60], [76], biology [47], [60] and many other fields. Turing patterns have been observed in Belousov-Zhabotinsky reaction [79]. Another article [29] studied the effect of convection on Turing instability where they argued that the chemical concentration variation correspond to velocity variation which is the basic principle of driving convection and it stabilizes the patterns. For the basic understanding of Turing instabilities in one, two and three dimensional we refer the reader to [40].

In order to analyze the stability also with respect to spatially dependent

perturbations we have to resort to the linearized reaction diffusion system.

$$\begin{aligned}\frac{\partial}{\partial t}u_1(\boldsymbol{x},t) &= D_u\Delta u_1(\boldsymbol{x},t) + J_{11}u_1(\boldsymbol{x},t) + J_{12}v_1(\boldsymbol{x},t)\\ \frac{\partial}{\partial t}v_1(\boldsymbol{x},t) &= D_v\Delta v_1(\boldsymbol{x},t) + J_{21}u_2(\boldsymbol{x},t) + J_{22}v_2(\boldsymbol{x},t)\end{aligned} \tag{4.20}$$

We can also formulate this set of equations in matrix form for the vector $\boldsymbol{w}(\boldsymbol{x},t) = [u(\boldsymbol{x},t), v(\boldsymbol{x},t)]$

$$\frac{\partial}{\partial t}\boldsymbol{w}(\boldsymbol{x},t) = D\Delta\boldsymbol{w}(\boldsymbol{x},t) + J\boldsymbol{w}(\boldsymbol{x},t) \tag{4.21}$$

For the perturbed fields we can now perform a Fourier ansatz $\boldsymbol{w} = w_{\boldsymbol{k}}\exp(\mathrm{i}k\cdot\boldsymbol{x}+\lambda t)$. This ansatz leads us to the following eigenvalue problem

$$\lambda w_k = (J - k^2D)w_k \tag{4.22}$$

Here we use $B = (J - k^2D)$ and $D = \begin{pmatrix} D_u & 0 \\ 0 & D_v \end{pmatrix}$.

Applying the condition of stability as mentioned above.

$$Tr(B) = -(D_u + D_v)k^2 + Tr(J) < 0 \tag{4.23}$$

$$Det(B) = D_uD_vk^4 - (D_uJ_{22} + D_vJ_{11})k^2 + Det(J) > 0 \tag{4.24}$$

where $Tr(J)$ and $Det(J)$ are given in above eq. (4.11).

In order to obtain a Turing instability, we have to ensure that the fixed point is stable with respect to disturbances with $k = 0$. This condition yields

$$TrJ < 0 \qquad , DetJ > 0 \tag{4.25}$$

For large values of k, the conditions for stability, $TrB \approx -(D_u + D_v)k^2 < 0$, $DetB \approx D_uD_vk^4 > 0$ is met. In order to obtain an instability with a single real eigenvalue we have the condition

$$TrB < 0 \qquad , \qquad DetB = 0 \tag{4.26}$$

This yields:

$$k^4 - \frac{(D_uJ_{22} + D_vJ_{11})}{D_uD_v}k^2 + \frac{DetJ}{D_uD_v} = 0 \tag{4.27}$$

Furthermore, the critical wave number is given by the minimum of $DetB$ with respect to k:

$$k_c^2 = \frac{(D_u J_{22} + D_v J_{11})}{2 D_u D_v} \tag{4.28}$$

Inserting eq. (4.28) into eq. (4.27) we obtain the inequality

$$-k_c^4 + \frac{DetJ}{D_u D_v} = 0 \tag{4.29}$$

As a consequence

$$-(D_u J_{22} + D_v J_{11})^2 + 4DetJ(D_u D_v) = 0 \tag{4.30}$$

This amounts to

$$-(D_u J_{22} - D_v J_{11})^2 - 4J_{12}J_{21}(D_u D_v) = 0 \tag{4.31}$$

This relation can only be satisfied (for positive values of $DetJ$) provided the diffusion coefficients are different. This fact was the major obstacle for the experimentalists. However the experimental group of De Keppers were successful in achieving a stationary pattern in a chemical reaction famous as (CIMA reaction)[76].

4.4 The Inclusion of Advection

The effect of adding advection in reaction-diffusion results in highly interesting pattern forming processes. The problem of considering advection can be divided into two issues

- **Passive advection**:
  In the case of passive advection the chemicals are transported by a given velocity field, which is not influenced by the chemical reaction itself.
- **Active advection**:
  In the case of active advection the velocity field itself is determined by the configurations of the chemical components. As a consequence, there is a back-reaction onto the chemical kinetics by the advection. This is a source of nonlinearity and the reason for a large variety of spatio-temporal processes.

For both cases, the advection-reaction-diffusion equations are obtained by taking into account the fluxes due to an external velocity field $\boldsymbol{U}(\boldsymbol{x},t)$. The result are the advection-diffusion-reaction equations for the $\alpha = 1,..,n$ chemical species with concentrations C_α:

$$\dot{C}_\alpha + \boldsymbol{U} \cdot \nabla C_\alpha = R_\alpha[C_1,..,C_n] + D_\alpha \Delta C_\alpha \tag{4.32}$$

4.5 Fluid Dynamics

We now have to specify the evolution of the velocity field $\boldsymbol{U}(\boldsymbol{x},t)$. For *passive advection*, there is no back-reaction of the chemical fields onto the velocity field. The dynamics of $\boldsymbol{U}(\boldsymbol{x},t)$ is governed by e.g. the Navier-Stokes equation.

For *active advection* the back reaction of the reaction-diffusion system onto fluid motion has to be taken into account. Both cases are described by the Navier-Stokes equation

$$\rho[\frac{\partial}{\partial t}\boldsymbol{U}(\boldsymbol{x},t) + \boldsymbol{U}(\boldsymbol{x},t) \cdot \nabla \boldsymbol{U}(\boldsymbol{x},t)] = -\nabla p + \eta \Delta \boldsymbol{U}(\boldsymbol{x},t) + \nabla \cdot \Sigma(\boldsymbol{x},t) \tag{4.33}$$

Here, we have considered an incompressible fluid

$$\nabla \cdot \boldsymbol{U}(\boldsymbol{x},t) = 0 \tag{4.34}$$

ρ denotes the density of the fluid, η the viscosity, $\nu = \eta/\rho$ the kinematic viscosity. Stresses, which are generated by a coupling of the chemical kinetics to the fluid dynamics, are included in the stress tensor Σ. For passive advection, Σ vanishes. For *active advection*, one has to specify a material law relating the stresses Σ to the chemical reaction under consideration.

In the following we shall consider several models. The first example will be an extension of a model by Lega and Passot [50] for active fluids. The second example will concern a model of a chemical surface reaction. Both models will lead us to an extensions of the generalized Swift-Hohenberg equation including mean flow.

4.6 A Model for Active Fluids

In this subsection, we specify the fluid dynamics in order to make contact with the generalized Swift-Hohenberg equation including mean field dynamics for spiral defect chaos.

We assume that the chemical reaction generates an additional stress, which results in a force which is proportional to the gradient of the concentrations $C_\alpha(\boldsymbol{x}, t)$:

$$\nabla \cdot \Sigma = \sum_{\alpha=1}^{n} g^\alpha(C_1, .., C_n) \nabla C_\alpha(\boldsymbol{x}, t) \tag{4.35}$$

The geometry is a thin fluid layer, such that the fluid motion is essentially two dimensional, with a Poiseuille profile in vertical direction. Therefore, the velocity field is given by the stream function $\chi(\boldsymbol{x}, t)$

$$\boldsymbol{U}(\boldsymbol{x}, t) = \nabla \times \boldsymbol{e}_z \chi(\boldsymbol{x}, t) \tag{4.36}$$

which, in turn, obeys the two dimensional equation for the vorticity

$$\begin{aligned} [\frac{\partial}{\partial t} + \boldsymbol{U}(\boldsymbol{x}, t) \cdot \nabla]\omega &= \nu(\Delta - c^2)\omega + \sum_\alpha \boldsymbol{e}_z \cdot [\nabla \times g^\alpha(C_1, ..C_n) \nabla C_\alpha(\boldsymbol{x}, t)] \\ &= \nu(\Delta - c^2)\omega + \sum_{\alpha,\beta} \frac{\partial g^\alpha}{\partial C_\beta} \boldsymbol{e}_z \cdot [\nabla C_\beta(\boldsymbol{x}, t) \times \nabla C_\alpha(\boldsymbol{x}, t)] \end{aligned}$$

As in the case of the generalized Swift-Hohenberg equation we have taken into account a spatially uniform damping $-c^2\omega$, which accounts for dissipation due to a varying velocity profile in the vertical direction of the thin layer.

The inhomogeneity couples the fluid motion to the chemical reaction. The coupling arises in the case where

$$\frac{\partial g^\alpha}{\partial C_\beta} \neq \frac{\partial g^\beta}{\partial C_\alpha} \tag{4.37}$$

Otherwise, the inhomogeneity vanishes.

The property (4.37) points at an interesting feature, as we will discuss in the next subsection, considering *active fluids*.

4.6.1 Active Fluids and Bacterial Colonies

Recently, so-called active fluids have been considered, arising from the investigations of colonies of amoeba and colonies, or swarms. Active fluids contain elements, which are able to undergo directed motion by itself. Examples of active fluids are microorganisms such as the Amoeba, Bacterias etc. Self-organization processes in such systems are rather diverse. The different kinds of patterns seen in these systems exhibit larger spatial scales of kilometers for bird flocks to micrometers for bacterial colonies [28].

Lega and Passot [51] recently proposed a hydrodynamic model for the description of the evolution of colonies of bacteria on the surface of agar plate. They considered the reaction-diffusion equation for the concentration of bacteria-water mixture (where the density of both was assumed to be constant) coupled to an advection equation for the velocity field of the mixture. Their advection term describes the role of gradient forces due to nutrients which means that the nutrients are consumed by bacteria and as a result mass of bacteria grows.

Lega and Passot [51] arrived at advection-reaction-diffusion models quite similar to the set of equations (4.35), (4.37). However, they assumed that the fluid motion is generated by a gradient volume force, meaning that

$$g^{\alpha}(C_1, ..C_n) = const \tag{4.38}$$

In the present case, we focus on forces, which do not fulfill this requirement. It would be interesting to formulate models of active fluid elements leading to such types of behavior.

4.7 Advection-Reaction-Diffusion Systems at Interfaces

The studies of interfaces between different fluids is an active field of research. It will become important especially when considering pattern formation at the micro- and nano-scale, like e.g. pattern formation in Langmuir-Blodgett transfer systems.

Pattern formation at the interface is a separate field of research and, from the point of view of basic research, many patterns like spirals , targets, finger like patterns are studied in this context. Its importance in industrial applications

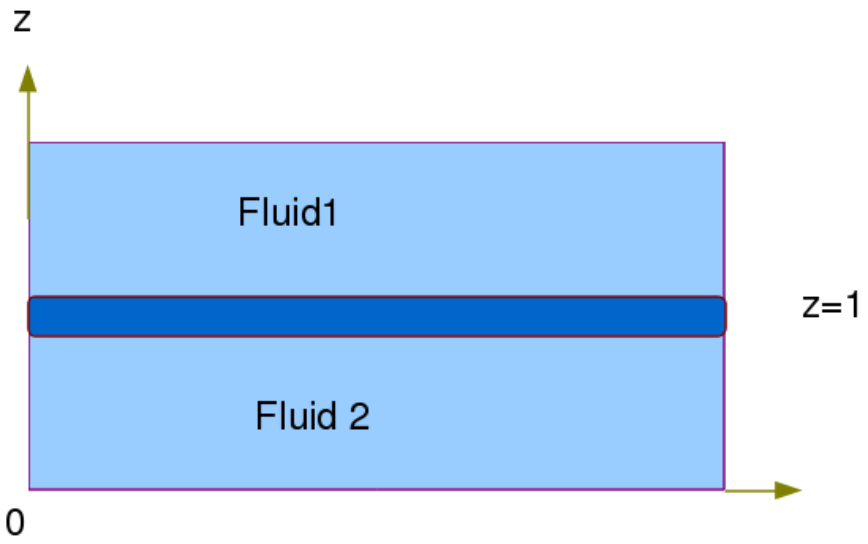

Figure 4.1 Schematic view of the model: A chemical reaction takes place in the interface between the fluids

like polymer coating techniques, semiconductor industry, micro-fluidics etc make this field very interesting and demanding. Pearson [58] was amongst the pioneers who studied the instability of the interface and pointed at the importance of surface tension in connection with temperature induced instabilities. Sternling and Scriven [71] studied the interface for the concentration gradient model. A historical contribution by Rowlinson and Widom [67] who characterized different cases of inter facial liquids on the basis of density gradients, viscosity variations etc. at the interface.

In this section, we focus on patterns emerging on the inter-facial area between two fluids. We consider a very general case of two layer fluid lying one above the other. The result is a thin interface between the two along the $x - y$ plane. The thickness of the interface is assumed to be small, i.e., zero. Therefore, gravitational acceleration can be ignored for simplification. Furthermore, the two fluids are assumed to have similar viscous properties. We assume that a chemical reaction takes place exactly within the fluid interface involving n chemical species. The schematic diagram (4.42) depicts the situation. The coupling between inter-facial chemical reaction and hydrodynamic flow is assumed to be due to a variation of the inter-facial tension.

Let the vertical direction be denoted by the vector $\boldsymbol{e}_z$, the vertical coordinate by $z\epsilon[0,2]$. We assume that the interface between the two fluids is located at $z=1$. The basic assumption is that this interface remains planar. The coordinates in the interface are denoted by the vector $\boldsymbol{x}=[x,y]$.

4.7.1 Chemical Subsystem

We now formulate the reaction diffusion system describing the concentration of the chemicals at the interface:

$$\dot{C_\alpha}(\boldsymbol{x},t) = R_\alpha(C_1 \dots C_n) - \nabla_x \cdot \boldsymbol{J}_\alpha(\boldsymbol{x},t) \tag{4.39}$$

Here C_α denotes the concentration of the chemical species α where $(\alpha = 1.2.\dots n)$, ∇ is the two-dimensional gradient within the $x-y$ plane. The flux $J_\alpha(\mathbf{x},t)$ corresponding to the concentration C_α is a superposition of a diffusional flux, $-D_\alpha \nabla_x C_\alpha(\boldsymbol{x},t)$, and advective transport by the two-dimensional velocity field $U(\boldsymbol{x},t)$

$$\boldsymbol{J}_\alpha(\boldsymbol{x},t) = \boldsymbol{U}(\boldsymbol{x},t)C_\alpha(\boldsymbol{x},t) - D_\alpha \nabla_x C_\alpha(\boldsymbol{x},t) \tag{4.40}$$

Plugging this eq.(4.40) into eq.(4.39), we end up with the following advection-reaction-diffusion equation:

$$\dot{C_\alpha}(\boldsymbol{x},t) + \boldsymbol{U}(\boldsymbol{x},t)\cdot\nabla C_\alpha(\boldsymbol{x},t) = R_\alpha(C_1 \dots C_n) + D_\alpha \Delta_x C_\alpha(\boldsymbol{x},t) \tag{4.41}$$

4.7.2 Hydrodynamic Subsystem

Now we wish to specify the fluid dynamics of the above system. The equation of motion of the two fluids at the interface can be represented by the Navier-Stokes equation for the velocity field $\boldsymbol{U}(\boldsymbol{x},z,t)$

$$\begin{aligned}[\frac{\partial}{\partial t} &+ \boldsymbol{U}(\boldsymbol{x},z,t)\cdot\nabla]\boldsymbol{U}(\boldsymbol{x},z,t) \\ &= -\nabla P(\boldsymbol{x},z,t) + \nu\Delta\boldsymbol{U}(\boldsymbol{x},z,t) + (\nabla\cdot\Sigma(\boldsymbol{x},z,t))\end{aligned} \tag{4.42}$$

where $P(\boldsymbol{x},z,t)$ denotes the pressure, ν is the viscosity. We explicitly specify the horizontal coordinates $\boldsymbol{x}=[x,y]$ and the vertical coordinate z. Here the fluids

are assumed to be incompressible,

$$\nabla \cdot \boldsymbol{U} = 0 \tag{4.43}$$

The surface tension, described by the stress tensor Σ is a result of the variations of the concentrations along the surface. Denoting the location of the interface by

$$z = h(\boldsymbol{x}, t) \tag{4.44}$$

the surface tension is concentrated at the boundary:

$$\Sigma(\boldsymbol{x}, z, t) = \sigma(\boldsymbol{x}, t)\delta(z - h(\boldsymbol{x}, t)) \tag{4.45}$$

The stress tensor $\sigma(\boldsymbol{x}, t)$ only has components tangential to the surface. For isotropic tension one makes the ansatz

$$\sigma = \sigma_0 \left(E - \boldsymbol{n}\boldsymbol{n}\right) \tag{4.46}$$

Here, $\boldsymbol{n}$ is a vector normal to the interface, E denotes the identity matrix.

For the following we assume that the surface remains planar, $z = 1$. The surface tension reads

$$\Sigma = \sigma_0 \delta(z-1) \begin{pmatrix} 1 & 0 & 0 \\ 0 & 1 & 0 \\ 0 & 0 & 0 \end{pmatrix} \tag{4.47}$$

and the additional force at the surface takes the form

$$\nabla \cdot \Sigma = \delta(z-1) \begin{pmatrix} \nabla_{\boldsymbol{x}} \sigma_0 \\ 0 \end{pmatrix} \tag{4.48}$$

Usually, the quantity σ_0 is assumed to depend on the concentrations $C_j(\boldsymbol{x}, t)$ on the surface.

Model for Surface Tension

However, for the following we shall assume that the tensor σ does depend on the gradients of the concentrations $C_j(\boldsymbol{x}, t)$ within the interface,

$$\sigma_{i,j} = \sum_{i,j=1}^{n} g_\alpha \frac{\partial C_\alpha}{\partial x_i} \frac{\partial C_\beta}{\partial x_j} \tag{4.49}$$

This modeling ansatz leads us to the force

$$\nabla \cdot \Sigma = \delta(z-1)\boldsymbol{\kappa} \tag{4.50}$$

generated by the surface tension, where the vector field $\boldsymbol{\kappa}$ is explicitly given

$$\boldsymbol{\kappa} = \sum_{\alpha,\beta} g_{\alpha,\beta} \left[\Delta C_\alpha \nabla C_\beta\right] \tag{4.51}$$

Fluid Velocity

Our next simplification consists in neglecting the inertia of the fluid, i.e. assuming Stokes flow. Under the assumption that the interface remains planar, i.e. the vertical velocity vanishes, we obtain from the Navier-Stokes equation

$$-\nu[\Delta^(2) + \frac{\partial^2}{\partial z^2}]\boldsymbol{U}(\boldsymbol{x}, z, t) + \nabla P = \delta(z-1)\boldsymbol{\kappa}(\boldsymbol{x}, t) \tag{4.52}$$

In order to determine the velocity field we perform a decomposition into a poloidal field and a vortical field in terms of the scalar fields $S(\boldsymbol{x}, z, t)$ and $T(\boldsymbol{x}, z, t)$

$$\boldsymbol{U}(\boldsymbol{x}, z, t) = \nabla \times \nabla \times \boldsymbol{e}_z S(\boldsymbol{x}, z, t) + \nabla \times \boldsymbol{e}_z T(\boldsymbol{x}, z, t) \tag{4.53}$$

It is well-established that each solenoidal velocity field can be expressed in such a form. We point out that the velocity field corresponding to the toroidal field $T(\boldsymbol{x}, z, t)$ is purely horizontal.

The following identities are of considerable use:

$$\begin{aligned} \boldsymbol{e}_z \cdot [\nabla \times \boldsymbol{U}] &= -\Delta^{(2)} T(\boldsymbol{x}, z, t) \\ \boldsymbol{e}_z \cdot [\nabla \times [\nabla \times \boldsymbol{U}]] &= \Delta\Delta^{(2)} S(\mathbf{x}, z, t) \end{aligned} \tag{4.54}$$

A straightforward calculation yields the following two equations

$$\begin{aligned} \nu\Delta^{(2)}\Delta T &= \delta(z-1)\boldsymbol{e}_z\cdot[\nabla\times\boldsymbol{\kappa}] \\ \nu\Delta^{(2)}\Delta^2 S &= \delta(z-1)\Delta^2\boldsymbol{e}_z\cdot\boldsymbol{\kappa} \end{aligned} \tag{4.55}$$

However, for a planar surface,

$$\boldsymbol{e}_z\cdot\boldsymbol{\kappa}=0 \tag{4.56}$$

and, for the surface tension following the ansatz (4.49), there is no excitation of a poloidal field. However, a toroidal field is excited by this type of surface tension. As a consequence, we explicitly obtain for the toroidal part

$$\begin{aligned} \nu\Delta^{(2)}[\Delta^{(2)}+\frac{\partial^2}{\partial z^2}]T(\boldsymbol{x},z,t) &= \boldsymbol{e}_z\cdot[\nabla\times\delta(z-1)\boldsymbol{\kappa}(\boldsymbol{x},t)] \\ &= \delta(z-1)\sum_{\alpha,\beta}g_{\alpha,\beta}\boldsymbol{e}_z\cdot[\nabla\Delta C_\alpha\times\nabla C_\beta] \\ &= \delta(z-1)g(\boldsymbol{x},t) \end{aligned} \tag{4.57}$$

We are now in the position to determine the solution for the toroidal part of the velocity, which is specified by the field $T(\mathbf{x},z)$. To this end we consider the equation (4.57) in Fourier space, yielding

$$-\nu k^2[\frac{\partial^2}{\partial z^2}-k^2]T(\boldsymbol{k},z,t)=\delta(z-1)g(\boldsymbol{k},t) \tag{4.58}$$

Thereby, we have defined the Fourier transform $g(\boldsymbol{k},t)$.

The field $T(\boldsymbol{k},t)$ is determined by the equation

$$[\frac{\partial^2}{\partial z^2}-k^2]T(\boldsymbol{k},z,t)=0 \tag{4.59}$$

under the condition

$$\frac{\partial}{\partial z}T(\boldsymbol{k},z,t)|_{z=1-\epsilon}^{z=1+\epsilon}=-\frac{g(\boldsymbol{k},t)}{\nu k^2} \tag{4.60}$$

The last condition is obtained by integrating (4.58) from $z=1-\epsilon$ to $z=1+\epsilon$,

assuming that $T(\boldsymbol{k}, z, t)$ to be continuous across the boundary:

$$-\nu k^2 \int_{z=1-\epsilon}^{z=1+\epsilon} dz[\frac{\partial^2}{\partial z^2} - k^2]T(\boldsymbol{k}, z, t) = g(\boldsymbol{k}, t) \tag{4.61}$$

Taking into account this condition we obtain the solution

$$T(\boldsymbol{k}, z, t) = e^{-k|z-1|}\tilde{T}(\boldsymbol{k}, t) = e^{-k|z-1|}\frac{g(\boldsymbol{k}, t)}{2\nu k^3} \tag{4.62}$$

which holds, if the fluid extends to infinity in z-direction. In case of layers of thickness $d = 1$ we obtain the more general expression:

$$T(\boldsymbol{k}, z, t) = e^{-k|z-1|}\tilde{T}(\boldsymbol{k}, t) = e^{-k|z-1|}\frac{g(\boldsymbol{k}, t)}{2\nu k^3(1 + e^{-2kd})} \tag{4.63}$$

The toroidal field exactly at the interface, i.e. $z = 1$ is given by

$$T(\boldsymbol{x}, t) = \int K(\boldsymbol{x} - \boldsymbol{x}')\boldsymbol{e}_z \cdot \sum_{\alpha,\beta} g_{\alpha,\beta}[\nabla_{x'} C_\alpha(\boldsymbol{x}', t) \times \nabla C_\beta(\boldsymbol{x}', t)] \tag{4.64}$$

The kernel $K(\boldsymbol{x} - \boldsymbol{x}')$ is given by the Fourier transform

$$K(\boldsymbol{x} - \boldsymbol{x}') = \int d\boldsymbol{k} e^{i\boldsymbol{k}\cdot(\boldsymbol{x}-\boldsymbol{x}')}\frac{1}{2\nu k^3(1 + e^{-2kd})} \tag{4.65}$$

We calculate the two dimensional velocity field from the stream function $T(\boldsymbol{x}, t)$ according to

$$\boldsymbol{v}(\boldsymbol{x}, t) = \nabla \times \boldsymbol{e}_z T(\boldsymbol{x}, t) \tag{4.66}$$

4.7.3 Reactions at Interfaces: Summary

Let us now summarize our treatment of advection-reaction-diffusion system. We consider the interface between two different fluids, where the chemical reaction occurs in the two-dimensional interface and the chemicals are allowed to diffuse in the interface. Furthermore, the varying chemical concentrations allow for the emergence of a surface tension, which leads to an additional driving force in the direction tangent to the interface. In the adiabatic approximation, i.e. neglecting

inertial effects of fluid motion, we obtain the velocity field of the form

$$\boldsymbol{v}(\boldsymbol{x},t) = \nabla_{\boldsymbol{x}} \times \boldsymbol{e}_z \int d\boldsymbol{x}' K(\boldsymbol{x}-\boldsymbol{x}') \sum_{\alpha\beta} g_{\alpha\beta} \boldsymbol{e}_z \cdot [\nabla C_\alpha \times \nabla C_\beta] \tag{4.67}$$

We remind the reader that this velocity field is a functional of the concentrations $C_\alpha(\boldsymbol{x},t)$ itself, i.e. the velocity field depends on the field configuration of the concentrations.

The chemical reaction occurring inside the interface are given by the advection-reaction-diffusion equations

$$[\frac{\partial}{\partial t} + \boldsymbol{v}(\boldsymbol{x},t) \cdot \nabla_{\boldsymbol{x}}] C_\alpha(\boldsymbol{x},t) = R_i[C_1(\boldsymbol{x},t), .., C_n(\boldsymbol{x},t)] + D_\alpha \Delta_{\boldsymbol{x}} C_\alpha(\boldsymbol{x},t) \tag{4.68}$$

The main effect of the advection term is to render the nonlinear dynamics essentially nonlocal. As we shall discuss in the following, this fact will allow for instabilities of chemical fronts with fractal boundaries. Furthermore, we can investigate systems exhibiting Turing structures and explore the possibilities to find states which are analogous to the spiral defect chaos observed in small Prandtl number Rayleigh-Bénard convection.

Let us explicitly write down the dynamics of an activator-inhibitor system, described by the activator concentration $u(\boldsymbol{x},t)$ and the inhibitor concentration $v(\boldsymbol{x},t)$.

The force at the interface leads us to the velocity field

$$\boldsymbol{v}(\boldsymbol{x},t) = \nabla_{\boldsymbol{x}} \times \boldsymbol{e}_z \alpha \int d\boldsymbol{x}' K(\boldsymbol{x}-\boldsymbol{x}') \boldsymbol{e}_z \cdot [\nabla u(\boldsymbol{x},t) \times \nabla v(\boldsymbol{x},t)] \tag{4.69}$$

4.8 Summary

In this chapter, we started from the general description of the reaction-diffusion systems and discussed the stability analysis of spatially homogeneous solutions of such model equations. Then we proceeded to the description of advection-reaction-diffusion processes. To this end we considered two models. The first model describes fluid motion of active media. The second model was concerned with the treatment of chemical reactions arising at the interface of two fluids. For both cases we showed that the formulation of suitable ansätze for the additional stress tensor

arising in active fluids and the surface tension for interface reaction leads to model equations, which are extensions of the generalized Swift-Hohenberg equation with mean flow modeling spiral defect chaos in Rayleigh-Bénard convection.

5 From Spiral Defect Chaos to Fractal Fronts

In the present chapter we shall investigate pattern formation in a two-component advection-reaction-diffusion system, consisting of the FitzHugh-Nagumo model coupled to fluid motion. Based on numerical treatment of the underlying equations we explicitly discuss the following issues:

- Reduction of the model to generalized Swift-Hohenberg equation in the presence of a mean flow
- Observation of spiral defect chaos
- Transition to states with fractal fronts

Let us summarize our starting point, the two-component activator-inhibitor model, with activator $u(\boldsymbol{x},t)$ and inhibitor $v(\boldsymbol{x},t)$.

$$\frac{\partial}{\partial t}u(\boldsymbol{x},t)+\boldsymbol{U}(\boldsymbol{x},t)\cdot\nabla u(\boldsymbol{x},t)=\epsilon u(\boldsymbol{x},t)-u(\boldsymbol{x},t)^3+D_u\Delta u(\boldsymbol{x},t)-\kappa v(\boldsymbol{x},t) \quad (5.1)$$

$$\tau\left[\frac{\partial}{\partial t}v(\boldsymbol{x},t)+\boldsymbol{U}(\boldsymbol{x},t)\cdot\nabla v(\boldsymbol{x},t)\right]=D_v\Delta v(\boldsymbol{x},t)-v(\boldsymbol{x},t)+u(\boldsymbol{x},t) \quad (5.2)$$

The evolution equation for the stream function takes the form

$$\left[\frac{\partial}{\partial t}+\boldsymbol{U}(\boldsymbol{x},t)\cdot\nabla\right]\Delta\chi(\boldsymbol{x},t)= \nu(\Delta-c^2)\Delta\chi(\boldsymbol{x},t)+\alpha\boldsymbol{e}_z\cdot[\nabla u(\boldsymbol{x},t)\times\nabla v(\boldsymbol{x},t)] \quad (5.3)$$

Here, the velocity field $\boldsymbol{U}(\boldsymbol{x},t)$ is derived from the stream function in the usual way:

$$\boldsymbol{U}(\boldsymbol{x},t)=\nabla\times\boldsymbol{e}_z\chi(\boldsymbol{x},t) \quad (5.4)$$

5.1 Derivation of Generalized Swift Hohenberg Equation

In the present section we shall show that a Swift-Hohenberg type equation can be derived in a certain parameter regime for the following two-component reaction-diffusion equation

$$\dot{u}(\boldsymbol{x},t) = D_u \Delta u(\boldsymbol{x},t) + f\left(u(\boldsymbol{x},t)\right) - \kappa v(\boldsymbol{x},t) \tag{5.5}$$

$$\dot{v}(\boldsymbol{x},t) = \frac{1}{\tau}\left[D_v \Delta v(\boldsymbol{x},t) - v(\boldsymbol{x},t) + u(\boldsymbol{x},t)\right] \tag{5.6}$$

5.1.1 Case 1: $\tau = 0$

Let us first consider the limiting case $\tau \to 0$. As a consequence, we can neglect the first term on the left hand side of eq.(5.6). We obtain for the inhibitor

$$(1 - D_v\Delta)v(\boldsymbol{x},t) = u(\boldsymbol{x},t) \tag{5.7}$$

This shows that the inhibitor follows the activator adiabatically. Using the Green's function $G(\boldsymbol{x}-\boldsymbol{x}')$ of the operator $1 - D_v\Delta_v$,

$$(1 - D_v\Delta)\, G(\boldsymbol{x}-\boldsymbol{x}') = \delta(\boldsymbol{x}-\boldsymbol{x}') \tag{5.8}$$

we end up with the representation

$$v(\boldsymbol{x},t) = \int d\boldsymbol{x}' G(\boldsymbol{x}-\boldsymbol{x}')u(\boldsymbol{x}',t) \tag{5.9}$$

and obtain the nonlocal evolution equation for the activator $u(\boldsymbol{x},t)$

$$\dot{u}(\boldsymbol{x},t) = D_u\Delta u(\boldsymbol{x},t) + \epsilon u(\boldsymbol{x},t) - u(\boldsymbol{x},t)^3 - \kappa \int d\boldsymbol{x}' G(\boldsymbol{x}-\boldsymbol{x}')u(\boldsymbol{x}',t) \tag{5.10}$$

It is interesting to note that this evolution equation can be written in variational form,

$$\dot{u}(\boldsymbol{x},t) = -\frac{\delta}{\delta u(\boldsymbol{x},t)} V\left[u\right] \tag{5.11}$$

with the potential

$$V[u] = \int d\boldsymbol{x} \left(-\frac{1}{2}\epsilon u(\boldsymbol{x},t)^2 + \frac{1}{4}u(\boldsymbol{x},t)^4 - \frac{1}{2}D_u(\nabla u)^2 \right) + \frac{1}{2}\kappa \int d\boldsymbol{x} \int d\boldsymbol{x}' u(\boldsymbol{x},t) G(\boldsymbol{x}-\mathbf{x}') u(\boldsymbol{x}',t) \tag{5.12}$$

The elimination of the inhibitor $v(\boldsymbol{x},t)$ leads to a nonlocal potential $V[u]$.

In order to make contact with the generalized Swift-Hohenberg equation, we have to look at a situation, where the nonlocal term can be approximated by a local one. To this end we look for an iterative solution of equation (5.7).

$$v = [1 + D_v\Delta + D_v^2\Delta^2 + ..]u \tag{5.13}$$

It should be emphasized here that the above approximation is valid if the evolving patterns are slowly varying in space, i.e. in situations where the critical wave number k_c in the resulting generalized Swift-Hohenberg equation remains small.

We can now summarize. Our new set of equations for the activator and inhibitor reads

$$\begin{aligned} \frac{\partial}{\partial t}u(\boldsymbol{x},t) &+ \boldsymbol{U}(\boldsymbol{x},t)\cdot\nabla u(\boldsymbol{x},t) = \epsilon u(\boldsymbol{x},t) - u(\boldsymbol{x},t)^3 \\ &+ (D_u - D_v)\Delta u(\boldsymbol{x},t) - D_v^2\Delta^2 u(\boldsymbol{x},t) - u(\boldsymbol{x},t) \end{aligned} \tag{5.14}$$

Using the condition $(D_u - D_v) < 0$, we arrive at the following formulation.

$$\begin{aligned} (\frac{\partial}{\partial t} + \boldsymbol{U}(\boldsymbol{x},t)\cdot\nabla)u(\boldsymbol{x},t) &= (\epsilon-1)u(\boldsymbol{x},t) - u^3(\boldsymbol{x},t) \\ -D_v^2(\frac{D_v - D_u}{2D_v^2} + \Delta)^2 u(\boldsymbol{x},t) &+ \frac{(D_v - D_u)^2}{4D_v^2}u(\boldsymbol{x},t) \end{aligned} \tag{5.15}$$

Here, we have again included the advection term.

As a consequence, we obtain a Swift-Hohenberg equation for the activator u coupled to a mean flow given by eq.(5.3) where by comparing eq.(5.15) with the Swift-Hohenberg equation, we get the relations,

$$\epsilon - 1 + \frac{(D_v - D_u)^2}{4D_v^2} = \varepsilon \tag{5.16}$$

$$k_c^2 = \frac{D_v - D_u}{2D_v^2} \tag{5.17}$$

This relation shows that instability occurs when $\epsilon > 1 - \frac{(D_v - D_u)^2}{4D_v^2}$ Furthermore, our expansion is justified if k_c is small, i.e., if D_v is slightly larger than D_u.

It remains to consider the coupling term to the fluid dynamics, which arises via the equation for the stream function $\chi(\boldsymbol{x}, t)$. The decisive term is the inhomogeneity

$$\boldsymbol{e}_z \cdot [\nabla u \times \nabla v] = \boldsymbol{e}_z \cdot [\nabla u \times \nabla [u + D_v \Delta u + ..]] \tag{5.18}$$

where we have used the expansion (5.13). As a consequence, the mean field equation reads

$$\begin{aligned} [\frac{\partial}{\partial t} + \boldsymbol{U}(\boldsymbol{x}, t) \cdot \nabla] \Delta \chi(\boldsymbol{x}, t) = \\ \nu(\Delta - c^2)\Delta\chi(\boldsymbol{x}, t) + \alpha D_v \boldsymbol{e}_z \cdot [\nabla u(\boldsymbol{x}, t) \times \nabla \Delta u(\boldsymbol{x}, t)] \end{aligned} \tag{5.19}$$

and exactly takes the form used in the description of spiral defect chaos.

5.1.2 Case 2: Small τ Expansion

In this subsection we want to discuss the case when first order corrections in τ are taken into account. To this end we have to take into account the above mentioned equations of activator and inhibitor once again. For simplicity let us consider the case first without advection terms and, then at the end, take them into account.

We first state the result

$$\begin{aligned} (\partial_t + \mathbf{U} \cdot \nabla)\, u(\boldsymbol{x}, t) = \{L(\Delta) - \kappa\tau \frac{L(\Delta)}{(1 - D_v\Delta)^2}\} u(\boldsymbol{x}, t) \\ -(1 - \frac{\kappa\tau}{(1 - D_v\Delta)^2}) f(u(\boldsymbol{x}, t)) \end{aligned} \tag{5.20}$$

The derivation is described in the next subsection. For this equation, we were not able to find a potential, as we did for $\tau = 0$.

Derivation of the first order correction in τ

We can write the above eq.(5.6) in spectral space as

$$(\tau\frac{\partial}{\partial t} + D_v k^2 + 1)v(\boldsymbol{k}, t) = u(\boldsymbol{k}, t) \tag{5.21}$$

This first order differential equation can be solved

$$v(\boldsymbol{k}, t) = \frac{1}{\tau}\int_{-\infty}^{t} dt' e^{-(\frac{D_v k^2+1}{\tau})(t-t')} u(\boldsymbol{k}', t') \tag{5.22}$$

Applying the Taylor expansion on $u(\mathbf{s}', t')$, i.e.,

$$u(\boldsymbol{k}', t') = u(\boldsymbol{k}, t) + (t' - t)\dot{u}(\boldsymbol{k}, t) + \dots \tag{5.23}$$

using the first two terms we can write

$$v(\boldsymbol{k}, t) = \frac{1}{\tau}\int_{-\infty}^{t} dt' e^{-(\frac{D_v k^2+1}{\tau})(t-t')} \left(u(\boldsymbol{k}, t) + (t' - t)\dot{u}(\boldsymbol{k}, t)\right) \tag{5.24}$$

Next, we perform the time integrals. As a consequence the equation reads

$$v(\boldsymbol{k}, t) = \frac{1}{D_v k^2 + 1}(u(\boldsymbol{k}, t) - \frac{\tau}{(D_v k^2 + 1)^2}\dot{u}(\boldsymbol{k}, t)) \tag{5.25}$$

Converting the equation back to real space, we get

$$v(\boldsymbol{x}, t) = \left(\frac{1}{(1 - D_v\Delta)} - \frac{\tau}{(1 - D_v\Delta)^2}\frac{\partial}{\partial t}\right) u(\boldsymbol{x}, t) \tag{5.26}$$

Hence we can write the activator equation by plugging in eq.(5.26) into eq.(5.5) for $\kappa = 1$. We obtain

$$(1 + \frac{\kappa\tau}{(1 - D_v\Delta)^2})\partial_t u(\boldsymbol{x}, t) = \{\epsilon + D_u\Delta - \frac{1}{1 - D_v\Delta}\}u(\boldsymbol{x}, t) - f(u\boldsymbol{x}, t) \tag{5.27}$$

$$\partial_t u(\boldsymbol{x}, t) = \{1 - \frac{\kappa\tau}{(1 - D_v\Delta)^2}\}\{L(\Delta)u(\mathbf{x}, t) - f(u(\boldsymbol{x}, t))\} \tag{5.28}$$

where we denote the $L(\Delta)$ term for simplicity as

$$L(\Delta) = (\epsilon + D_u\Delta - \frac{1}{1 - D_v\Delta})$$

Hence the activator equation can be simplified finally as

$$\partial_t u(\boldsymbol{x}, t) = \{L(\Delta) - \kappa\tau \frac{L(\Delta)}{(1 - D_v\Delta)^2}\} u(\boldsymbol{x}, t) - (1 - \frac{\kappa\tau}{(1 - D_v\Delta)^2}) f(u(\boldsymbol{x}, t)) \quad (5.29)$$

No we can consider the advective term and obtain the final result (5.20), stated above.

5.2 Numerical Results of Spiral Defect Chaos in Reaction Diffusion Systems

As we have shown in the previous section, it has been possible to derive generalized Swift-Hohenberg equations for our two-component reaction diffusion system in the limiting case $\tau \to 0$, $D_v - D_u > 0$, $D_v - D_u$ small. Therefore, we expect that states similar to spiral defect chaos can, in principal, be observed in reaction diffusion systems. We remind the reader, however, that this spiral defect chaos has nothing to do with spiral waves, e.g. observed in Belousov-Zhabotinsky reactions.

Figures (5.1), (5.2) exhibit patterns of the activator field obtained from numerical solutions of the advection reaction diffusion system (left coulum) with patterns emerging without coupling to the velocity field (right coulum). In both cases, random initial conditions had been choosen. Without advection the patterns evolve into so-called labyrinths, the coupling to advection leads to the emergence of patterns similar to spiral defect chaos.

Figures (5.3), (5.4) show that the sign of α in the mean field equation has an influence on the emerging patterns. For positive values of α spiral defect chaos is observed. For negative values of α disordered patterns emerge. Here, the wavelength of the cellular structures apparently is smaller than for the spiral defect chaotic patterns.

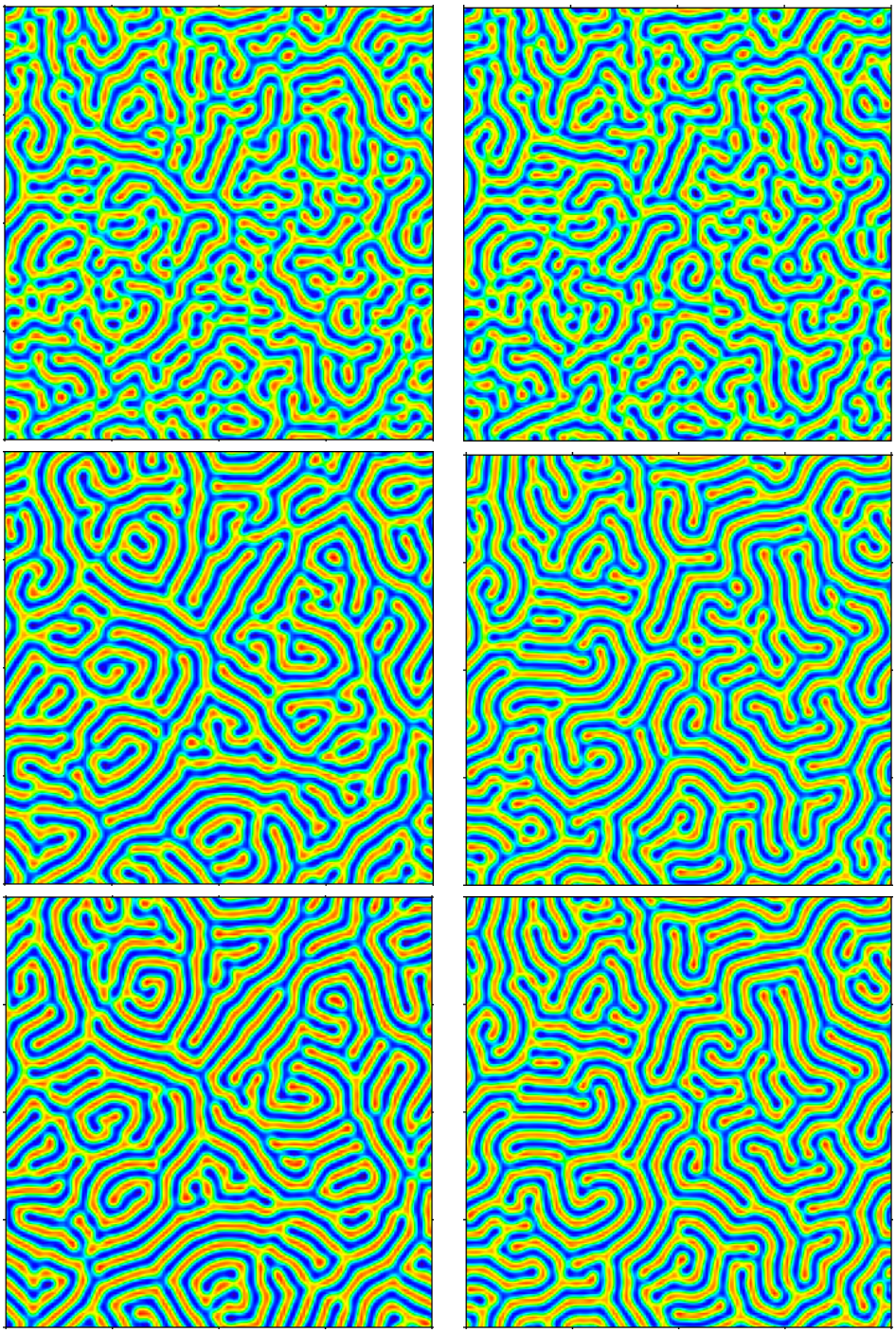

Figure 5.1 Starting from random initial conditions: Spiral defect chaos is developed, as shown in the activator field (left column), for the case of advection $\alpha = 1.15$. Labyrinths emerge without advection $\alpha = 0.0$ (right column). Patterns are shown at the same time instants, while all other parameters are equal for both cases: $D_u = 1.5e-4$, $D_v = 2D_u$, $\epsilon = 0.96$, $\tau = 0.01$, $\kappa = 1$. Time step for calculation was $dt = 0.02$, $resolution = 128 \times 128$, system length=2

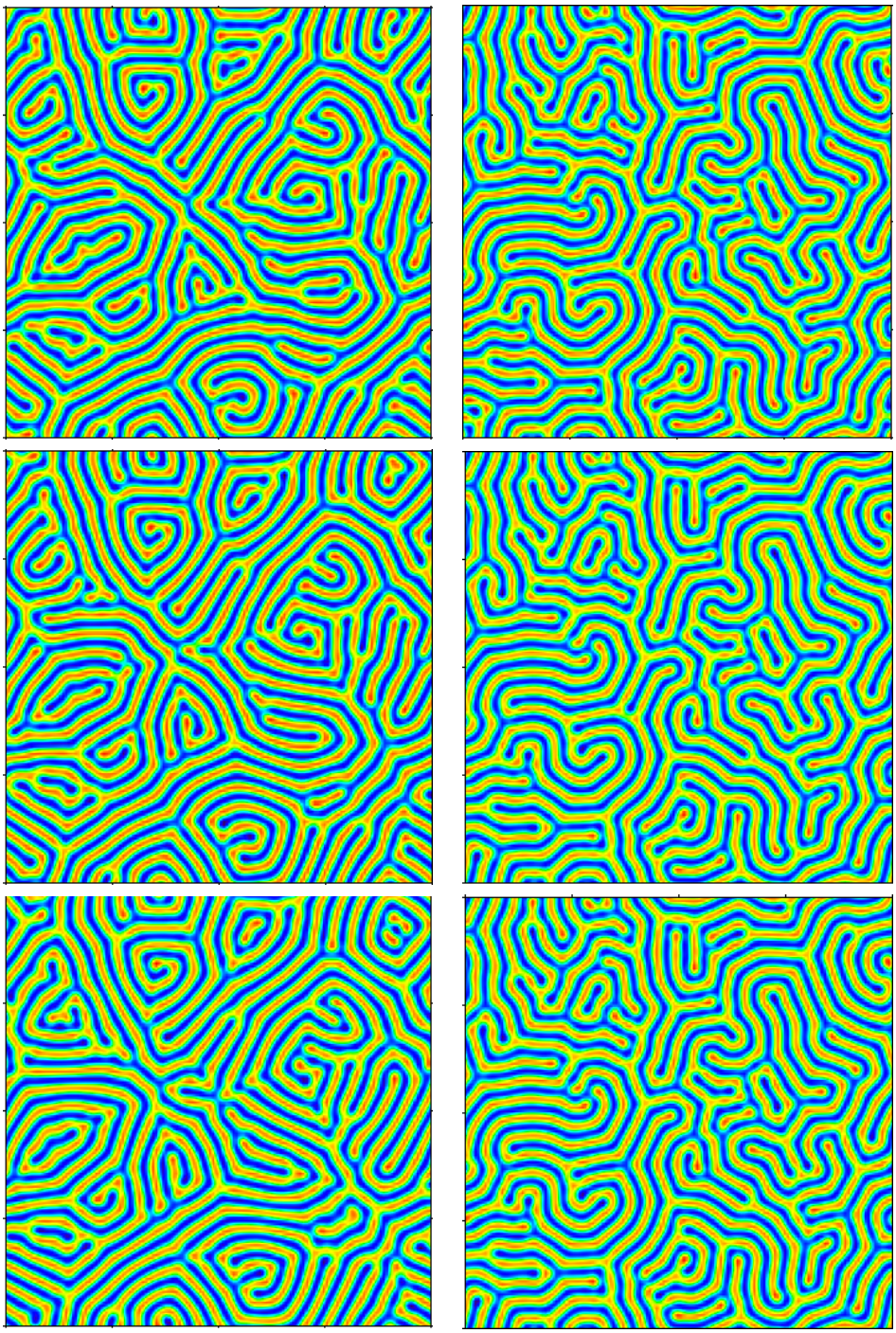

Figure 5.2 Continuation of above case, fig. (5.1): Spiral defect chaos is developed, as shown in the activator field (left column), for the case of advection $\alpha = 1.15$. Labyrinths emerge without advection $\alpha = 0.0$ (right column). Patterns are shown at the same time instants, while all other parameters are equal for both cases: $D_u = 1.5e-4$, $D_v = 2D_u$, $\epsilon = 0.96$, $\tau = 0.01$, $\kappa = 1$. Time step for calculation was $dt = 0.02$, $resolution = 128 \times 128$, system length=2.

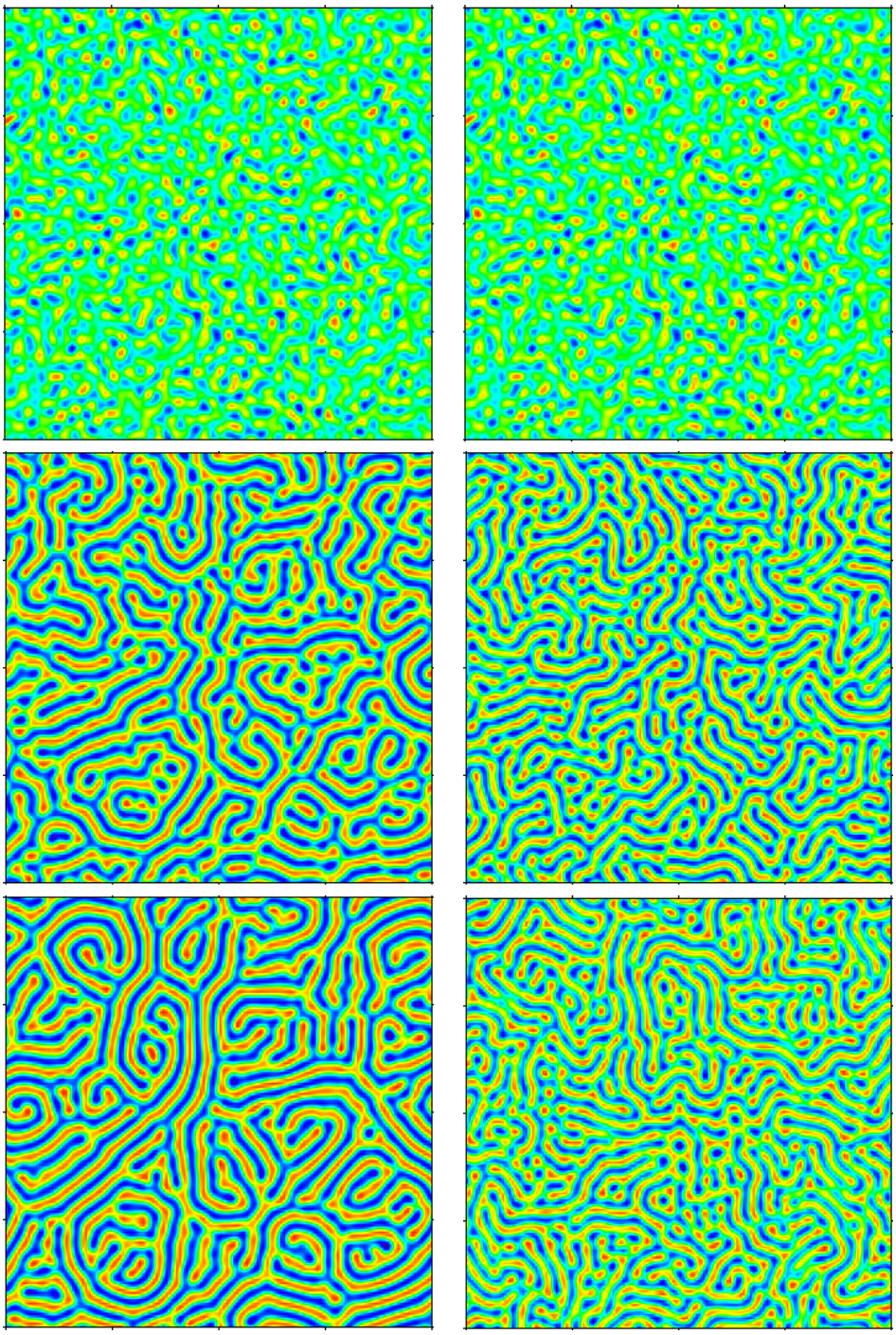

Figure 5.3 Starting from random initial conditions: Spiral defect chaos is developed in the presence of advection, $\alpha = 3.0$. In the right column, the field is shown for the case $\alpha = -3.0$ at the same time intervals. Disordered cellular patterns are observed. For both cases the parameters are $D_u = 1.5e-4$, $D_v = 2D_u$, $\epsilon = 0.96$, $\tau = 0.01$, $\kappa = 1$. Time step is $dt = 0.02$,$resolution = 128 \times 128$, system length=2.

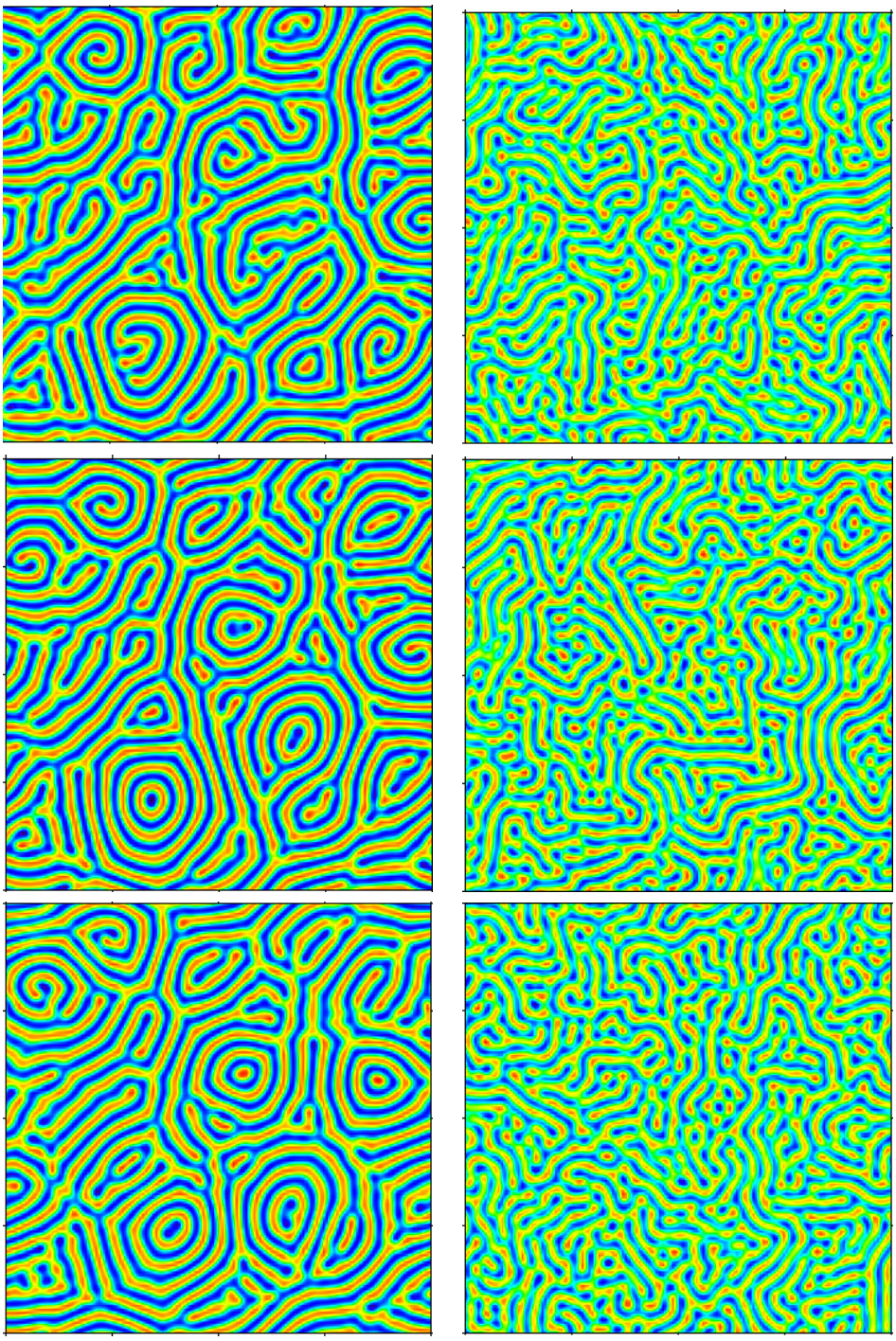

Figure 5.4 Continuation of the fig. 5.3: Spiral defect chaos is developed in the presence of advection, $\alpha = 3.0$. In the right column, the field is shown for the case $\alpha = -3.0$ at the same time intervals. Disordered cellular patterns are observed. For both cases the parameters are $D_u = 1.5e - 4$, $D_v = 2D_u$, $\epsilon = 0.96$, $\tau = 0.01$. Time step is $dt = 0.02$, $resolution = 128 \times 128$, system length=2

5.3 Development of Fractal Like Structures

5.3.1 A Brief History of Fractals

In 1967 Benoit Mandelbrot developed the concept of a fractal object. He was interested in the shapes of coastlines of islands and revealed that they are best characterized by a scaling behaviour, dependent on the resolution used for measuring this length [54]. He found out that such boundaries are characteristic for Nature, and termed the objects as fractal. The term *fractal* comes from the Latin word 'Fractus' meaning fractured or irregular [73].

Fractal structures have been known since long ago. For example, George Christoph Lichtenberg, a German Physicist discovered in his laboratory a two dimensional pattern on the dust settled on electrostatically charged resin plates in early 1700s, which were named Lichtenberg figures. These are actually produced by passing high voltage on the surface of the electrical insulators [2]. He used high voltage currents to charge the insulating surfaces like glass, rubber etc. He used then powdered lead and sulfur on the charged surface so that sulfur being negatively charged was attracted to the positive charges and lead being positively charged was attracted to the negative charges. The result are the famous Lichtenberg patterns. Two examples are shown in figs. (5.5), (5.6).

In the following we shall show, based on numerical calculations of the advection-reaction-diffusion systems, eqs. (5.1), (5.2), (5.3), that fractal like behaviour emerge in certain parameter regimes also in this model system. This fractal behaviour is based on an instability of fronts. Crucial for the process is the coupling of reaction-diffusion process to advection.

It is well-known that the two-component reaction-diffusion system (5.1) and (5.2) has front solutions due to the fact that there are two stable, spatially homogeneous solutions determined by the set of equations

$$\begin{aligned} 0 &= \epsilon u - u^3 - \kappa v \\ 0 &= -v + u \end{aligned} \tag{5.30}$$

The two stable states are given by

$$u = \pm\sqrt{\epsilon - \kappa} \qquad , \qquad v = \pm\sqrt{\epsilon - \kappa} \tag{5.31}$$

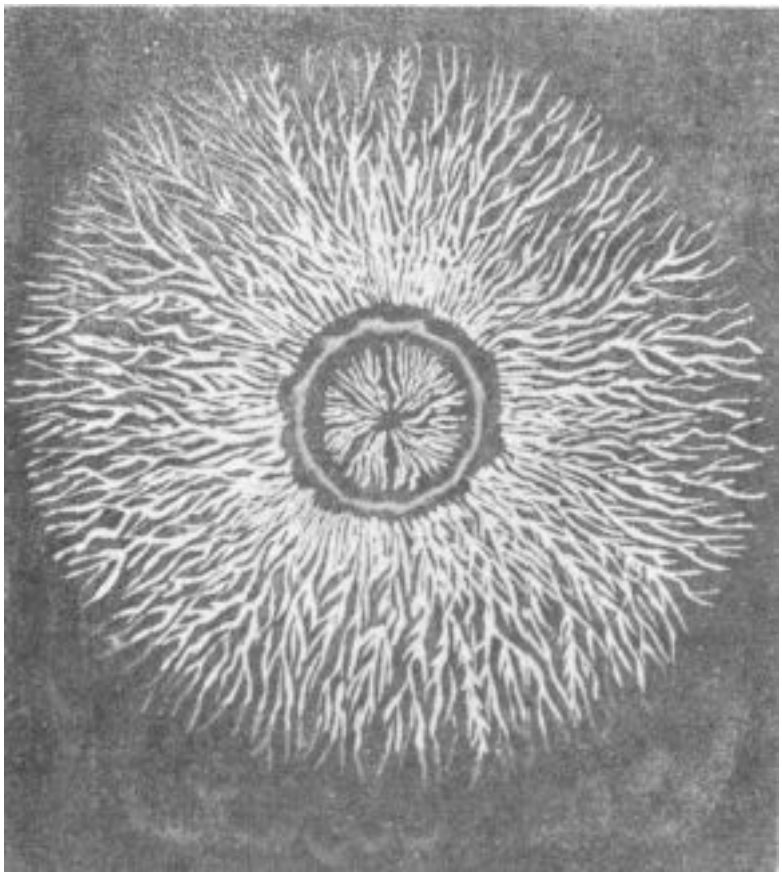

Figure 5.5 Positive Lichtenberg Figure (courtesy of website[1])

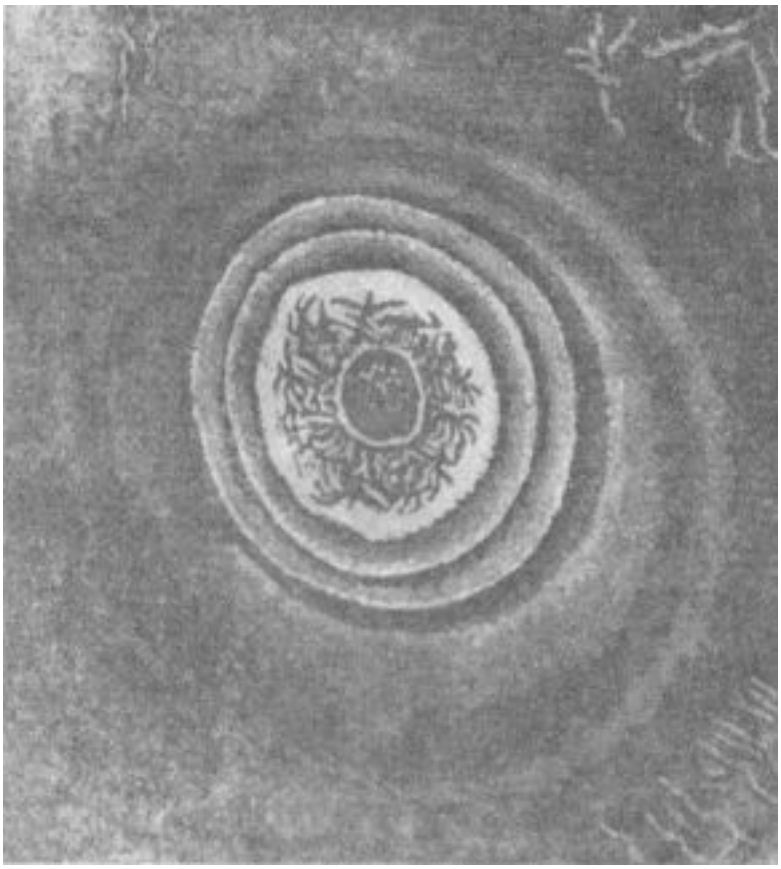

Figure 5.6 Negative Lichtenberg Figure (courtesy of website[1])

A stationary front connects these two different states. Its form is entirely determined by the dynamical system

$$D_u \frac{\partial^2}{\partial x^2} u = -(\epsilon u - u^3) + \kappa v$$
$$D_v \frac{\partial^2}{\partial x^2} v = v - u \tag{5.32}$$

We have performed numerical simulations of the basic model equations (5.1), (5.2), (5.3) in a control parameter region, where the two stable states (5.31) exist, i.e., $\epsilon > \kappa$

Our numerical solutions show that, for positive values of α the fronts are unstable eventually leading to fractal like boundaries between the two stationary homogeneous states, resembling Mandelbrot's fractal coastlines of islands.

Examples are shown in figs. (5.7) and (5.8). We show the mean field on the left hand side and on the right hand side the activator field. Starting from a simple circular spot we show how instability sets in.

The control parameter α which is a measure for the back-reaction of the induced velocity field plays a crucial role. For the model of interface reaction introduced in the previous section α is related to the magnitude of surface tension. For the model of active media, it is related to the additional stress induced by the undrlaying microstructure of the active media. As fig. (5.11) indicates, there is no front instability for the case of negative values of α.

5.3.2 Power Law Behavior

In this subsection we want to show that the above argument about the fractal behavior is true. To this end we introduce a quantity, which measures the fractal behaviour of the boundary. The relevant quantity is the length of the front, taken from the idea of Mandelbrot on the fractal nature of coastlines. To estimate this quantity directly from the fields $u(\boldsymbol{x}, t)$ and $v(\boldsymbol{x}, t)$ we remind the reader that the quantity

$$(\nabla u(\boldsymbol{x}, t))^2 + (\nabla v(\boldsymbol{x}, t))^2 \tag{5.33}$$

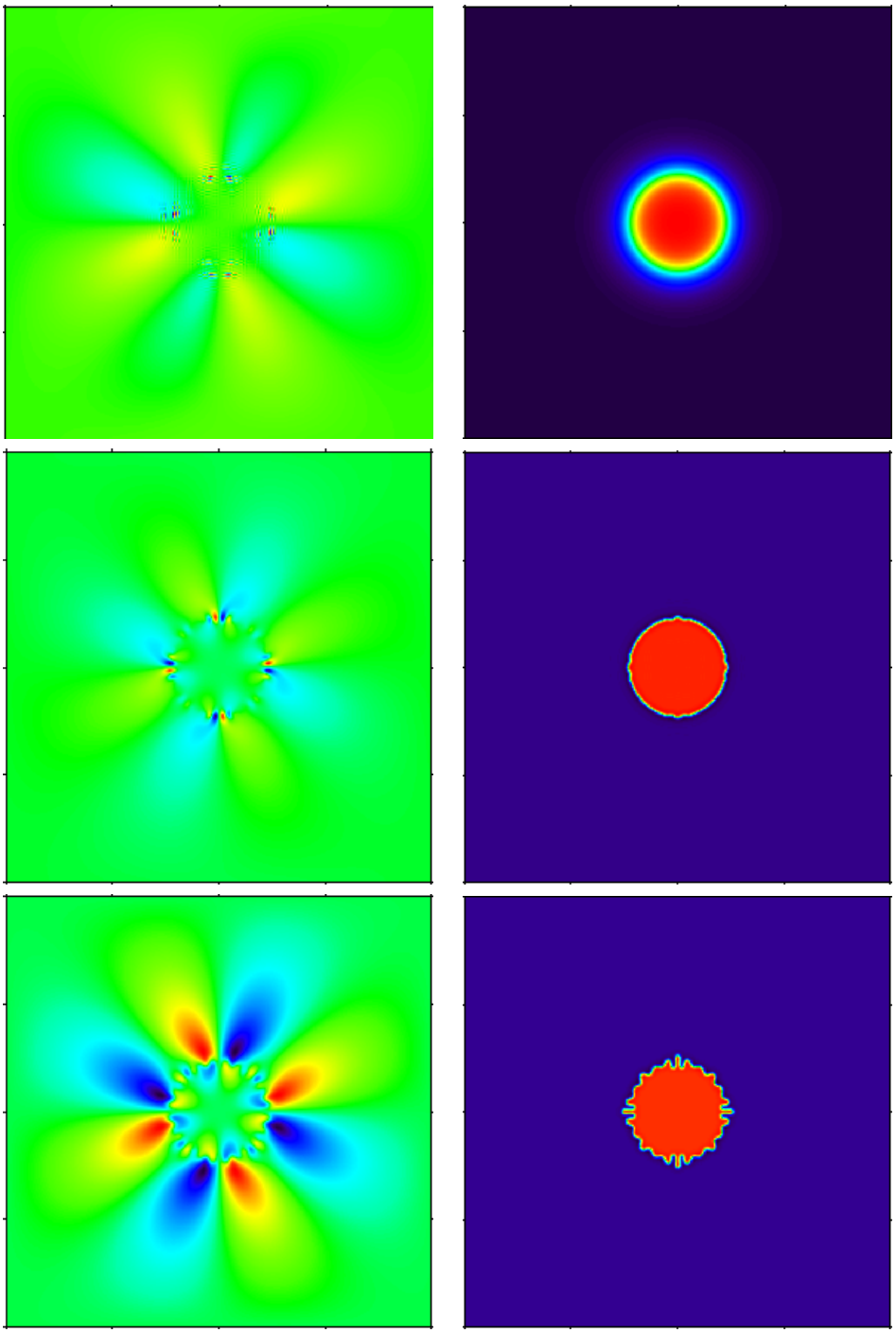

Figure 5.7 Instability of front starting from a small spot: Mean field on left hand column and Activator on right hand column with parameters at $\alpha = 5.0$, $D_u = 1.5e-4$, $D_v = 2D_u$, $\epsilon = 2.5$, $\tau = 0.005$, $\kappa = 1$. Time step was $dt = 0.0001$, resolution 256×256, system length=4.

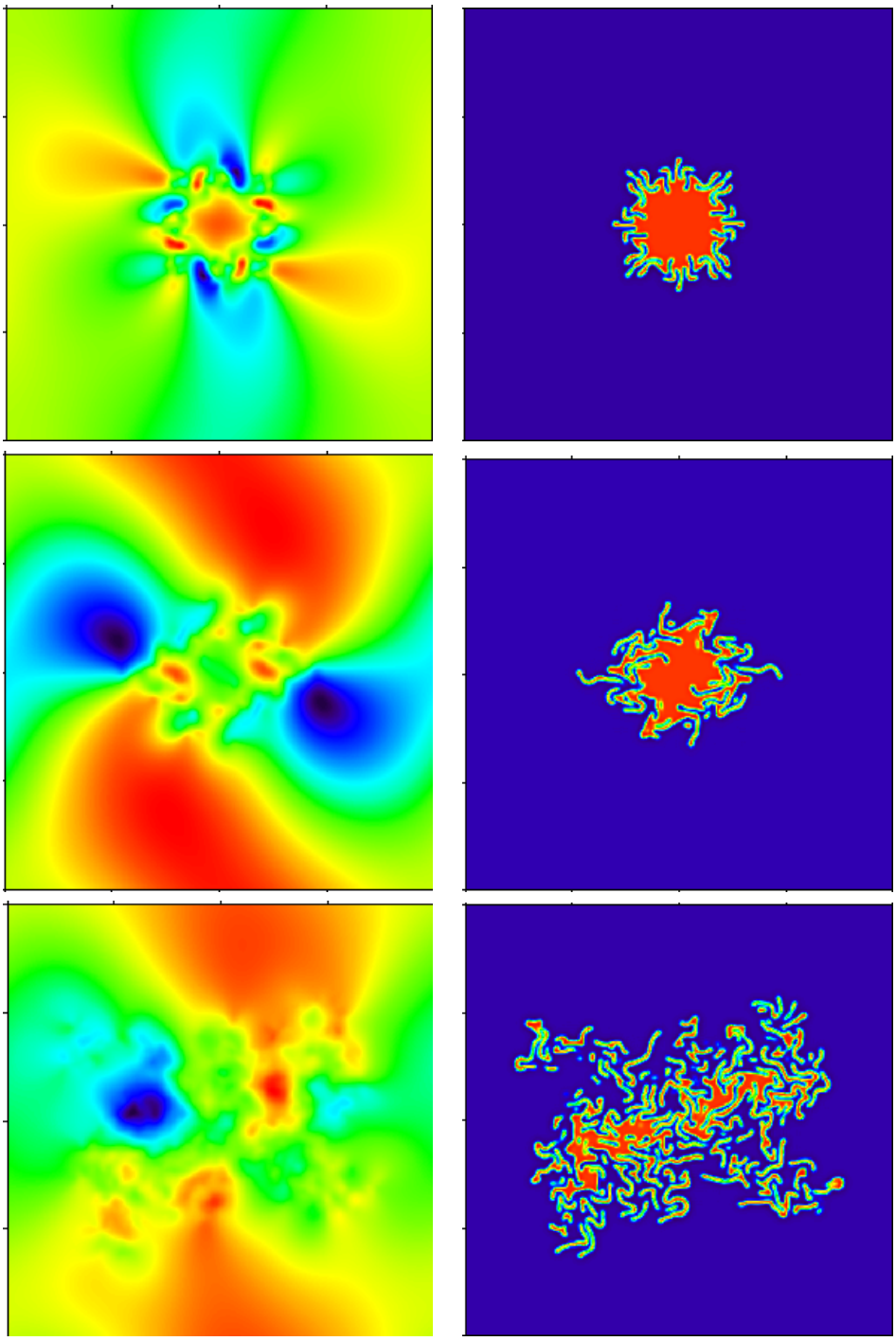

Figure 5.8 Continuation of the fig. (5.7): Instability of front starting from a small spot: Mean field on left hand column and Activator on right hand column with parameters at $\alpha = 5.0$, $D_u = 1.5e-4$, $D_v = 2D_u$, $\epsilon = 2.5$, $\tau = 0.005$, $\kappa = 1$. Time step was $dt = 0.0001$, resolution 256×256, system length=4.

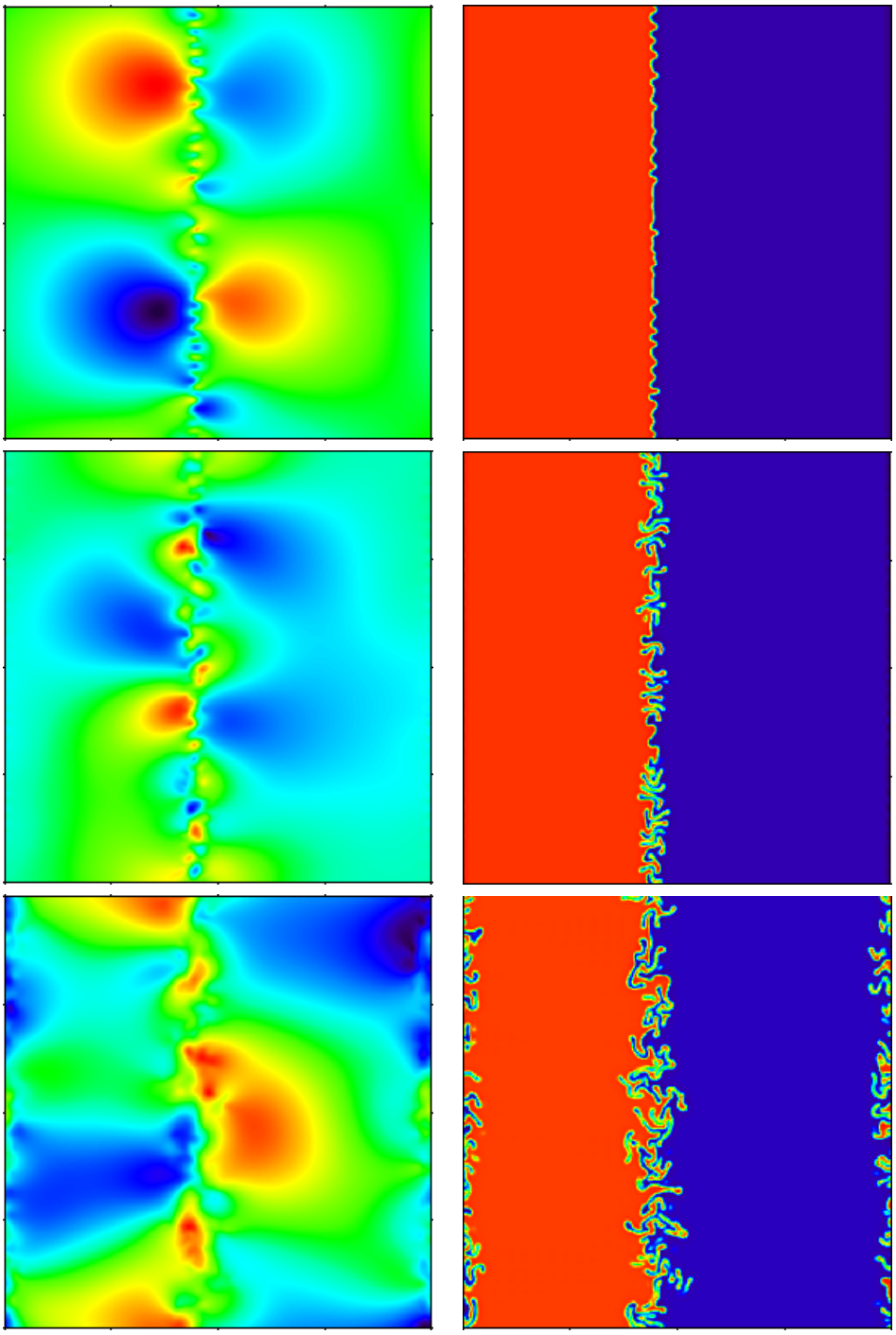

Figure 5.9 Instability of planar fronts: Mean field on left hand column and activator on right hand column for the parameters $\alpha = 10.0$, $D_u = 1.5e-4$, $D_v = 2D_u$, $\epsilon = 2.5$, $\tau = 0.005$, $\kappa = 1$. Time step was $dt = 0.0001$, resolution 256×256, system length=4.

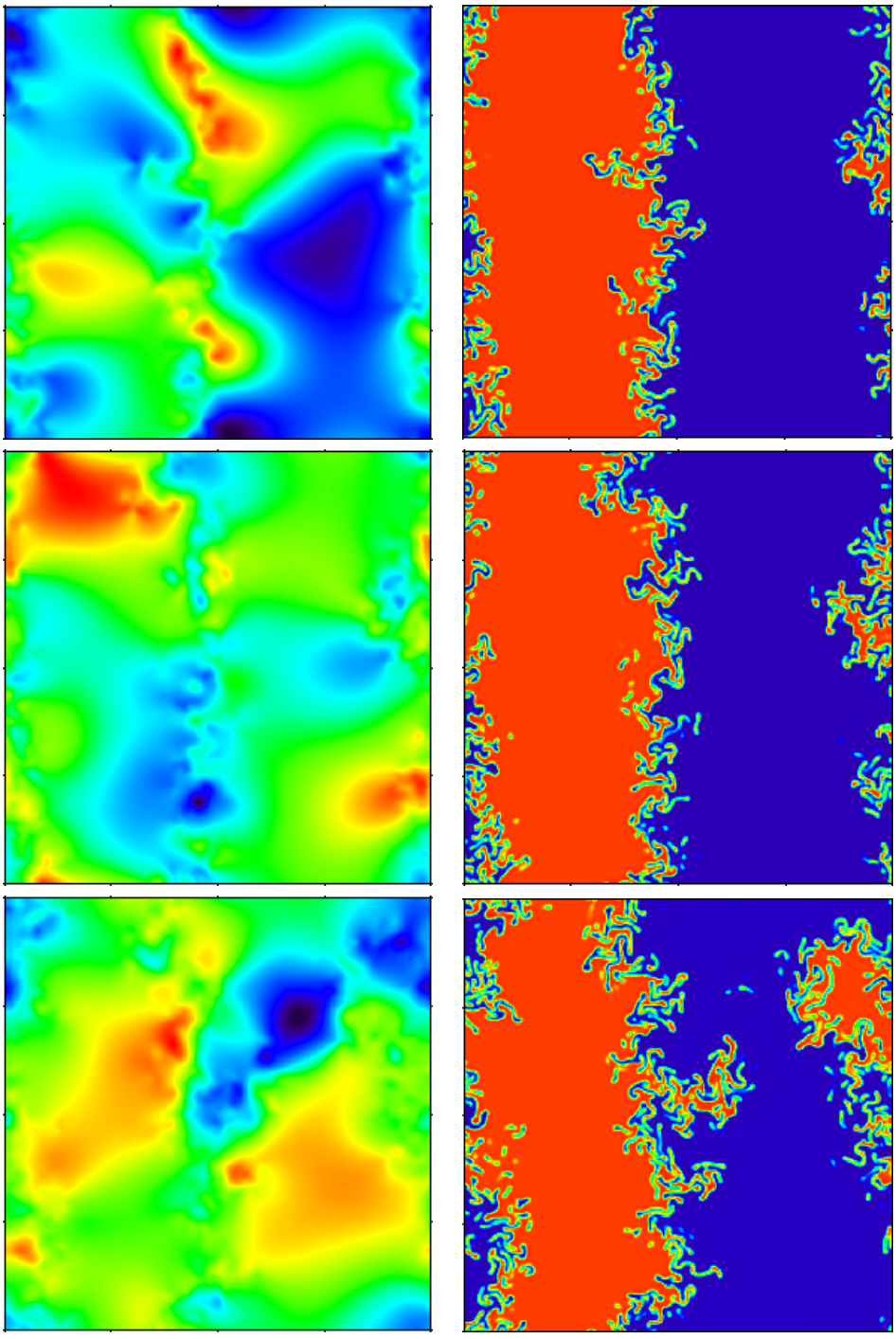

Figure 5.10 Continuation of fig. (5.9): Mean field on left hand column and Activator on right hand column at with parameters $\alpha = 10.0$, $D_u = 1.5e-4$, $D_v = 2D_u$, $\epsilon = 2.5$, $\tau = 0.005$, $\kappa = 1$. Time step was $dt = 0.0001$, resolution 256×256, system length=4.

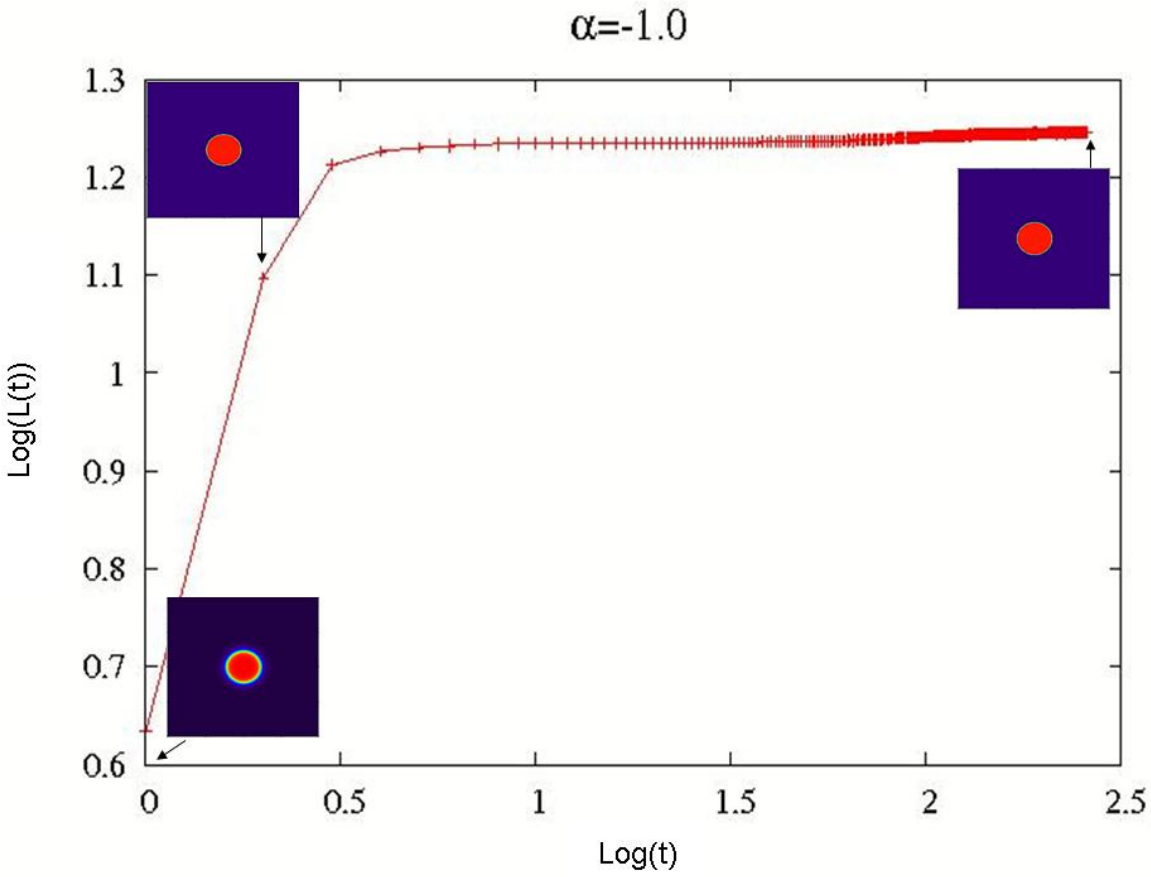

Figure 5.11 Graph showing different stages of the dynamics of activator field, where $\alpha = -1.0$, $dt = 0.0001$,$resolution = 256 \times 256$, system length=4.

is located at the front. As a consequence, the quantity

$$L(t) = \int d\boldsymbol{x}\{(\nabla u(\boldsymbol{x},t))^2 + (\nabla v(\boldsymbol{x},t))^2\} \tag{5.34}$$

is a direct estimate of the length of the curve. In fig. (5.12) we have plotted the logarithm of $L(t)$ with respect to the logarithm of time for various values of positive αs. It is seen that there exist different regimes with different slopes γ:

$$L(t) \approx t^{\gamma} \tag{5.35}$$

The slope $\gamma = 1$ belongs to a nonfractal growth, usually seen at the onset of instability. However, if fractal growth sets in, the curves become steeper indicating $\gamma > 1$.

If we compare computations with different values of α we can see first that this control parameter plays a decisive role in the development of fractal like structures. Also from fig(5.13), fig.(5.14) and fig(5.15), we show that the temporal evolution of the instabibility in the three cases is different. This is not surprising since we expect that the temporal dynamics is chaotic and sensitivity with respect to initial disturbances influences the fine details of the temporel evolution.

5.4 Summary and Results

In this chapter we have show that, for certain values of the control parameters, the advection reaction diffusion system, eqs. (5.1), (5.2), 5.3) can be reduced to the generalized Swift-Hohenberg equation with mean flow, exhibiting spiral defect chaos patterns. Consequently, we were able to find such patterns also in the chemical system under consideration. Furthermore, approaching regimes of control parameters, where the chemical kinetics exhibits bistability, we found that chemical fronts may become unstable leading to the emergence of fractal type boundaries separating the two different chemical phases. Our findings suggest to view the emergence of spiral defect chaos in connection with instabilites of fronts induced by the back-reaction of advection onto the chemical kinetics. Further studies could be devoted to the investigation of the formation of fractal boundaries.

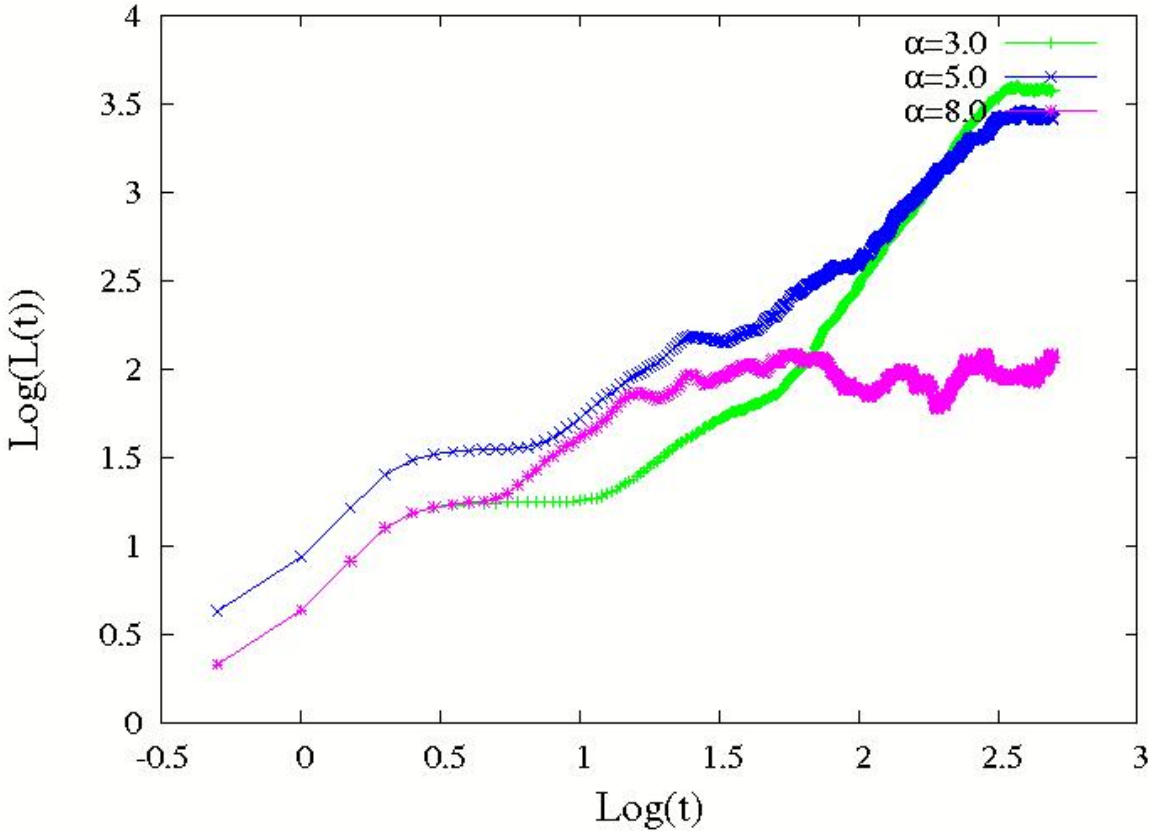

Figure 5.12 Graph summarizes the behavior of the instability at different values of surface tension coefficient, where red line denotes $\alpha = 3$, green color shows at $\alpha = 5$, blue color shows at $\alpha = 8$

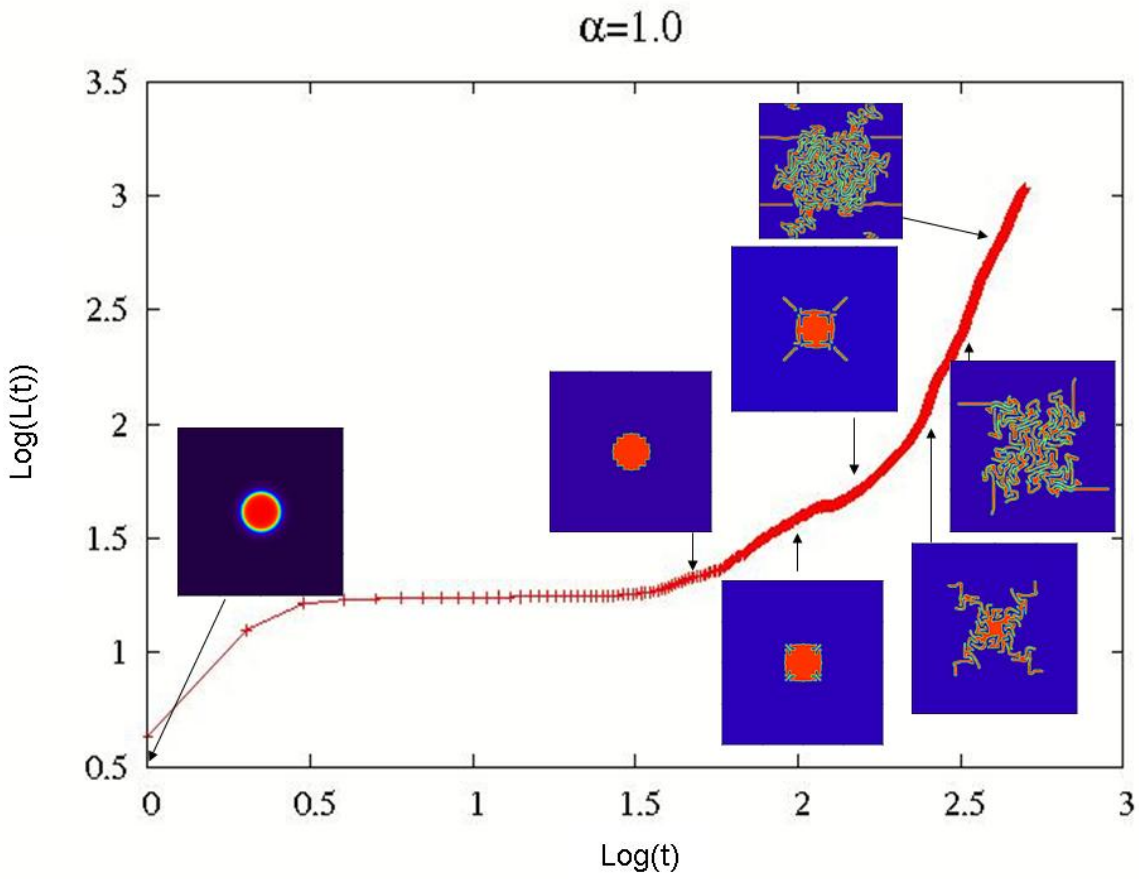

Figure 5.13 Graph showing different stages of the development of fractal boundaries in time. Parameters: $\alpha = 1.0$, $dt = 0.0001$,$resolution = 256 \times 256$, system length=4.

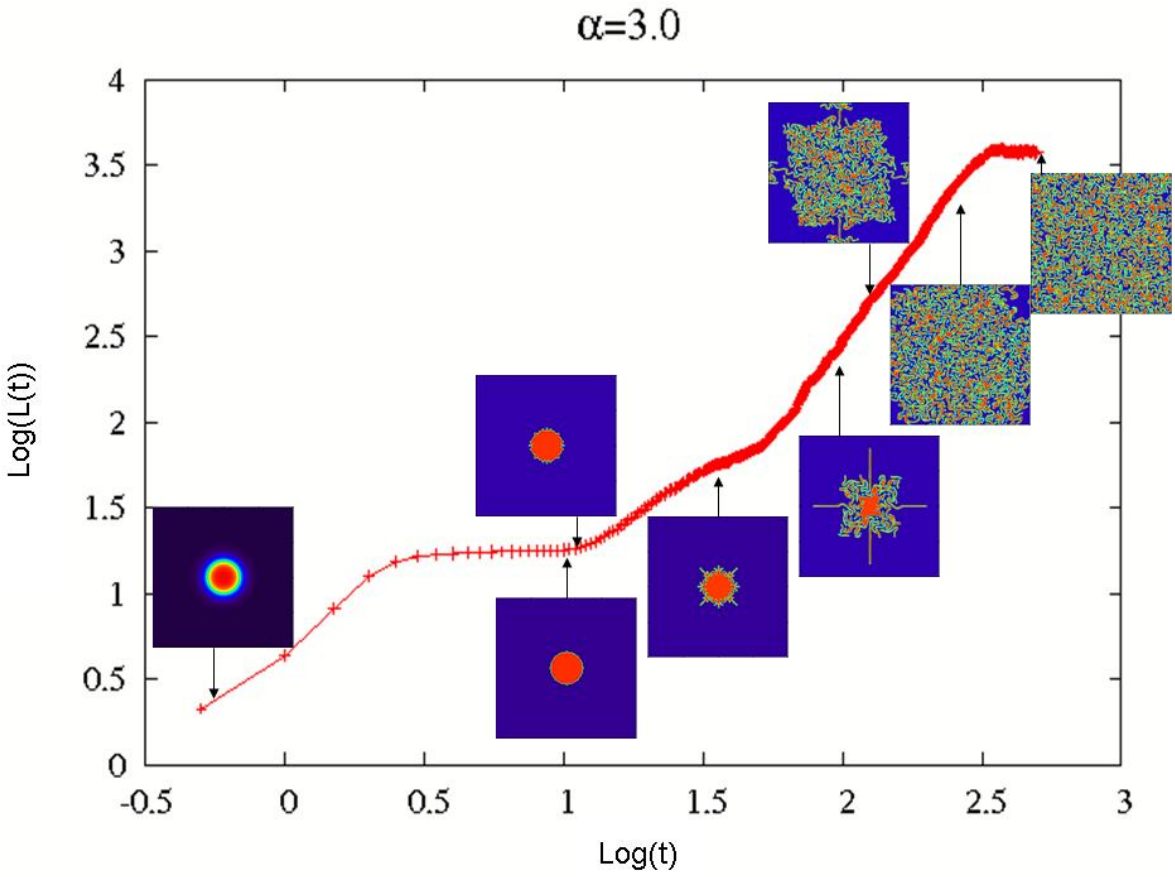

Figure 5.14 Graph showing different stages of the development of fractal boundaries in time. Parameters: $\alpha = 3.0$, $dt = 0.0001$,$resolution = 256 \times 256$, system length=4.

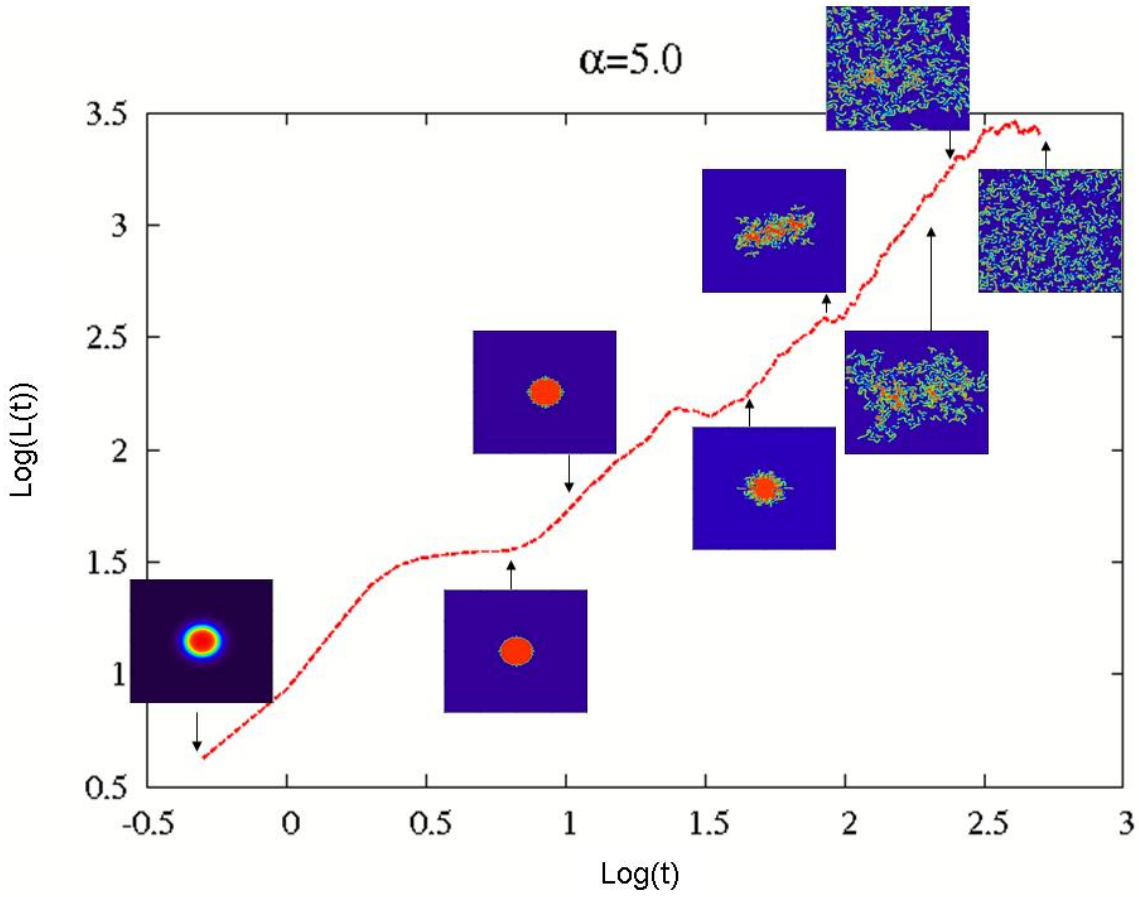

Figure 5.15 Graph showing different stages of the development of fractal boundaries in time. Parameters: $\alpha = 5.0$, $dt = 0.0001$,$resolution = 256 \times 256$, system length=4.

6 Fractal Evolution of Fronts

The investigation of fronts in non-equilibrium pattern formation has a long tradition. The history of studies of front propagation, relevant for the present work, started with the seminal work of Fisher [36] and Kolmogorov, Petrovskii, and Piscounov [5]. They explicitly demonstrated the existence of moving fronts in a reaction-diffusion equation for a single chemical concentration. Since then, the investigation of reaction fronts has been an important topic in the field of chemical reactions far from equilibrium.

In principle, two different problems have to be addressed investigating the spatio-temporal evolution of fronts in non-equilibrium systems. The first problem is concerned with the investigation of fronts between stable and unstable states of a system. It is evident that the front moves into the direction of the unstable state eventually leaving the system in its stable state. Here, the main issue is the determination of the selected velocity of the moving front, since there are continuously many front solutions differing in their propagation velocity, as can be seen from the Fisher-Kolmogorov-Petrovskii-Piscounov equation.

Let us briefly touch this aspect, although this problem will not be addressed in the following. According to von Saarloos [78], *Associated with any given unstable state is a well defined and easily calculated so called "linear" spreading velocity $v*$, the velocity with which arbitrarily linear small perturbations about the unstable state grow out and spread according to the dynamical equations obtained by linearising the full model about the unstable state; nonlinear fronts can either have their asymptotic speed v_{as} equal to $v*$ (a so called pulled front) or larger than $v*$ (pushed front).*

An experiment on Taylor vortex flow in a Taylor Couette flow by Ahlers and Cannell [9] is very illuminating as the measured velocity of the front between Taylor vortices and basic Couette flow differed from the calculated one. Nevertheless the experimental work of Fineberg and Steinberg [35] on the velocity of fronts in Rayleigh-Bénard convection agreed well with the theoretical predictions and

they were successful also in measuring the wavelength of roll pattern. Up to now, it seems that the question of the selection of the front velocity is still an open problem. We refer the reader to the review article of von Saarloos [78].

The other important issue in the investigation of fronts in non-equilibrium systems is concerned with the instability of planar or curved fronts. This has been studied in relationship to flame instabilities in the work of Sivashinsky [70]. For an overview we refer to the recent monograph of Pelce [59]. Of considerable interest is the growth of fractal boundaries arising, e.g. in dendritic growth. The field caught its attention by physicists in early 1980's when Dee [27] and coworkers studied dendritic growth, and a variety of models have been formulated [33].

Fractal growth behavior of fronts have also been detected by Lega and Passot [50] within there model for the growth of bacterial colonies. In the previous chapter, we have also found fractal growth of fronts in the investigated advection diffusion reaction models.

In this chapter we want to derive the evolution equation which describes the instability of boundaries between different states in reaction-diffusion equations eventually leading to fractal fronts. We have already observed their appearance in the previous chapter in the case of activator-inhibitor model. Here, the instability sets in due the presence of advection. The aim is to understand the dynamics between chemical kinetics and hydrodynamics leading to instability of the planar front.

Front instabilities as discussed in the present section are relevant for a large variety of systems ranging from processes in the atmosphere and the ocean to industrial chemical reactors where the transport of chemicals in the solution is a must. The spatio-temporal dynamics in these systems is certainly more complex due to the variation in the density, pressure, viscosity etc. However, the treatment of idealized systems yields important insight into the spatio-temporal properties of fronts in systems far from equilibrium.

6.1 Zeldovich Equation

In order to investigate the interplay between hydrodynamics and chemical kinetics, we consider a one-component reaction-diffusion system consisting of a single species. Furthermore, we deal with a bistable system having two stable states

separated by an unstable one. Such systems allow for the existence of stationary domain walls separating the two states. They can be modeled by the Zeldovich-Frank- Kamenetski equation which originally has been developed to discuss phenomenon related with flame propagation [82].

$$\dot{\psi} = \varepsilon\psi - \psi^3 + D\Delta\psi \tag{6.1}$$

This equation allows for front solutions. An example of a stationary front is depicted in fig.(6.1). The two stable homogeneous states are at $\psi = \pm\sqrt{\varepsilon}$ and the unstable state is $\psi = 0$.

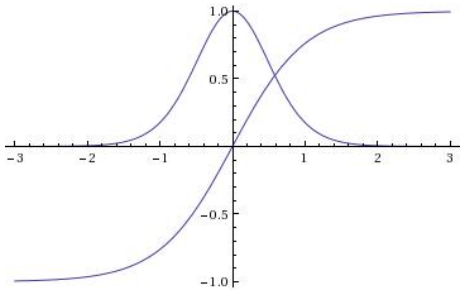

Figure 6.1 A stationary front in a bistable system. The slope of the front between two stable states is given by $\frac{\varepsilon}{\sqrt{2D}}$

6.1.1 Advection in the Zeldovich-Equation

In the following we shall extend our treatment to the case where advection is taken into account. Adding the advection term to above eq.(6.1), we obtain this equation as

$$\dot{\psi} + \boldsymbol{U} \cdot \nabla\psi = \varepsilon\psi - \psi^3 + D\Delta\psi \tag{6.2}$$

We can either consider the velocity field $\boldsymbol{U}$ to be given, in which case we would consider the advection of a passive scalar field $\psi(\boldsymbol{x}, t)$, which, however, exhibits nonlinear effects. On the other hand, we can consider the case where the velocity field is generated by the concentration field $\psi(\boldsymbol{x}, t)$ itself.

Since we consider a two dimensional system the velocity field can be represented in terms of the stream function $\chi(\boldsymbol{x}, t)$ according to

$$\boldsymbol{U} = \nabla \times \mathbf{e}_z\chi$$

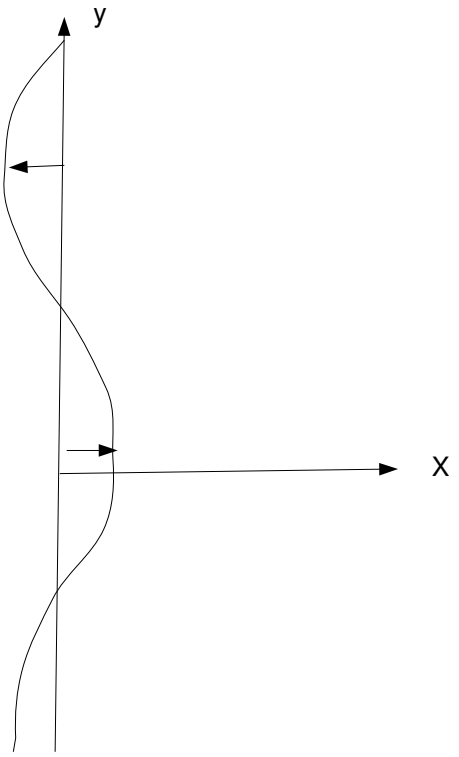

Figure 6.2 Front propagation due to the advection in Y direction

.

The stream function is determined by the basic fluid dynamic equation, neglecting inertia of the fluid,

$$G(-\Delta)^{(-1)}\chi(\boldsymbol{x},t) = \alpha \mathbf{e}_z \cdot [\nabla\psi(\boldsymbol{x},t) \times \nabla\Delta\psi(\boldsymbol{x},t)] \tag{6.3}$$

Here, we have introduced the operator $G(-\Delta)^{(-1)}$, which in general is a differential operator. For the model, which relates the fluid velocity to the concentration field in close analogy to the generalized Swift-Hohenberg equation for spiral defect chaos, we have

$$G(-\Delta)^{(-1)} = (\Delta - c^2)\Delta \tag{6.4}$$

For the model of a surface reaction, the operator $G(-\Delta)^{(-1)}$ has the form

$$G(-\Delta)^{-1}) = (-\Delta)^{3/2}(1 + e^{d\Delta}) \tag{6.5}$$

Both operators are defined via their Fourier transforms.

In the following we shall perform our treatment for a general operator $G(-\Delta)^{(-1)}$. In the case of the Zeldovich equation, it is convenient to replace the quantity $\Delta\psi(\boldsymbol{x}, t)$ with $\dot{\psi}(\boldsymbol{x}, t)/D$. since we can use

$$\Delta\psi = \frac{1}{D}[\dot{\psi} - \epsilon\psi + \psi^3] \tag{6.6}$$

which leads us to the representation

$$G(-\Delta)^{(-1)}\chi(\boldsymbol{x}, t) = \frac{\alpha}{D}\boldsymbol{e}_z \cdot [\nabla\psi(\mathbf{x}, t) \times \nabla\dot{\psi}(\boldsymbol{x}, t)] \tag{6.7}$$

6.2 Front Solution

Let us consider first the front solution of the advection-reaction- diffusion equation, eq. (6.2), given by

$$\psi^0(x - x_0, t) \tag{6.8}$$

Since the cross product $\nabla\psi^0 \times \dot{\nabla}\psi^0$ vanishes identically, the corresponding velocity field vanishes. The front is stationary and is determined by the equation:

$$\varepsilon\psi^0 - (\psi^0)^3 + D\frac{\partial^2}{\partial x^2}\psi^0 = 0 \tag{6.9}$$

It is straightforward to show that the solution reads

$$\psi(x - x_0) = \pm\sqrt{\varepsilon}\tanh\sqrt{\frac{\varepsilon}{2D}}(x - x_0) \tag{6.10}$$

It is exhibited in fig. (6.1). Due to translational symmetry, the position x_0 of the front is arbitrary.

6.3 Evolution of Fronts

In the following we shall be interested in moving fronts and instabilities, which are induced by a spatial variation of the planar front (6.10). To this end we shall perform the ansatz

$$\psi = \psi(x - X(y,t), y, t) \tag{6.11}$$

An approximate representation, which should be reasonably good, would be the representation $\psi = \psi^0(x - X(y,t))$, which describes a front located at the position $X(y,t)$. For the following we introduce the time dependent coordinate

$$\xi = x - X(y,t) \tag{6.12}$$

We now insert our ansatz into eq. (6.2). First, we have to determine the time derivative and the gradient terms.

$$\dot{\psi} = -\dot{X}(Y,t)\frac{\partial \psi}{\partial \xi} + \frac{\partial \psi}{\partial t} \tag{6.13}$$

$$\frac{\partial \psi}{\partial x} = \frac{\partial \psi}{\partial \xi} \tag{6.14}$$

$$\frac{\partial \psi}{\partial y} = -\frac{\partial X}{\partial y}\frac{\partial \psi}{\partial \xi} + \frac{\partial \psi}{\partial y} \tag{6.15}$$

The Laplacian reads

$$\Delta\psi = \frac{\partial^2 \psi}{\partial \xi^2} - \frac{\partial^2 X}{\partial y^2}\frac{\partial \psi}{\partial \xi} + (\frac{\partial X}{\partial y})^2\frac{\partial^2 \psi}{\partial \xi^2} + \frac{\partial^2 \psi}{\partial y^2} - \frac{\partial X}{\partial Y}\frac{\partial^2 \psi}{\partial \xi \partial y} \tag{6.16}$$

Collecting all these terms in eq.(6.2), we get

$$\begin{aligned} -\dot{X}\frac{\partial \psi}{\partial \xi} + \frac{\partial \psi}{\partial t} + U_x\frac{\partial \psi}{\partial \xi} - U_y\frac{\partial X}{\partial y}\frac{\partial \psi}{\partial \xi} + U_y\frac{\partial \psi}{\partial y} = \\ \varepsilon\psi - \psi^3 + D[\frac{\partial^2}{\partial \xi^2} + \frac{\partial^2}{\partial y^2} + (\frac{\partial X}{\partial y})^2\frac{\partial^2}{\partial \xi^2}]\psi - D\frac{\partial^2 X}{\partial y^2}\frac{\partial \psi}{\partial \xi} \end{aligned} \tag{6.17}$$

Rearranging the terms we obtain

$$\frac{\partial\psi}{\partial\xi}[-\dot{X}(y,t)+U_x-U_y\frac{\partial X(y,t)}{\partial y}+D\frac{\partial^2 X(y,t)}{\partial y^2}]+\frac{\partial\psi}{\partial t}$$
$$+U_y\frac{\partial\psi}{\partial y}=\varepsilon\psi-\psi^3+D(\frac{\partial^2}{\partial\xi^2}+\frac{\partial^2}{\partial y^2}+(\frac{\partial X}{\partial y})^2\frac{\partial^2}{\partial\xi^2})\psi \tag{6.18}$$

This equation can now be used to perform our approximation, trying to replace ψ by the expression of the planar front

$$\psi(x-X(y,t),y,t)=\psi^0(x-X(y,t))=\psi^0(\xi) \tag{6.19}$$

We recognize that the derivative of this function with respect to ξ, $\frac{\partial}{\partial\xi}\psi^0(\xi)$ is a function, which is strongly localized at $\xi=0$, i.e. at $x=X(y,t)$. Therefore, we can replace the velocity field $\boldsymbol{U}(x,y,t)$ with $\boldsymbol{U}(\mathbf{X}(y,t),y,t)$. Furthermore, we assume that

$$\psi^0(x-X(y,t))(\frac{\partial X(y,t)}{\partial y})^2 \tag{6.20}$$

is small and, hence, can be disregarded.

These approximations leads us to the evolution equation for the front location $X(y,t)$ in the form

$$\dot{X}(y,t)+U_y(X(y,t),y)\frac{\partial X(y,t)}{\partial y}=U_x(X(y,t),y)+D\frac{\partial^2 X(y,t)}{\partial y^2} \tag{6.21}$$

This evolution equation determines the location $X(y,t)$ of the front as a function of time.

The remaining terms in eq. (6.18) determine the front solution $\psi^0(\xi)$,

$$0=\epsilon\psi^0(\xi)-\psi^0(\xi)^3+D\frac{\partial^2}{\partial\xi^2}\psi^0(\xi) \tag{6.22}$$

6.4 Evolution of Velocity Field

In this section we shall calculate the mean field $\mathbf{U}(\mathbf{x},t)$, given in eq.(6.7).

Taking into account the fact that the front is propagating in x-direction,

$$\psi=\psi^0(x-X(y,t))=\psi^0(\xi) \qquad , \tag{6.23}$$

we may express the time derivative as

$$\dot{\psi}^0 = -\dot{X}(y,t)\frac{\partial \psi^0}{\partial \xi} \tag{6.24}$$

Furthermore, we calculate the gradient

$$\nabla \psi^0 = \begin{pmatrix} \frac{\partial \psi}{\partial \xi} \\ -\frac{\partial X(y,t)}{\partial y}\frac{\partial \psi}{\partial \xi} \end{pmatrix} \tag{6.25}$$

as well as

$$\nabla \dot{\psi} = \begin{pmatrix} -\dot{X}(y,t)\frac{\partial^2 \psi^0}{\partial \xi^2} \\ -\frac{\partial \dot{X}(y,t)}{\partial y}\frac{\partial \psi^0}{\partial \xi} + \dot{X}(y,t)\frac{\partial X(y,t)}{\partial y}\frac{\partial^2 \psi^0}{\partial \xi^2} \end{pmatrix} \tag{6.26}$$

Using above definitions, the right hand side of eq.(6.7) can be rewritten as

$$(\nabla \psi \times \nabla \dot{\psi}) \cdot \boldsymbol{e}_z = -(\frac{\partial \psi^0}{\partial \xi})^2 \frac{\partial \dot{X}(y,t)}{\partial y} \tag{6.27}$$

The next step consists in determining the stream function. Using the kernel $G(\mathbf{s}-\mathbf{s}')$ defined as the inverse of the operator $G(-\Delta)^{(-1)}$,

$$G(-\Delta)^{(-1)} G(\boldsymbol{x}-\boldsymbol{x}') = \delta(\boldsymbol{x}-\boldsymbol{x}') \tag{6.28}$$

we end up with

$$\begin{aligned} \chi(\boldsymbol{x},t) &= \frac{\alpha}{D}\int d\boldsymbol{x}' G(\boldsymbol{x}-\boldsymbol{x}')\boldsymbol{e}_z \cdot [\nabla \psi^0 \times \nabla \dot{\psi}^0] \\ &- \frac{\alpha}{D}\int d\boldsymbol{x}' G(\boldsymbol{x}-\boldsymbol{x}') \left(\frac{\partial \psi^0(x'-X(y',t))}{\partial x'}\right)^2 \frac{\partial \dot{X}(y',t)}{\partial y'} \end{aligned} \tag{6.29}$$

The velocity field is obtained from the stream function by calculating

$$\begin{aligned} \boldsymbol{U}(\boldsymbol{x},t) &= \nabla_x \times \boldsymbol{e}_z \chi(\boldsymbol{x},t) \\ &= -\frac{\alpha}{D}\int d\boldsymbol{x}' \boldsymbol{K}(\boldsymbol{x}-\boldsymbol{x}')(\frac{\partial \psi^0(x'-X(y',t))}{\partial x'})^2 \frac{\partial \dot{X}(y',t)}{\partial y'} \end{aligned} \tag{6.30}$$

Here, we have defined the vector kernel

$$\boldsymbol{K}(\boldsymbol{x}-\boldsymbol{x}') = \nabla_x \times \boldsymbol{e}_z G(\boldsymbol{x}-\boldsymbol{x}') = \boldsymbol{K}(x-x', y-y') \tag{6.31}$$

We remind the reader that the derivative of the function $\psi(x - X(y,t))^0$ is strongly peaked at the location $X(y,t)$. As a consequence, we can replace the integral

$$\begin{aligned}
&\int dx'dy' \boldsymbol{K}(\boldsymbol{x} - \boldsymbol{x}')(\frac{\partial \psi^0(x' - X(y',t))}{\partial x'})^2 \frac{\partial \dot{X}(y',t)}{\partial y'} \approx \\
&\quad \int dy' \boldsymbol{K}(x - X(y',t), y - y') \frac{\partial \dot{X}(y',t)}{\partial y'} \int dx' (\frac{\partial \psi^0(x' - X(y',t))}{\partial x'})^2 \\
&\quad \approx \delta \int dy' \mathbf{K}(x - X(y',t), y - y') \frac{\partial \dot{X}(y',t)}{\partial y'}
\end{aligned} \tag{6.32}$$

where we have defined the positive quantity

$$\delta = \int dx' (\frac{\partial \psi^0(x' - X(y',t))}{\partial x'})^2 \tag{6.33}$$

Collecting all these terms in the main equation of front eq.(6.21), we arrive at

$$\begin{aligned}
&\dot{X}(y,t) - \frac{\alpha\delta}{D} \int dY' K_y(X(y,t) - X(y',t), y - y') \frac{\partial \dot{X}(y',t)}{\partial y'} \partial_y X(y,t) \\
&= -\frac{\alpha\delta}{D} \int dy' K_x(X(y,t) - X(y',t), y - y') \frac{\partial \dot{X}(y',t)}{\partial y'} + D \frac{\partial^2 X(y,t)}{\partial y^2}
\end{aligned} \tag{6.34}$$

The velocity contains the temporal derivative $\dot{X}(y,t)$. Since to lowest order, $\dot{X}(y,t) = D\frac{\partial^2}{\partial y^2} X(y,t)$ we can approximate

$$\begin{aligned}
&\dot{X}(y,t) - \alpha\delta \int dy' K_Y(X(y,t) - X(y',t), y - y') \frac{\partial^3 X(y',t)}{\partial y'^3} \partial_y X(y,t) \\
&= -\alpha\delta \int dy' K_X(X(y,t) - X(y',t), y - y') \frac{\partial^3 X(y',t)}{\partial y'^3} + D \frac{\partial^2 X(y,t)}{\partial y^2}
\end{aligned} \tag{6.35}$$

This equation is our central result. It describes the evolution of the front between the two stable solutions $\psi = \pm\sqrt{\epsilon}$ of the Zeldovich equation in the presence of advection. Due to the coupling of the front dynamics to the velocity field the evolution of the front is nonlocal.

6.5 Linear Stability Analysis of a Planar Front

For planar fronts the velocity field vanishes identically, indicating that a planar front is a stationary solution. A planar front obeys

$$X(y,t) = X(y',t) = X_0 \tag{6.36}$$

Let us now investigate the stability of such a planar front. The vectorial kernel $\boldsymbol{K}(X(y,t) - X(y',t), y - y')$ to lowest order in $X(y,t) - X(y',t)$ is given by the Taylor series

$$\boldsymbol{K}(X(y,t)-X(y',t), y-y') = \begin{pmatrix} K_x(0, y-y') \\ 0 \end{pmatrix} + O\left(X(y,t) - X(y',t)\right) \tag{6.37}$$

The linear evolution of a planar front is then given by the nonlocal equation

$$\dot{X}(Y,t) = -\alpha\delta \int dy' K_x(0, y-y') \frac{\partial^3 X(y',t)}{\partial y'^3} + D\frac{\partial^2 X(y,t)}{\partial y^2} \tag{6.38}$$

Partial integration with respect to y' yields

$$\dot{X}(y,t) = -\alpha\delta \int dy' \kappa(y-y') \frac{\partial^2 X(y',t)}{\partial y'^2} + D\frac{\partial^2 X(y,t)}{\partial y^2} \tag{6.39}$$

Thereby, the kernel $\kappa(y - y')$ is defined according to

$$\kappa(y-y') = \frac{\partial K_x(0, y-y')}{\partial y} = \frac{\partial^2 G(0, y-y')}{\partial y^2} \tag{6.40}$$

Although the linear evolution equation for the front location is nonlocal, it can be solved by a Fourier transform, since the nonlocality is a convolution. Fourier transform yields

$$\dot{X}(k,t) = [-Dk^2 + \alpha\kappa(k)k^2]X(k,t) \tag{6.41}$$

Thereby, $\kappa(k)$ denotes the Fourier transform of $\kappa(y)$. The solution for the Fourier amplitude reads

$$X(k,t) = X(k,0)e^{\lambda(k)t} \tag{6.42}$$

where we have defined the growth rate

$$\lambda(k) = [-D + \alpha\delta\kappa(k)]k^2 \tag{6.43}$$

If this growth rate is positive, the corresponding perturbation growth exponentially in time. Disturbances with k-values having negative growth rates decay. Here, we emphasize that the growth rate actually is determined by the quantity $\kappa(y - y')$, given by (6.40).

We can relate the Fourier transform $\kappa(k)$ to the Fourier transform of $G(0, y)$. Denoting the Fourier transform of the kernel

$$G(x, y) = \int dk_1 dk_2 e^{ik_1 x + ik_2 y} G(k_1, k_2) \tag{6.44}$$

we obtain

$$G(0, y) = \int dK dk e^{iky} G(K, k) = \int dk e^{iky} \Gamma(k) \tag{6.45}$$

Since $\kappa(y) = \frac{\partial^2}{\partial y^2} G(0, y)$ the Fourier transform is explicitly given by

$$\kappa(k) = -k^2 \Gamma(k) \tag{6.46}$$

and is directly linked to the Fourier transform of the kernel $G(x, y)$.

6.5.1 The Kernel $G = [\Delta(\Delta - c^2)]^{-1}$

In the following we shall determine the quantity $\kappa(k)$ for the kernel $G = [\Delta(\Delta - c)]^{-1}$, whose Fourier transform $G(\mathbf{k})$ is just

$$G(k) = \frac{1}{k^2(k^2 + c^2)} \tag{6.47}$$

This calculation is based on the definition (6.40). As a consequence, the Fourier transform of $\kappa(y)$ reads

$$\kappa(k) = -k^2 \Gamma(k) = -k^2 \int dK G(K, k) = -k^2 \int dK \frac{1}{(k^2 + K^2)(k^2 + K^2 + {}^2 c)} \tag{6.48}$$

The integral can be evaluated by considering

$$\frac{1}{(k^2+K^2)(k^2+K^2+c^2)} = \frac{1}{c^2}[\frac{1}{k^2+K^2} - \frac{1}{k^2+K^2+c^2}] \tag{6.49}$$

using the integral

$$\int_{-\infty}^{\infty} dK \frac{1}{K^2+a^2} = \frac{\pi}{a} \tag{6.50}$$

Therefore,

$$\Gamma(k) = \int dK \frac{1}{(k^2+K^2)(k^2+K^2+c^2)} = \frac{\pi}{c^2}[\frac{1}{\sqrt{k^2}} - \frac{1}{\sqrt{k^2+c^2}}] \tag{6.51}$$

and the growth rate $\lambda(k)$ of the disturbances of the Fourier amplitudes $X(k,t)$ are given by

$$\lambda(k) = -Dk^2 + \alpha\delta\frac{\pi}{c^2}[\frac{k^2}{\sqrt{k^2}} - \frac{k^2}{\sqrt{k^2+c^2}}] \tag{6.52}$$

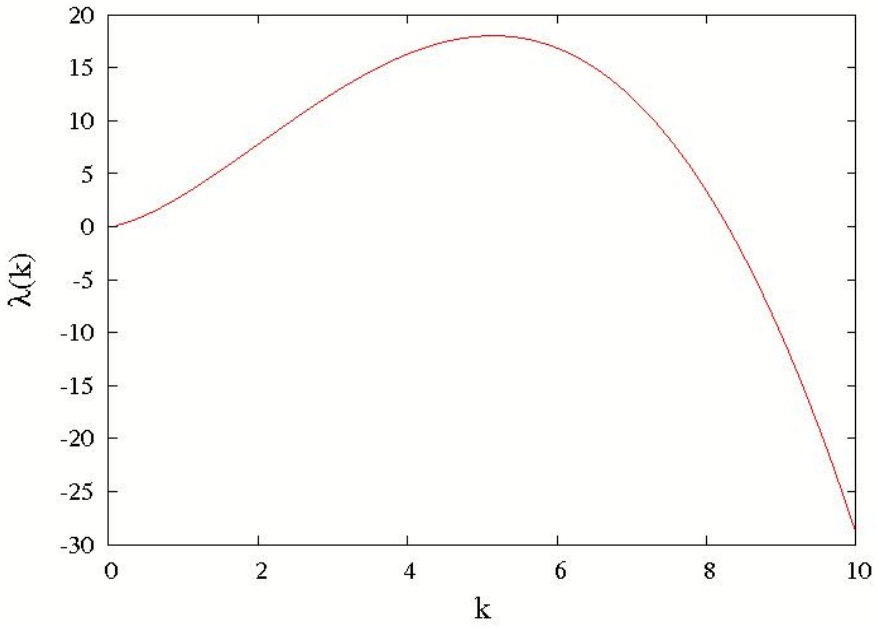

Figure 6.3 Growth rate given by eq. (6.52).

This function is depicted in fig. (6.3). For small values of k, we obtain

$$\lambda(k) = \alpha\delta\frac{\pi}{c^2}k \tag{6.53}$$

whereas for large values of k the growth rate is given by $-Dk^2$. The wave number with maximal growth rate, k_{max} is determined from the condition

$$\frac{d}{dk}\lambda(k) = 0 \tag{6.54}$$

We want to determine the growth rate for the case of large values of c, where we can approximate $c + k^2 \approx c$. Here we obtain

$$\lambda(k) = -(D + \frac{\alpha\delta\pi}{c^3})k^2 + \frac{\pi}{c^2}\alpha\delta k \tag{6.55}$$

As we explicitly see, instability sets in for positive values of α.

Here, k_{max} is given by

$$k_{max} = \frac{\pi\alpha}{2(Dc^2 + \alpha\pi/c)} \tag{6.56}$$

6.5.2 The Kernel $G = (-\Delta)^{-3/2}$

Let us briefly discuss the case of the kernel $G = (-\Delta)^{-3/2}$. This belongs to the model of an interface reaction between two fluid layers in the limiting case of infinite depth. As in the previous subsection we have to evaluate the quantity $\Gamma(k)$

$$\Gamma(k) = \int dK \frac{1}{(k^2 + K^2)^{3/2}} = \frac{2}{k^2} \tag{6.57}$$

The growth rate is then given by

$$\lambda(k) = (-D + 2\alpha\delta)k^2 \tag{6.58}$$

Thus, instability of the planar front arises when

$$\alpha\delta > \frac{D}{2} \tag{6.59}$$

The growth rate is quadratic in k, for the limiting case of infinitely deep fluid layer. It is expected that for finite fluid layers, the growth rate again becomes negative for large values of k.

6.6 Summary

Motivated by our numerical findings of fractal like behavior of fronts in chemical advection-reaction-diffusion systems we have, in this chapter, investigated the stability of planar fronts for a bistable one-component reaction diffusion system, the Zeldovich equation, in the presence of advection. We have considered two different models, a model for an active fluid and a model for an interface reaction. Depending on the sign of the quantity α we obtained either a stable or an unstable front. It would be interesting to formulate the evolution equation for the location of the fronts also for curved geometries, as in the work of Goldstein et al. [63] for a two-component reaction-diffusion system without advection. This gives the perspective to actually calculate the fractal boundaries, parametrized by the vector $\mathbf{X}(s,t)$ depending on arc-length s and time t, between the two stable states.

7 Numerical Methods

In this chapter we wish to give the outlook of the method we employed in the numerical simulation of the model equations for our first system. The simulation of our second system is done on the basis of the same procedure. So we give here a mere introduction of the pseudospectral scheme in general. The pseudospectral scheme is known to be efficient method as it converges very fast [38] as long as there is no discontinuity due to initialization or nonlinearity at each time step which can develop e.g., shock waves. Although for a very deep understanding, we refer to the monographs of Gottlieb and Orszag [10], Fornberg [38], Canuto et al. [21] and many others. In the following first we give general definitions used in the methods following [34] and then in later sections describe the iteration steps necessary for our coupled set of equations.

7.1 Discretization Method

7.1.1 General Representation of the field

The pseudospectral method uses the Fast Fourier Transform (FFT) rediscovered by Cooley and Turkey [22] was originally invented by Carl Friedrich Gauss.

In the pseudospectral method, the field is expanded in terms of some specified set of basis function and then truncated at some specified point in the domain. For generalization let us consider that $\psi(\mathbf{r})$ is a scalar field of a single variable $\boldsymbol{r}$ which is expanded in the Fourier series as follows:

$$\psi(\boldsymbol{r}) = \sum_{k_x,k_y=-\infty}^{\infty} \tilde{\psi}(\boldsymbol{k}) \exp^{\mathrm{i}(\boldsymbol{k}\cdot\boldsymbol{r})} \tag{7.1}$$

Here $\boldsymbol{k}$ is the wave vector and represents the spectral space and $\tilde{\psi}(\boldsymbol{k})$ represents the magnitude of the field in spectral space. For the two-dimensional field $\boldsymbol{r} = (x, y)$

Also the wave vector $\boldsymbol{k} = k_x\hat{\boldsymbol{x}} + k_y\hat{\boldsymbol{y}}$ as we are dealing with two-dimensional field. For finite representation of the field, only first $N+1$ coefficients are retained at the grid points so that we have

$$\psi(\boldsymbol{r}) = \sum_{k=0}^{N} \tilde{\psi}(\boldsymbol{k}) \exp^{\mathrm{i}(\boldsymbol{k}\cdot\boldsymbol{r})}$$

The properties of a transform of a real field is

$$\tilde{\psi}^*(\boldsymbol{k}) = \tilde{\psi}(-\boldsymbol{k})$$

where $*$ represents the complex conjugate of the field. This condition shows that the field is assumed as real. Another very important property of the Fourier transform is that the differentiation of the field is represented as follows

$$\partial_x \tilde{\psi}(\boldsymbol{x}) \rightarrow \mathrm{i}k_x \tilde{\psi}(\boldsymbol{k}) \tag{7.2}$$

7.1.2 Spatial Discretization

Consider a two-dimensional domain of finite size length, $\Omega = [0, L_x] \times [0, L_y]$. It is discretized in x and y direction with spacing Δx and Δy given by $\frac{L_x}{I}$ and $\frac{L_y}{J}$ respectively where i and j are integers. On the grid points $(x_i, y_j) = (i\Delta x, j\Delta y)$ with $i\epsilon 0, 1, ..., I-1$ and $j\epsilon 0, 1, ..., J-1$, the solution is approximated as $\psi_{i,j}(t)$. The components of wave vector are denoted by $k_x = \frac{2\pi p}{L_x}$ and $k_y = \frac{2\pi q}{L_y}$ where $p\epsilon(-\frac{I}{2}+1, ..., -1, 0, 1, ..., \frac{I}{2})$ and $q\epsilon(-\frac{J}{2}+1, ..., -1, 0, 1, ..., \frac{J}{2})$. In the following we will use $\mathcal{F}$ for FFT and $\mathcal{F}^{-1}$ for inverse FFT. The discrete Fourier Transform of the field ψ is given by

$$\begin{aligned} \mathcal{F}(\psi(x,y,t)) = \sum_{0}^{I-1}\sum_{0}^{J-1} \tilde{\psi}(k_p, k_q, t) \exp -\mathrm{i}(k_p x_i + k_q y_j) = \\ p = (-\frac{I}{2}+1, ..., -1, 0, 1, ..., \frac{I}{2}) \\ q = (-\frac{J}{2}+1, ..., -1, 0, 1, ..., \frac{J}{2}) \end{aligned} \tag{7.3}$$

where k_x and k_y are the wave vectors in x and y directions. The inverse discrete Fourier Transform is given by

$$\mathcal{F}^{-1}\tilde{\psi}(k_p, k_q, t) = \frac{1}{IJ}\sum_{p=\frac{I}{2}}^{\frac{I}{2}-1}\sum_{q=\frac{J}{2}}^{\frac{J}{2}-1}\psi(x, y, t)\exp^{-\mathrm{i}(k_p x_i + k_q y_j)}$$
$$i = (0, 1, ..., I-1)$$
$$j = (0, 1, ..., J-1) \tag{7.4}$$

If we have N dimensions then the total operation due to this method is of the $O(N\log(N))$ if $N = 2^m$ where m is an integer. We introduce our set of equations namely the Generalized Swift Hohenberg model given in Chapter 3 which can generally be written in Fourier space as

$$\frac{\partial}{\partial t}\tilde{\psi}(\boldsymbol{k}) = L\tilde{\psi}(\boldsymbol{k}) + N\tilde{\psi}(\boldsymbol{k}) \tag{7.5}$$

where ψ is the field, L denotes the linear term and N denotes the nonlinear term. We represent the equation in this way because the linear and nonlinear terms are treated in different ways in the pseudospectral method. The linear term is simply transformed into the Fourier space and is given by

$$L\tilde{\psi}(\boldsymbol{k}) = (\epsilon - (1-k^2)^2)\tilde{\psi}(\boldsymbol{k}) \tag{7.6}$$

Whereas the nonlinear term is first calculated in real space and then transformed to the Fourier space i.e.,

$$N\tilde{\psi}(\boldsymbol{k}) = \mathcal{F}(\boldsymbol{U}\cdot\nabla\psi(x) - \psi^3(x)) \tag{7.7}$$

whereby we have $\boldsymbol{U} = (-\partial_x\phi, \partial_y\phi)$. Hence using eq. (7.6) and eq. (7.7), we can write eq. (7.5) as

$$\frac{\partial}{\partial t}\tilde{\psi} = \epsilon\tilde{\psi} - (-k^2+1)^2\tilde{\psi} + \mathcal{F}(\mathbf{U}\cdot\nabla\psi(x)) - \tilde{\psi}^3(\boldsymbol{k}) \tag{7.8}$$

Hence the above eq.(7.8) represents the temperature equation in spectral space. As we describe earlier that we have two coupled equations, so using the same

approach we can discretize the mean field in spectral domain as

$$-\left(\frac{\partial}{\partial t}+Pr(k^2+c^2)\right)k^2\tilde{\phi}+\mathcal{F}(\boldsymbol{U}\cdot\nabla\Delta\phi)=\mathcal{F}\left(\nabla\psi(\boldsymbol{x},t)\times\nabla\Delta\psi(\boldsymbol{x},t)\cdot e_z\right) \quad (7.9)$$

Hence eqs. (7.8) and (7.9) are the spectral equation to be proceeded. Next we discuss how these equations are discretized in time.

For all multiplicative terms, we transform the fields into real space and perform the multiplication and then transform the product into the Fourier space.

7.1.3 Temporal Discretization

Here we describe the method for temporal discretization of our coupled fields. Since the field equations contain both the diffusive and advection terms so we use the mixed schemes for our both equations which is widely used in such kind of situation where there are restrictions on the time step [75]. We use the Runge-Kutta method for the diffusive term as described below for out first equation and Implicit Euler scheme for the advective equation given in the next subsection. Also we mention here that for our second system, we use Implicit Euler scheme for the all the equations.

Equation (7.8) is discretized in time by the explicit fourth order Runge-Kutta method. If $\tilde{\psi}_n$ represents the field at initial time then $\tilde{\psi}_{n+1}$ denotes at the next time step. We forwarded the field equation first in spectral space, i.e., right hand side of the eq. (7.8) is advanced in space and the result is stored as $\tilde{\psi}_n(\mathbf{k})$ where n denotes the time index. Before we give any further detail, we give the basic definitions of Runge-Kutta method.

$$\tilde{\psi}_{n+1}(k)=\tilde{\psi}_n(k)+\frac{1}{6}(k_1+2k_2+2k_3+k_4) \quad (7.10)$$

where k_1, k_2 ,k_3 and k_4 are the slopes in spectral space given by

$$\begin{aligned} k_1 &= f(t_j, \tilde{\psi}_j)\Delta t \\ k_2 &= f\left(t_j + \frac{1}{2}\Delta t, \tilde{\psi}_j + \frac{1}{2}k_1\right)\Delta t \\ k_3 &= f\left(t_j + \frac{1}{2}\Delta t, \psi_j + \frac{1}{2}k_2\right)\Delta t \\ k_4 &= f\left(t_j + \Delta t, \tilde{\psi}_j + k_3\right)\Delta t \end{aligned} \tag{7.11}$$

Here Δt denotes the smallest time step. How do we choose this time step? We will come to this point later. But first we describe that how do we proceed once we calculate initial field $\tilde{\psi}_n$ as described in the above paragraph. Then we find the value of the field at each slope interval according to above eq. (7.11) and then putting back into eq. (7.10), we iterate the model eq. (7.8) and eq. (7.9) until we get some consistent patterns (in convection case, namely spiral chaos). For the choice of time step, we use CFL (Courant Friedrichs Levy) condition which simply requires that $dt < \frac{dx}{V}$ where dt is the time step, $dx = \frac{2\pi}{N}$ is the space resolution and V is the maximum velocity of the field.

7.1.4 Implicit Euler

In this subsection, we illustrate the method for Implicit Euler since we use this scheme for our second field which is the advection equation. Here we just want to define the basic steps. The details can be found in any numerical text book. The equation is given by

$$-\left(\frac{\partial}{\partial t} + Pr(k^2 + c^2))\right) k^2\tilde{\phi} + \mathcal{F}(\boldsymbol{U}\cdot\nabla\Delta\phi) = \mathcal{F}\left(\nabla\psi(\boldsymbol{x},t)\times\nabla\Delta\psi(\boldsymbol{x},t)\cdot e_z\right) \tag{7.12}$$

If $\phi_{n+1}(k)$ denotes the field at time $t+1$ and $\phi_n(k)$ at time t then the above equations in this scheme can be expressed as

$$\left(1 + Pr(k^2 + c^2)\right) k^2\tilde{\phi}_{n+1} = \mathcal{F}\left(\nabla\psi(\boldsymbol{x},t)\times\nabla\Delta\psi(\boldsymbol{x},t)\cdot e_z\right) - \mathcal{F}\left(\boldsymbol{U}\cdot\nabla\Delta\phi_n(\boldsymbol{k})\right. \tag{7.13}$$

7.1.5 Boundary Conditions

We use the simplest periodic boundary conditions in the horizontal direction because they are consistent with the ideal periodic solutions and are appropriate for the consideration of the infinite layer i.e., large aspect ratio systems($l \gg d$) for convection problem, where l is the physical length of the system and d is the depth of the fluid. Also another reason is that pseudospectral method is inherently made for periodic boundaries

$$\psi(x + L) = \psi(x)$$

$$\phi(x + L) = \phi(x)$$

7.1.6 Test Case

Here we give a brief solution of a test case of Swift-Hohenberg model in order to check the validity of our code. We consider a simple two-dimensional system which give rise to hexagonal structures. Our dimensionless equation is

$$\partial_t \psi(\boldsymbol{x}, t) = \epsilon\psi(\boldsymbol{x}, t) - (k_c^2 - \nabla^2)^2\psi(\boldsymbol{x}, t) - c\psi^2(\boldsymbol{x}, t) - \psi^3(\boldsymbol{x}, t) \tag{7.14}$$

where ψ represents the temperature field at the mid plane, k_c is the critical wavenumber and c is a coefficient which appears due to the non-dimensionalization of the equation. This a gradient model and we get stationary patterns.

We apply here above mentioned scheme and for the resolution of $128 * 128$ in real space. We use the value for $k_c = 1$. For time discretization, we use Implicit Euler for this test where typical time step is 0.01. Nonlinearities were calculated as mentioned above.

7.2 Summary

It is very cumbersome to solve the nonlinear partial differential equations analytically so we made use of numerical methods to solve such type of equations. Simulations can complement the experiments and are helpful to aid the experiments. We solve our set of equations in a domain of length L using periodic boundary conditions. All the equations are solved in spectral space except the

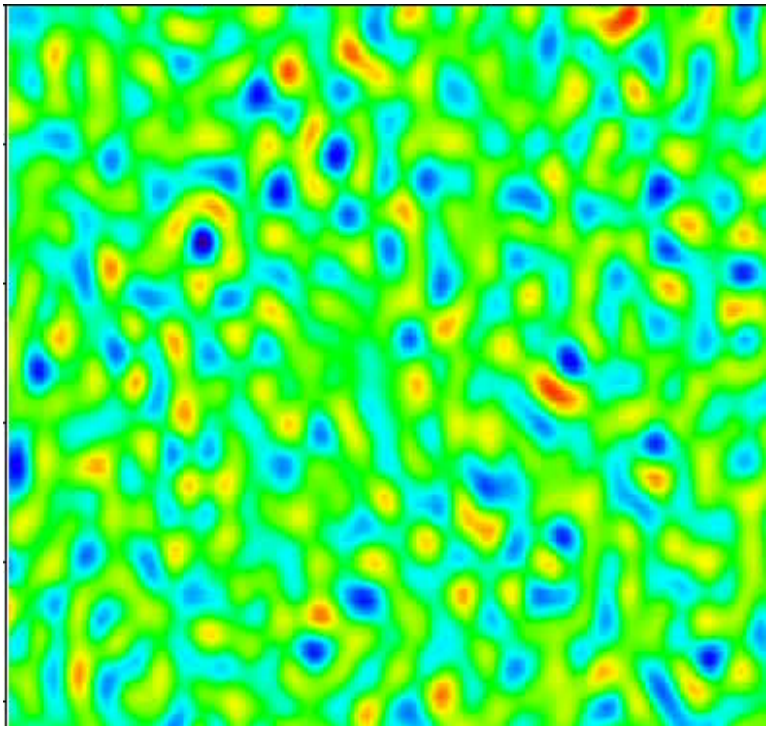

Figure 7.1 Starting with initial random numbers for eq. (7.14), $c = 0.5$, $\epsilon = 0.3$

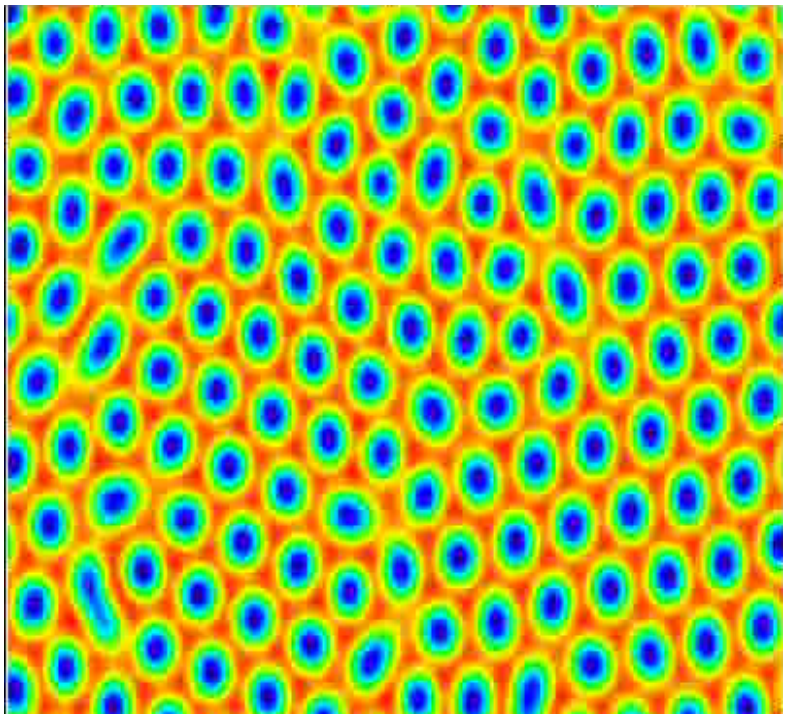

Figure 7.2 Appearance of Hexagons where red indicates high temperature and blue lower temperature.

nonlinear terms and convolution terms which are first solved in physical space and then converted back to the spectral space.

We employ high resolution N^2 grid for our simulations. The highest Nyquist frequency occurs at $\frac{N}{2}$. Mostly for our simulations we use resolutions 256×256 and 512×512. We iterate the temperature field using Runge-Kutta method because it is known to be highly convergent for periodic boundaries while for the case of mean field, use the Implicit Euler scheme.

8 Summary and Outlook

This universe is full of colors and amazing patterns. When a physicist looks into the sky, the colors and the different geometries cannot make him silent and compel him to think about how these patterns are there? What is the mechanism through which these patterns are formed? Why are patterns found which resemble other patterns despite of the fact that they arise in quite different systems, viewed from the microscopic point of view. When once they are formed how can they be stable or how can one understand the long transients? These are the questions which arise in the field of pattern formation in non-equilibrium systems.

The study of pattern formation is not a new field. It has a long history of exploration. With the advancement of science and history, it has turned out that the study of pattern formation is not a single branch of sciences but belongs to the field of complex systems far from equilibrium, which ranges from the natural sciences up to economics, sociology, informatics etc.

Pattern formation is directly associated with instability. An instability occur when a system is driven away from a state by a variation of the control parameters, or,in other words, by imposing a flow of energy and flow. We study the pattern formation in spatially extended systems by considering two important systems: One is the Rayleigh-Bénard system and the other is a reaction-diffusion system modeling a chemical system. Considerable amount of efforts have been made to investigate pattern formation in these two systems still many questions remain to be answered, which are especially concerned with so-called spatio-temporal chaos. There has been a close interaction between theory, experiment and numerical studies which have helped to come to the present knowledge in the field.

A basic theoretical concept of the field of pattern formation has been to look for universal features. Such an approach has been formulated in terms of the order parameter concept valid for systems close to the first instabilities. Mathematically this means that we can reduce the description to the order parameter equation, which is devoted to the dynamics of those modes which are active in describing

the phenomenon.

In Chapter 2, we introduce the Rayleigh-Bénard experiment as one of the paradigms of pattern forming systems. We formulate the basic equations, which rely on the Boussinesqian description of a fluid. Then we introduce a model equation, the so-called Swift-Hohenberg equation, which is applied to understand pattern formation in large aspect ratio systems, whose behavior is actually quasi two-dimensional.

In Chapter 3, we give an introduction to the mathematical treatment of pattern formation leading from the basic pattern forming equation to the order parameter equation describing the system close to instability. This approach underlines the concept of universality since the procedure applies to quite different pattern forming systems. Then we give a review of the derivation of the order parameter equation connecting it to the model of the Swift Hohenberg equation. This model equation has proved its importance since decades and its basic form and variants are useful in capturing the characteristics of pattern formation in large aspect ratio systems.

To study the patterns of spatio-temporal chaos, one needs to study the formation within the class of non-potential systems. Since the Swift-Hohenberg equation represents a system which has a non-equilibrium potential, and, hence, the long-term behavior is governed by its local minima, we discuss modified models of the Swift-Hohenberg equation. For Rayleigh-Bénard convection we take into account the dynamics of a horizontal flow field in terms of a so-called mean-field dynamics.

By numerical calculations we investigate the state of so-called spiral defect chaos in chapter 4. As is well-known the evolution of spiral defect chaos is developed as a result of the coupling of convection to the mean field dynamics. The spirals rotate and they are created and annihilated continuously. In order to explicitly show that mean field is responsible for the spiral defect chaos, we quench the dynamics of the mean field after the domain is full of spirals. We observe that the spiral defect states relax to rolls with some angular bends. We support this calculation by showing that the rolls tend to align with the lines of constant stream function, except for regions close to the former spiral tips.

The evolution of spatio temporal chaos is not bound to just hydrodynamic convective flows as already mentioned. In chapter 5, another very important class of systems namely reaction-diffusion equations are introduced as a second

model of spatio-temporal pattern formation. The basic equations represent the concentration of chemical species involved in the reaction in terms of chemical concentrations. First a basic introduction into the field of research is given, especially pointing out the emergence of Turing structures in close analogy to Rayleigh- Bénard convection. Then we include the hydrodynamic flow velocity in the form of advection. Hence, our system is actually a so-called advection-reaction-diffusion system. We study two models, which demonstrate the possibility of a back-reaction of the chemical kinetics onto the fluid dynamics by invoking a) a model of active media, and, b) by considering a certain type of inter-facial chemical reaction.

In chapter 6 of the thesis we explicitly demonstrate that, based on a two-component activator-inhibitor system including advection the appearance of spiral defect chaotic states also in these types of systems. This is underlined by a treatment which allows one to adiabatically eliminate the inhibitor dynamics, resulting, for certain regimes in control parameter space, at the generalized Swift-Hohenberg equation used as a model for low Prandtl number convection.

As a further result we present our findings on chemical fronts arising in our two-component advection reaction diffusion model in parameter regimes where one observes bi-stability. Our numerical calculations demonstrate the existence of an instability of a front induced by the advective motion. The fronts in this type of instability are known to show the formation of fractal like structure similar to the phenomenon of fingering. This instability does not arise in the absence of advection. We characterize the evolution of the fractals by investigating the time dependence of the perimeter of the pattern, which is characterized by a power law behavior indicating the formation of the fractal boundary. In some way those simulations exhibits patterns similar to Lichtenberg figures as a paradigm of fractals.

In Chapter 7, we continue the study of fractal fronts and analytically derive the evolution equation for the fronts of a bistable system, the Zeldovich model, in the presence of advection. As an issue we investigate the stability of planar fronts and explicitly show that the coupling to advection on the basis of the model of active fluids' or, alternatively, on the model of an inter-facial reaction can lead to an instability of a planar front, eventually leading to a fractalization of the chemical fronts.

Our findings are based on a combined application of analytical methods and numerical calculations. The numerical integrations of the order parameter equations a pseudospectral method has been applied. In Chapter 8, we give the basic definitions of the numerical methods which have been used in our simulations and then introduce the pseudospectral method.

To summarize, we studied two models for pattern formation with the intention to get insight into complex spatio-temporal patterns. As new results we found the existence of spiral defect chaos also in advection reaction-diffusion systems and showed that advection can induce an instability of chemical fronts eventually leading to fractal like boundaries.

List of Figures

Bibliography

[1] http://www.capturedlightning.com/frames/lichtenbergs.html.

[2] Super nova methodo naturam ac motum fluidi electrici investigandi, 1777.

[3] T. Passot A. C. Newell and J. Lega. Order parameter equations for patterns. *Ann. Rev. Fluid Mech.*, 25:399, 1993.

[4] T. Passot A. C. Newell and M. Soulli. Convection at finite rayleigh nbumbers in large aspect ratio containers. *Phys. Rev. Lett*, 64:2378, 1990.

[5] I Petrovsky A. Kolmogoroff and N. Piscounoff. Study of the diffusion equation with growth of the quantity of matter and its application to a biological problem. *Bulletin de 1 'universite d' etat a' Moscou, Ser. Int., Section A*, 1:1–25, 1937.

[6] B. Pier A. Kurdolli and J. P. Gollub. Superlattice patterns in surface waves. *Physica*, 123:99, 1998.

[7] T. Passot A.C. Newell and M. Soulli. The phase diffusion and mean drift equations for convection at finite rayleigh numbers for large containers. *Journal of Fluid Mechanics*, 220:187, 1990.

[8] G. Ahlers and R. P. Behringer. Evolution of turbulence from rayleigh benard instability. *Physical Review Letter*, 40:712, 1978.

[9] G. Ahlers and D. S. Cannell. Vortex front propagation in rotating couette taylor flow. *Phys. Rev. Lett.*, 50:1583, 1983.

[10] and Orszag. *Numerical analysis of Spectral Methods.* SIAM, 1977.

[11] D. Anvir and M. L. Kagan. The evolution of chemical patterns in reactive liquids, driven by hydrodynamic instabilities. *Chaos*, 5:589, 1995.

[12] H. Arbell and J. Fineberg. Pattern formation in two frequency forced parametric waves. *Phys. Rev. E*, 65:036224, 2002.

[13] A Assenheimer and V. Steinberg. Rayleigh benard convection near the gas liquid critical point. *Phys. Rev. Lett*, 70:3888, 1993.

[14] A Assenheimer and V. Steinberg. Transition between spiral and target states in rayleigh benard convection. *Nature*, 367:345, 1994.

[15] Yu. Astrov, E. Ammelt, S. Teperick, and H. G. Purwins. Hexagon and stripe turing structures in a gas discharge system. *Physics Letters A*, 211(3):184 – 190, 1996.

[16] P. Alstrom B. Christiansen and M. T. Levinsen. Ordered capillary wave states: quasi-crystals, hexagons and radial waves. *Phys. Rev. Lett.*, 68:2157, 1992.

[17] H. Benard. Les tourbillons cellulaires dans une nappe liquide. *Rev'. Gen. Sciences Pure Appl.*, 11:1261–1271, 1900.

[18] M. Bestehorn and R. Friedrich. Rotationally invariant order parameter equations for natural patterns in nonequilibrium systems. *Phys. Rev. E*, 59:3, 1999.

[19] D. Binks and W. van de Water. Nonlinear pattern formationof faraday waves. *Phys. Rev. Lett*, 78:4043, 1997.

[20] F. H. Busse. On the stability of two dimensional convection in a layer heated from below. *J. Math Phys.*, 46:149, 1967.

[21] A. Quarteroni C. Canuto, M. Y. Hussaini and T. A. Zang. *Spectral Methods in Fluid Dynamics*. Springer verlag, New York, 1988.

[22] J. W. Cooley and J. Tukey. An algorithm of the machine computation of complex fourier series. *Mathematics of Computation*, 19:297, 1965.

[23] M. C. Cross. Phase dynamics of convective rolls. *Phys. Rev. A*, 27:490, 1983.

[24] M. C. Cross and P. C. Hohenberg. Pattern formation outside of equilibrium. *Rev. Mod. Phys.*, 65(3):851, Jul 1993.

[25] M. C. Cross and P. C. Hohenberg. Spatiotemporal chaos. *Sceince*, 263:1569, 1994.

[26] M. C. Cross and A. C Newell. Convection patterns in large aspect ratio systems. *Physica D*, 3:299, 1984.

[27] G. Dee and J. S. Langer. Propagating pattern selection. *Phys. Rev. Lett.*, 50:383, 1983.

[28] R. C. Desai and R. Kapral. *Dynamics of Self organised and self Assembeled Structues*. Cambridge press, 2009.

[29] M. Diewald and H. R. Brand. Chemically driven convection can stabilize turing patterns. *Phys. Rev. E*, 51:6, 1995.

[30] J. R. de Bruyn R. Ecke Y. C. HuK. Lerman E. Bodenschatz, D. S. Cannel and G. Ahlers. Experiments on thress systems with non variational aspects. *Physica D*, 61:77–93, 1992.

[31] Y. Hu. R. Ecke and G. Ahlers. Convection for prandtl numbers near 1: dynamics of textured patterns. *Phys. Rev. E*, 51:3263, 1995.

[32] H. M. Hastings F. H. Fenton, E. M. Cherry and S. J. Evans. Multiple mechansims od spiral wave breakup in a model of cardiac electrical activity. *Chaos*, 12:852, 2002.

[33] Fereydoon Family and TamaÂ´s Vicsek. *Dynamics of Fractal Surfaces*. World Scientific, 1991.

[34] Riccardo Fazio and Salvatore Iacono. Pseudospectral methods for linear advection and dispersive problems. *IAENG International Journal of Applied Mathematics*, 39:396, 2009.

[35] J. Finebreg and V. Steinberg. Voretx front propagation in rayleigh be'nard convection. *Phys. REv. Lett.*, 58:1332, 1987.

[36] R. A Fisher. The wave of advance of advantageous genes. *Ann. Eugenics*, 7:355, 1937.

[37] R. FitzHugh. Impulses and physiological states in theoretical models of nerve membrane. *Biophysical J.*, 1:445–466, 1961.

[38] Bengt Fornberg. *A Practical Guide to Pseudospectral Method*. Cambridge University Press, 1990.

[39] A. V. Getling. *Rayleigh-Bénard Convection: Structures and dynamics*. World Scientific, 1998.

[40] S. V. Gurevich. *Lateral self-organization in nonlinear transport systems described by reaction diffusion equations*. PhD thesis, WWU Muenster, 2006.

[41] W. M. Coughran Jr H. S. Greenside and M. C. Cross. Mean flows and the onset of chaos in large cell convection. *Phys. Rev. Lett*, 60:2269, 1988.

[42] H. Haken. *Pattern Formation and Pattern recognition*. Springer Verlag New York, 1979.

[43] H. Haken. *Advanced Synergetics*. Springer Berlin, 1987.

[44] G. Iooss and A. M. Rucklidge. On the existence of quasipattern solutions of the swiftâhohenberg equation. *Journal of Nonlinear science*, 20:361–394, 2010.

[45] M. C. Cross K. H. Chiam and H. S. Greenside. Mean flow and spiral defect chaos in rayleigh be'nard convection. *Phys.Rev. E*, 67:056206, 2003.

[46] R. Kapral and K. Showalter, editors. *Chemical Waves and Patterns*. Kulwer Academic Publishers, 1995.

[47] K. Kondo and R. Asai. A reactionâdiffusion wave on the skin of the marine angelfish pomacanthus. *Nature*, 376:765, 1995.

[48] Y. Kuramoto. *Chemical Oscillations, Waves and Turbulence*. Springer Series in Synergetics, 1984.

[49] L. D. Landau. On the problem of turbulence. *C. R. Acad. Sci. USSR*, 44:311, 1944.

[50] J. Lega and T. Passot. Hydrodynamics of bacterial colonies: A model. *Phys. Rev. E*, 67:031906, 2003.

[51] J. Lega and T. Passot. Hydrodynamics of bacterial colonies. *Nonlinearity*, 21:C1–C16, 2007.

[52] G. Liu and G. Ahlers. Spiral defect chaos in rayleigh benard convection with small prandtl numbers. *Phys. Rev. Lett*, 77:3126, 1996.

[53] R. Friedrich M. Bestehorn, M. Fantz and H. Haken. Hexagonal and spiral patterns of thermal convection. *Physics Letters A*, 174:48–52, 1993.

[54] Benoit Mandelbrot. *The Fractal Geometry of Nature*. W. H. Freeman and Company Newyork, 1977.

[55] P. Manneville. A two-dimensional model for three-dimensional convective patterns in wide containers. *J. Phys. France*, 44(7):759–765, 1983.

[56] J D Murray. *Mathematical Biology*. Springer Verlag, 2002.

[57] Q. Ouang and H. Swinney. Transition from a uniform state to hexagonal and striped turing patterns. *Nature*, 352:610, 1991.

[58] J. R. Pearson. On convection cells induced by surface tension. *J. Fluid Mech*, 4:489, 1958.

[59] Pierre Pelce. *New visions on form and growth Fingered Growth, Dendrites and Flames*. Oxford University Press, 2004.

[60] K. J. Painter P.K Maini and H. N. P. Chau. Spatial pattern formation in chemical and biological systems. *J. Chem. Soc. , Faraday Trans*, 93:3601, 1997.

[61] Y. Pomeau and P. Manneville. Wavelength selection in cellular flows. *Physics Letters A*, 75(4):296 – 298, 1980.

[62] Ilya Prigogine. Moderation et transformations irreversibles des systeme ouverts. *Bull. Acad. Roy. Bleg. Cl. Sci.*, 31:600, 1945.

[63] D. M. Petrich R. E. Goldstein, D.J. Muraki. Interface proliferation and the growth of labyrinths in a reaction-diffusion system. *Phys. Rev. E*, 53:3933, 1996.

[64] A. Aumann T. Ackermann Y. A. Logvin R. Herrero, E. G. Westhof and W. Lange. Twelvefold quasiperiodic patterns in a nonlinear optical system with continuous rotational symmetry. *Phys. Rev. Lett*, 82:4627, 1999.

[65] H. Diamant R. Lifshitz. Soft quasicrystals: why are they stable? *Philos. Mag.*, 87:3021, 2007.

[66] Lord Rayleigh. On convection currents in a horizontal layer of fluid, when the higher temperature is on the under side. *Phil. Mag.ser.*, 32:529–546, 1916.

[67] J. S. Rowlinson and B. Widom. *Molecular Theory of Capillarity*. Clarendon Press, 1982.

[68] D. S. Cannel S. W. Morris, E. Bodenschatz and G. Ahlers. Spiral defect chaos in large aspect ratio rayleigh-bénard convection. *Phys. Rev. Lett.*, 71:2026, 1993.

[69] E. D. Siggia and A. Zippelius. Pattern selection in rayleigh benard convection near threshold. *Phys. Rev. Lett*, 47:835, 1981.

[70] G. I Sivashinsky. On flame propagation under conditions of stoichiometry. *SIAM Journal on Applied Mathematics*, 39:136, 1980.

[71] C.V. Sternling and L. E. Scriven. Interfacial turbulence : Hydrodynamic stability and the marangoni effect. *AIChE J*, 5:514, 1959.

[72] J. Swift and P. C. Hohenberg. Hydrodynamic fluctuations at the convective instability. *Phys. Rev. A*, 15(1):319–328, Jan 1977.

[73] Richard P. Taylor. *Chaos, Fractals, Nature A New Look at Jackson Pollock*. Fractals Research (Eugene USA), 2010.

[74] Allan M. Turing. The chemical basis of morphogenesis. *Philos. Trans. R. Soc. London B*, 237:37, 1952.

[75] Steven J. Ruuth Uri M. Ascher and Raymond J. Spiteri. Implicit-explicit runge kutta methods for time dependant partial differential equations. *Applied Numerical Methamatics*, 25:151–167, 1997.

[76] J. Boissonade V. Castets, E. Dulos and P. De Kepper. Experimental evidence of a sustained standing turing-type nonequilibrium chemical pattern. *Phys. Rev. Lett.*, 64:2953, 1990.

[77] M. Mory V. Croquette and F. Schosseler. Rayleigh be'nard convective structures in a cylindrical container. *J. Phys. France*, 44:293–301, 1983.

[78] W. van Saarloos. Front propagation into unstable states. *Physics Reports*, 386:29–222, 2003.

[79] V. K. Vanang and I. R. Epstein. Pattern formation in a tunable medium: The belousov-zhabotinsky reaction in an aerosol ot microemulsion. *Phys. Rev. Lett.*, 87:228301, 2001.

[80] Daniel Walgraef. *Spatiotemporal Pattern Formation. with examples from Physics, Chemistry and Material Science.* Springer Verlag New York, 1997.

[81] A. N. Zaikin and A. M. Zhabotinsky. Concentration wave propagation in two-dimensional liquid phase self oscillating system. *Nature*, 225:535–537, 1970.

[82] Y. B. Zeldovich. K teorii rasprostranenia plasmeni. *Fizicheskoi Khimii (UDSSR)*, 22:1–38, 1948.

Acknowledgement

First of all I thank Almighty Allah, the most beneficent and merciful for all the blessings bestowed upon me. Then I thank my Supervisor, Prof. Dr Rudolf Friedrich whose motivation, encouragement and indescribable knowledge and experience made it possible to write this Dissertation. It was a great experience to work under his supervision and I feel myself lucky to work with such a nice and dedicated TEACHER.

I thank my friendly colleagues specially Michael Wilsczek and Johannes Lülff for answering many questions related to some basics of numeric and Latex which helped in beginning the Thesis. I thank Michael Wilsczek for corrections of some chapters. I also thank all group members, Svetlana Gurevich for her always welcome nature and friendly behavior, sweet Eva Baresal for the company we shared at times at some conferences and also sharing the stress during Thesis writing and also for translating the abstract. I also like to thank Oliver Kamps who also helped in correction of German abstract. I thank all other colleagues of the department. Many thanks goes to the office mate Max Theoder Kuchel for writing German letters for me whenever I needed and also for good atmosphere in the office.

I would also like to thank our Secretariat for sorting our institutional matters.

Outside the Institute I thank Eleni Dautsali whose company I enjoyed always and I did not went anywhere without her in whole Germany. I like to thank my best friend Ayesha Rehman for encouraging me when I start writing the Thesis and sharing the stress. I like to thank my all other friends whom I spent any time with.

Also my funding was from HEC (Higher Education Commission of Pakistan) and DAAD Germany. I like to thank them.

Last but not the least I like to thank my mother for her lifetime prayers, love and support without whom I would have been nothing. I thank my mother-in-law for her prayers for me. I thank my sisters Lubna, Saba and brothers Hassan,

Jawad, Sehban and Faizan and three naughty nephews and one niece whom I am anxious to meet. At the most I like to thank my very caring and loving husband Affan without whose help, understanding, motivation and love I would not be able to live alone and work. Thank you very much my Love.